Partial Discharge Properties and Gas Decomposition Analysis of Environmental Friendly Gas Insulation Media as a Basis of Diagnostic Technique Development

Mohamad Kamarol bin Mohd Jamil

Department of Electrical and Electronic Engineering
Graduate School of Engineering
Kyushu Institute of Technology

December, 2007

Doctoral Dissertation

Partial Discharge Properties and Gas Decomposition Analysis of Environmental Friendly Gas Insulation Media as a Basis of Diagnostic Technique Development

Mohamad Kamarol bin Mohd Jamil
(Student Number: 05586403)

Supervisor: Prof. Masayuki Hikita

Department of Electrical and Electronic Engineering
Graduate School of Engineering
Kyushu Institute of Technology

December, 2007

Table of Contents

Chapter 1 Introduction

Chapter 2 Experimental setup and method

Chapter 3 Discharge properties and emitted electromagnetic wave spectrum in low vacuum region of vacuum interrupter

Chapter 6 Summary

Appendix

Chapter 1

Introduction

1.1 The role of environmental friendly gas insulation media to the electric power apparatus.

An electric power apparatus in power station (transmission and distribution) such as gas insulated switchgear (GIS), gas circuit breaker (GCB) or gas insulated line (GIL) is implementing sulfur hexafluoride (SF_6) gas as an insulating medium in order to minimize the substation area. SF_6 gas is an inorganic compound used as an insulator because it has higher dielectric strength, excellent arc extinction properties, harmless and inactive. Although SF_6 gas is a perfect insulating media, it is a most potent greenhouse gas that has been evaluated. The emission of SF_6 gas to the atmosphere due to the leakage of power apparatus would give effect to the global warming potential (GWP). According to the Intergovernmental Panel on Climate Change (IPCC) the GWP affected by the emission of SF_6 gas is 22,200 times that of CO_2 over a100 year period [(1)]. While the GWP of SF_6 gas emission according to United Nations Framework Convention on Climate Change (UNFCCC) is 23,900 times that of CO_2 over 100 year period which is used as decorated at the 3rd Conference of the Parties (COP3) or the Kyoto Protocol [(1, 2)]. It is proved from the data of annual greenhouse gas emission by sector shown in Fig.1.1 [(3)], that the power substation is the higher percentage of the gas emission that contributed to the GWP. The electrical power gives a higher percentage of 34% of annual greenhouse gas emission of CO_2 gas. Thus, since SF_6 emission is 23,900 times that of CO_2 over 100 year, it depicts that the emission of SF_6 to the atmosphere obviously contributed to global warming effect.

The need to develop new gas became mandatory requirement to protect environment condition which was decided in Kyoto Protocol. For this reason various industries are recommended to decrease their consumption of SF_6 gas. At the same time, many researchers all over the world are trying all their best to search the best solution to minimize or to avoid the greenhouse gas emission and it became an ethically hoped. The researchers who involve in electrical power apparatus such as GIS, GCB and GIL

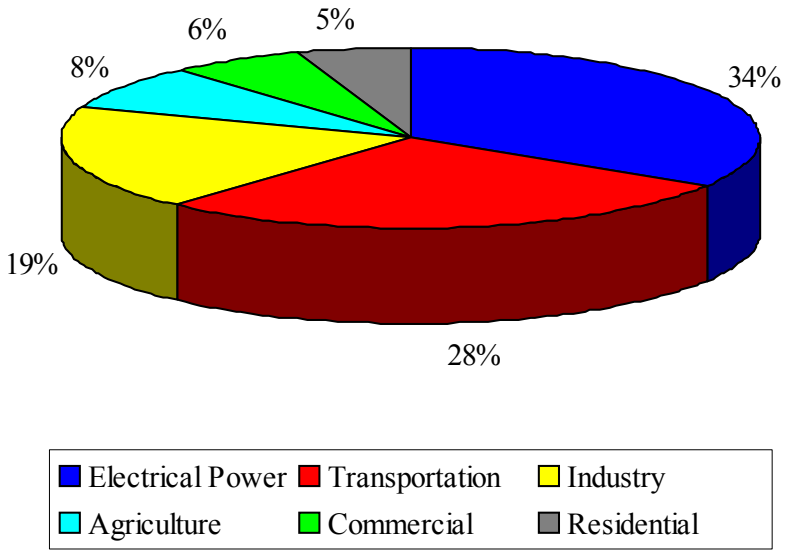

Fig. 1.1 Percentage of annual greenhouse gas emission by economic sector in 2005 [3]

are now being conducted a research extensively to find an environmental friendly gas insulation media that possible to substitute SF_6 gas.

1.2 Research and Development on the Alternative Gas

The conventional gases such as He, CO_2, N_2 and air has neither sufficiently enough insulation strength nor interruption ability, thus the gas with a mixture of SF_6 is considered as a potential to the solution which many works were carried out. Table1.1 shows the example of research and development trend on the alternative gases up to year 2000 and after year 2000 in Japan[4]. N_2-SF_6 gas mixtures were mainly studied up to year 2000. Then the research and development continue focused on the substitution of the equipment without SF_6 gas after year 2000. Vacuum is one of the promising environmental friendly dielectric media that has an excellent dielectric strength and provide nothing to support conduction. Vacuum circuit breaker (VCB) is a device that may be employed to replace the usage of SF_6 gas insulated apparatus in the future [4]. The VCB is widely implemented in power substation such as cubical-type insulated switchgear (C-GIS) and air insulated switchgear (AIS). Most of the VCB used in power

Table1.1 Research and development trend on alternative gases up year 2000 and after year 2000 [4]

	Categories	Contents	Gases	
			Up to year 2000	Year after 2000
Insulation / Interruption / Thermal properties	Insulation properties	Basic physics	N_2/SF_6,C-C_4F_8/N_2or CO_2,$N_2/SF_6/CO_2$, N_2/O_2,Air,N_2	N_2/C_2F_6,N_2/C_3F_8, CO_2/C_2F_6,CO_2/C_3F_8, CF_3I
		Uniform field	N_2/SF_6	Air,N_2,CO_2,C_3F_8, $CF_4/N_2/C_3F_8$, c-C_4F_8, CF_3I
		Non-uniform field	N_2/SF_6,C-C_4F_8/N_2 or CO_2,$N_2/SF_6/CO_2$, N_2/O_2,Air,N_2	N_2/SF_6,CO_2,N_2/CO_2, N_2 or CO_2/ C_3F_8, N_2 or CO_2/ C_2F_6,
		Practical equipment test	N_2/SF_6	CO_2 (Vacuum)
	Interruption capability	GCB	N_2/SF_6	CO_2
		VCB	Vacuum	Vacuum
		DS	N_2/SF_6	N_2/SF_6
	Current capacity	Temperature rise of conductor and enclosure	N_2/SF_6	N_2
Equipment	Equipment design	GIL / GIB	N_2/SF_6	N_2/SF_6, N_2
		GIS	N_2/SF_6	Silicon oil
		Transformer	N_2/SF_6	-
	Prototype	GCB	-	CO_2
		VCB	Vacuum	Vacuum
	Recycle	Pressure swing adsorption	N_2/SF_6	-
		Polymer membrane	N_2/SF_6	N_2/SF_6

Table 1.2 General properties of CF_3I gas[9].

Parameters	**CF_3I gas**	**SF_6 gas**
Molecular mass	195.91	146.05
Global Warming Potential (GWP)	less than 5	23,900
Ozone Depleting Potential (ODP)	0.0001	0
Life time in atmosphere	0.005 year	3,200 years
Boiling point at 0.1MPa	-22.5℃	-63.9℃

systems are in medium voltage class and research for the development of high rated voltage is proceeding now[5,6,7,8]. The successful of high rated voltage development may expand the application of vacuum technology in circuit breaker and switchgear for power substation.

At the same time, the quest on the other gas with the same or better dielectric strength has been carried out. Recently, an extremely low GWP effect gas with relatively low toxicity such as trifluro-iodo-methane (CF_3I) was innovated. CF_3I gas is colorless, nonflammable, has lower environmental impact to the effect of GWP less than 5 and 0.0001 of ozone depleting potential (ODP). The general properties of CF_3I gas compared with those SF_6 gas are shown in Table 1.2[9]. CF_3I gas may eventually replace SF_6 gas because recent studies have demonstrated the limiting electric field $(E/N)_{lim}$ (at α-η=0) under uniform configuration has relatively high of 440Td compared to that SF_6 gas as shown in Fig. 1.2 [10]. However there are still many uncertain items that should be investigated such as the insulation properties under non-uniform electric field of different electric field utilization factor and water content, partial discharge (PD) properties and by-product analysis of pure CF_3I and CF_3I mixture gas, the influence of gaseous by-products on electrical insulation properties of solid insulating material and

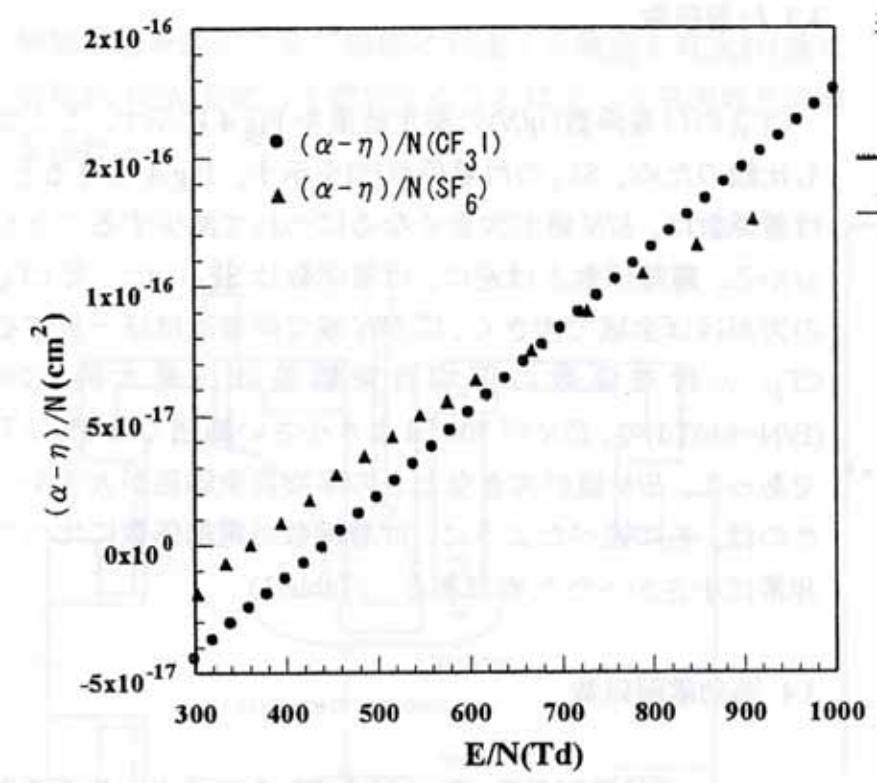

Fig. 1.2 Effective ionization coefficient in CF_3I compared with SF_6 gas [10]

the PD mechanism of CF_3I. Solving these issues would lead to contribution of design guideline for utilizing CF_3I gas as insulating medium of environmental friendly gas insulating power apparatus.

The utilizing of environmental friendly gas insulating media such as vacuum and CF_3I to the electric power apparatus give high impact to improve climate change due to the low GWP emission of greenhouse gases. It is realized that the rapid progress on technology development is essential and important for the better life with the conservation of environment.

1.2.1 Vacuum Circuit Breaker to medium and high voltage system application

Vacuum is an excellent candidate for switching at medium and high voltage. The vacuum was discovered as an insulating medium in 1920's [11, 12]. Later, the investigation on vacuum as a switching ambient was progressively carried out. Eventually in 1950's vacuum switches were commercialized and applied extensively in power system. The rapid research conducted on the vacuum technology for the power system application yield to the development of vacuum circuit breaker (VCB) [13].

The VCB is used extensively in electrical power distribution and transmission. Since VCB can interrupt a current in vacuum without producing any special gas harmful to the environment, and also has a lower thermal conductivity, it has become a most probable potential candidate in the substitution of SF_6 gas insulated switchgear. However, additional improvements are necessary to apply VCB completely to transmission system. The increments of VCB rated voltage to higher ones or same level with SF_6 gas type circuit breakers are desired. In 1978, the connection of two VCBs of 84 kV rated voltage with 31.5 kA for high voltage application were invented and commercialized in Japan. This gives the total rated voltage of 168 kV with two high voltage vacuum interrupters (VI) applied to the transmission systems [6,14]. Fig. 1.3 shows an example of the high voltage VCB utilized in the electrical transmission system. Later, the improvement on the capability of this VCB was carried out. In 1979, these double breaks VCB can interrupt a large short circuit current up to 40 kA at 168 kV of rated voltage. In 1985, the application of VI to 72 kV cubicle-type gas insulated (C-GIS) switchgear was commercialized [15]. The VI was installed inside the C-GIS and surrounded by the atmospheric pressure of SF_6 gas as insulator. The developments of this technology demonstrate a significant achievement to the reduction of size and reduction of SF_6 gas. Since C-GIS are compact, it was extensively utilized in both outside and inside of the buildings. Fig. 1.4 depicts the photograph and the internal

structure of C-GIS. The development towards the lower GWP of insulated switchgear is continued with the development of 72/84 kV tank-type VCB with ceramic type VI. The VI was insulated with high pressure of dry air [6, 14, 17] as shown in Fig. 1.5.

Later on, from year 2000 Japan have been engaged with the development of high voltage and high capacity of VCB. They have successfully developed a 145 kV, 40 kA single-break VCB by optimizing the electric field within the VI, introduced a new type of electrode and implementing a composite insulator [6, 14, 18]. Fig. 1.6 shows the example of 145 kV-40 kA single-break porcelain type VCB with prototype VI installed in the VCB. The VI has nominal current of 2 kA with 700 mm in length and 240 mm in diameter. It consists of axial magnetic field electrodes with some engineering technologies application to enhance the current interrupting and electrical insulation performance. These features enable the realization of cost reduction and simpler structure of VI. The other additional improvement necessary for the implementation of VCB to higher voltage transmission systems is by considering the thermal conductivity and gap configuration. Recent research reported that the implementation of silicone oil surrounding VI as insulation media combining with multi-gap configuration would enable VCB to apply at higher voltage level. The silicone oil will not only work as insulator but also effective for cooling agent. Newly designed silicone immersed vacuum switchgear is conceptually designed and intended to be applied to 550 kV

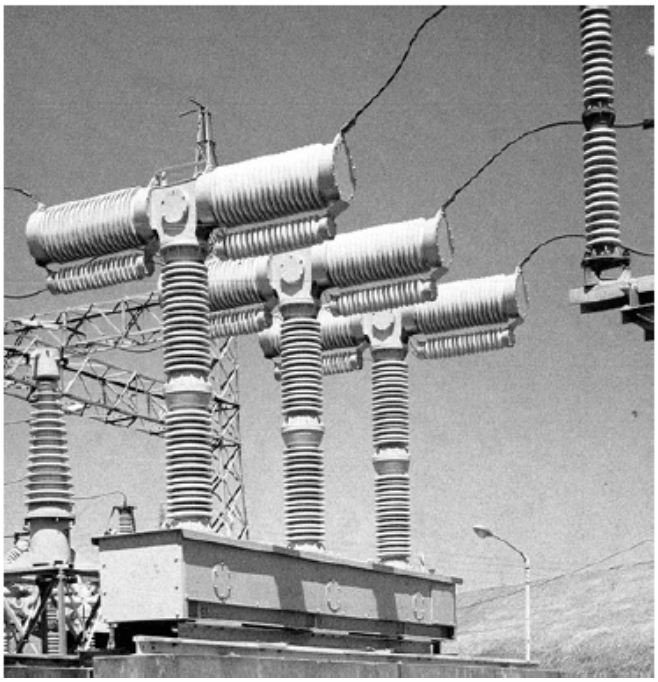

Fig. 1.3 A 168 kV, 40 kA double break VCB [6,14]

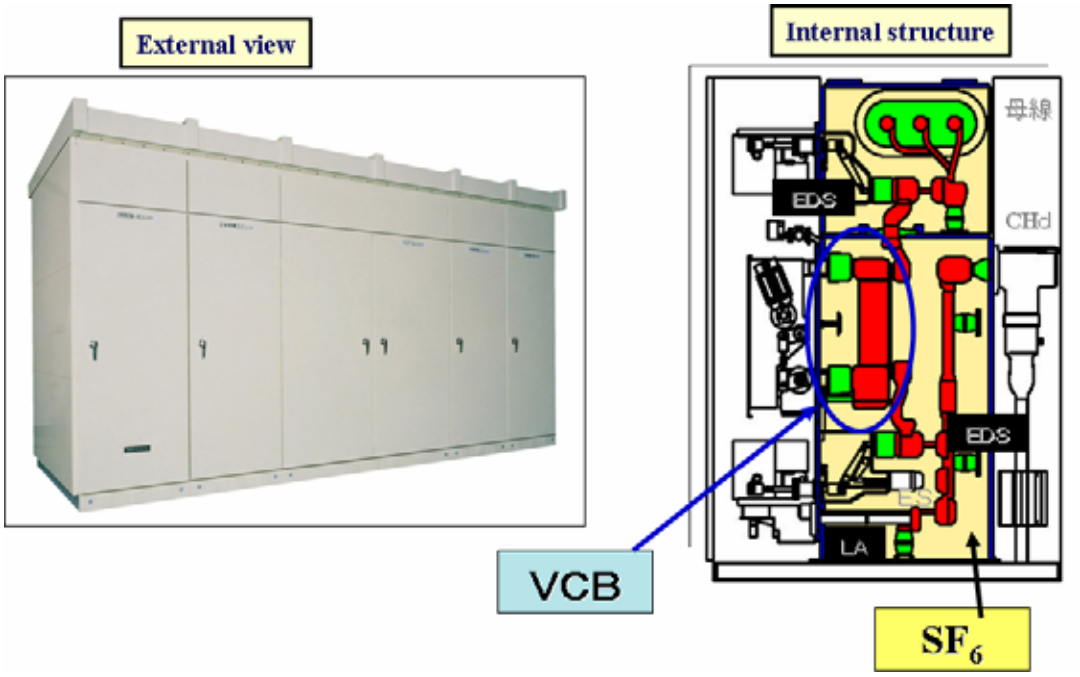

Fig. 1.4 One break 72 kV C-GIS [15,16]

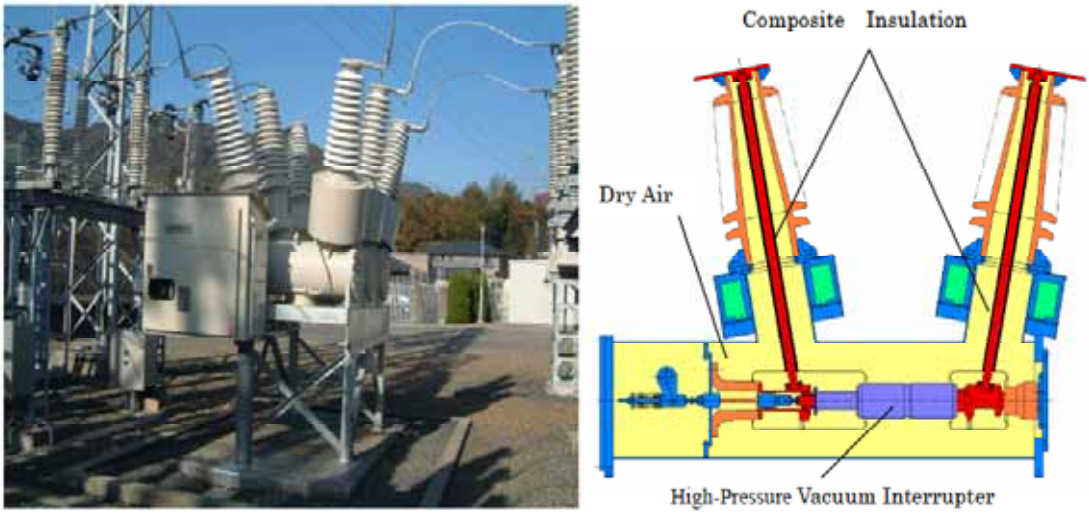

a) 72/84 kV, 31.5 kA SF_6 gas-free VCB b) Internal view of SF_6 gas-free VCB

Fig. 1.5 SF_6 gas –free of 72/84 kV vacuum circuit breaker [6, 14, 17]

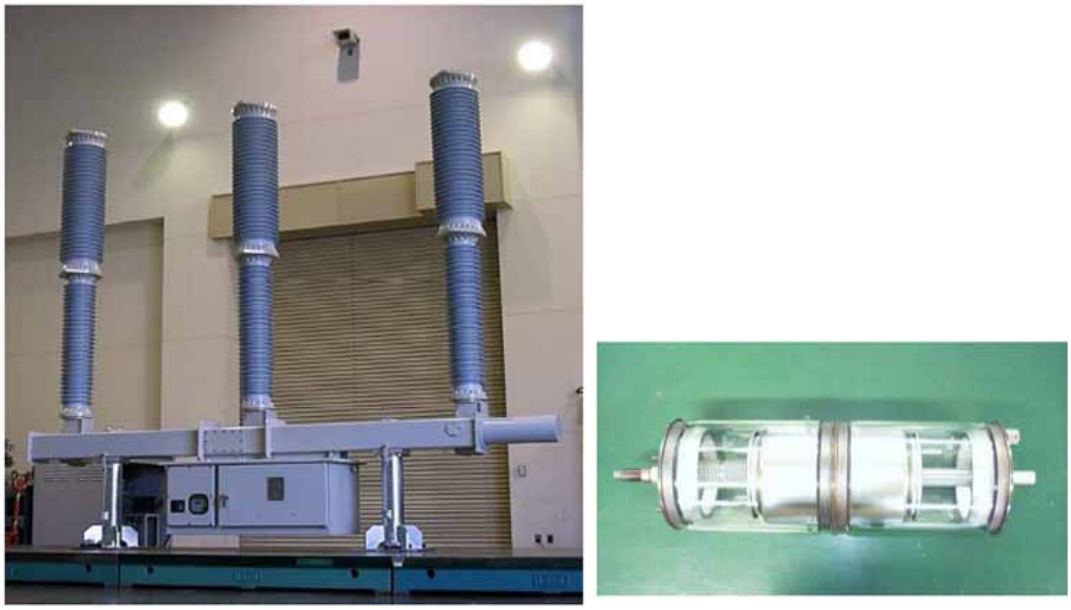

a) Porcelain type vacuum circuit breaker

b) Prototype vacuum interrupter used in the vacuum circuit breaker

Fig. 1.6 Single break vacuum circuit breaker of 145 kV, 40 kA[6, 14, 18]

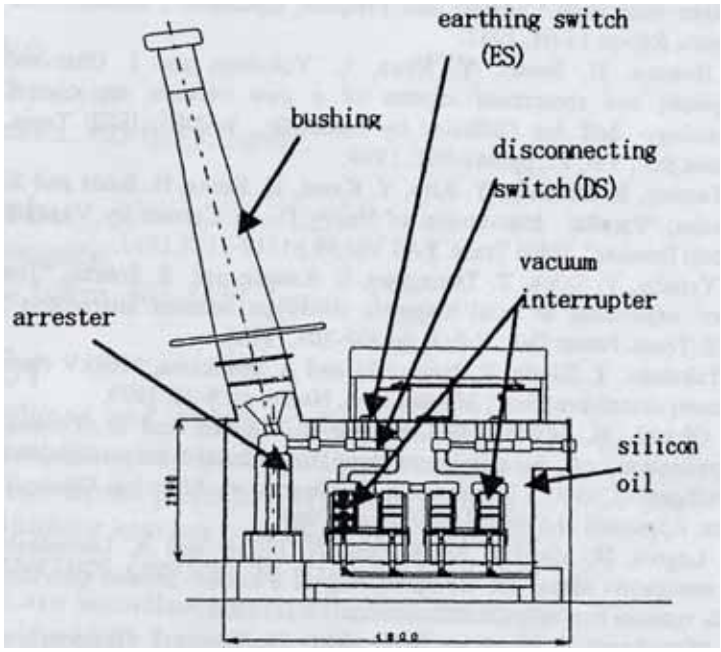

Fig. 1.7 New concept vacuum switchgear intended to be applied to 550 kV systems [14]

systems [14, 19]. This conceptual example is shown in Fig. 1.7 where it consists of four VIs connected in series together with earthing, disconnecting switches and arresters surrounded by the silicone oil. This report shows the feasibility of VCB to higher voltage systems where it consists of an environmental friendly media that can be one of the solution to future environmental issues.

In Europe, the evolution of VCB to the medium voltage circuit breaker (MVCB) markets was observed since 1980 [20]. At that time oil circuit breaker (OCB) was the highest of 65 % of the markets compared to vacuum and SF_6 of 10 % and 15 %, respectively. However the vacuum and SF_6 extensively replaced the oil medium as a circuit breaker in 1996. VCB and SF_6 occupied 40 % and 60 % respectively of the MVCB markets in Europe. The manufacturing of vacuum technology in MVCB by ABB company reported gradually increases from around 38 % in 1991 to 50 % in 1999 [21]. Moreover, the manufacturing of vacuum with SF_6 in MVCB reported increases 20% from 1991 to 1999. The worldwide market for MVCB 1998 reported that China, India, Asia and USA were among the highest percentage of 60 % to 90 % market of VCB. Countries like Latin America, Central and Eastern Europe obviously revealed the trend towards the use of vacuum technologies in circuit breaker. This indicates the application of VCB to the gas insulated switchgear apparatus has higher demand in future.

Although the application of VCB were achieved up to 145 kV class, the improvement and development for higher voltage application of VCB for utilization in power transmission and substation are still progressing [4-8,18, 22-27]. Several aspects have been taken into consideration to develop the high voltage VCB. One of the aspects is by the enhancement of electrical insulation performance in VI through the clarification of the fundamental electrical discharge characteristics in the vacuum and implementing the electrical insulation technique [22]. This study deals with uniform, quasi uniform and non uniform field electric field configuration under the affect of material, electrode surface roughness and pre-treatment, conditioning degree and area effect. From the perspective of higher voltage VCB it can be said that the material of the electrode, electrode conditioning and area affect were the potential critical electrical insulation techniques especially under the non-uniform and long gap electrode configurations. It means that by improving these critical factors the optimization on the electrical insulation performance in VI can be achieved. Therefore the electrical insulation design plays an important role in developing the high voltage VI. The study seeking to optimize level of electrical insulation performance in VI by charge simulation method was revealed that the electric field distribution in VI was greatly influence by floating potential of the center shielding [23]. Based on this factor the arrangement of VI in the VCB grounded

wall should be carefully considered. The maximum field strength between the VI and the VCB wall can be reduced by controlling the capacitance distribution in VI. Moreover, the curvature design of center shield tips yields to more uniform distribution of electric field and lower maximum electric field strength.

In the other aspects the interruption performance of VI also plays an important role in the development to higher voltage level. The VI should have a higher capability to interrupt fault current of high voltage system. The improvements of interruption performance require an understanding of the physical phenomena related to breaking process and the dielectric insulation. The physical phenomena such as breakdown characteristic in vacuum have been studied by many researches where many different mechanisms of breakdown in vacuum were proposed [28-33] such as anode heating mechanism and cathode heating mechanism. Moreover the interruption failure of VI may due to post-arc plasma sheath expand across the contact gap in the presence of molten metal on the contacts [34,35,36]. Metal vapors, residual plasma and metal droplets are also some of the potential sources contributing to the limitation of interruption performance.

Vacuum interruption has dominated the medium voltage (MV) range for many years and the application of VI to higher voltages level is not straightforward. There are a number of technical and economic factors to be taken into account. Nowadays, the technical aspects would not face any problems but it is not so simple to achieve. The fundamental problem with the high voltage VCB is the need to have up to a several number of interrupters in series per phase, which is very costly. One of the obvious ways to overcome this problem is development of high voltage VCB from a several number of interrupters to a single interrupter per phase. This immensely simplifies the design and reduces the cost of the circuit breaker substantially. With the advanced technology and extensive research the single interrupter up to 145 kV was developed [6,14,18]. Recently, a 252 kV single break VI prototype was proposed by China[5]. Based on this achieving it is possible to envisage solution using extrapolations of existing technology and it is expected that VCB for more than 252 kV will appear over the next few years. A work to realize this ambition is currently on going with a great deal to be done to understand the problems faced before technical solutions can be developed. This effort is most apparent in China where they are working to develop a 750 kV VCB [37,38]. From this point of view VCB seems to be possible for high voltage application and this indicates the diagnostic devices to monitor the performance of VI is highly recommended in future.

1.2.2 Diagnostic technique on the performance of vacuum interrupter

VCB is a dominant technology for MV class and extensively used in power transmission and distribution systems all over the world. In future it would appear to the high voltage class based on technical dominance at MV class and environmental concerns over the use of SF_6 gas. VCB is utilized to control and protect power lines and equipments under conditions of overload, short circuit, over current and other faults. The diagnosis of VI performance seems significance since the development on the VI to higher voltage application is extremely conducted. The success of high rated voltage development may expand the application of VCB in power substation systems. Consequently, the stability and reliability of the operation systems to the consumers are important and should be maintained for their satisfaction.

The diagnosis of vacuum interrupter performance can be classified under maintenance activity in order to keep it in a state in which it can operate properly according to the requirement. Condition based maintenance (CBM) is recently suggested where preventive actions are carried out depending on the condition of equipment [37-39]. The CBM strategy can improve the reliability of power system by avoiding a major failure and the consequent unplanned outage. It can delimitate the unnecessary maintenance work. Thus the repair and outage cost can be reduced. The key factor of CBM is the knowledge of the condition of the apparatus such as VCB.

Early detection on the performance of VCB can avoid a major failure to the power system and can save the repairing cost. VI would have a bad performance when the age achieved more than 30 years old in operation. The internal pressure of VI would gradually increase due to gas permeation, gas evolution or slow leak of vacuum [40]. The increasing of the internal pressure would lead to the decreasing of insulation performance in VI and cause the occurrence of PD. In 12 kV VCB, PD were found to occur above 2 Pa order of VI [41]. Fig. 1.8 depicts the breakdown performance of a 12 kV VCB at different pressures. At this moment, during the operation, if overcurrent or other fault occurs, VI would fail to interrupt and cause damage to the power apparatus. Therefore to alert possible trouble due to failure of VCB an effective measurement technique is necessary. For this purpose many kinds of devices with different technique were developed. In 1966, the magnetron method was discovered [42]. A few years later, the same methods with different way of measuring approachs were developed [40-44]. However these traditional methods require VCB to be detached and set into solenoid coil to measure the vacuum level of VI, so that it cannot be applied on-line. Moreover it needs a specialized and experienced operator to handle this task, which would increase

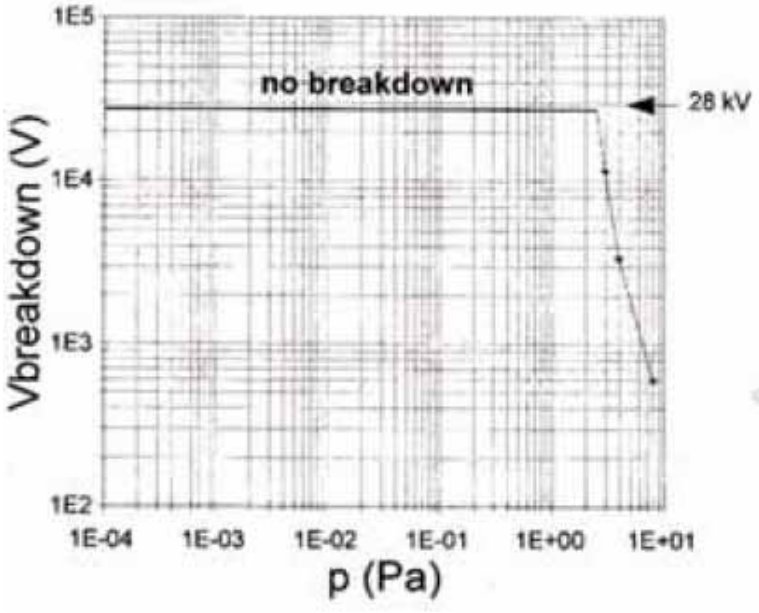

Fig. 1.8 Breakdown performance of a 12 kV VCB at different pressures during 1 min 20 kV test [41]

Table 1.3 Methods of vacuum measurement with relevant requirements [52]

Methods	Requirement			
	Range	Unambiguous	Accurate	Practicable in Field
Penning	◎	◎	◎	▽
Magnetron	◎	◎	◎	▽
Discharge noise	◎	◎	▽	◎
HF pre-discharge current	◎	▽	○	◎
HF emission current	◎	▽	○	◎
DC switching bahaviour	○	◎	▽	◎
AC switching behaviour	○	◎	○	◎
DC shield potential	○	▽	▽	◎
Air friction	○	◎	○	◎
Residual gas analysis	◎	◎	◎	▽

Captions:

▽ - Low expectation

○ - Indefinite

◎ - Promising

the maintenance cost and time. Later on, the detection of pressure variances in VI using magnetron method was continued with a Pockels electric field sensor [45]. This method was reported as on-line pressure detection of VI where the sensor needs to be attached at the center of VI envelope at the place where the shield is allocated. The sensor is connected to the monitoring system by the optical cable via the wall of the GIS tank. Since the sensor is directly attached at the envelope of VI, there is a possibility of discharge occurring between the external of VI and the other conductors inside the GIS tank. Moreover, the sensor located at the center where the shield is allocated may have a voltage of 80% of the applied voltage, thus it is not so reliable to higher voltage application.

The other measuring techniques like coupling electrode method, detection based on discharge with different kinds of methods were also reported [46-49]. The coupling electrode method was based on a potential change of the shield located at a few millimeters order distance from the envelope of VI. However this method is only applicable for the type of VCB which have installed coupling electrode and not for general type of VCB [46]. The measuring of vacuum performance based on PD can be classifying to a few numbers of methods. One of the methods is by measuring the electromagnetic wave (EMW) spectrum emitted by PD occurrence inside VI using the UHF sensor such as antenna [47-51]. The concept is advisable because the measurement can be done at a few meter distances, although the sensitivity of the measurement is not high enough to detect at lower frequency range at ten MHz order. This is because the PDs generated at this frequency range have lower intensity of EMW spectrum [41,49,50]. The other concept on measuring EMW spectrum reported by Guan Yonggang et al [48] is by adding floating point-plane gap in actual VI at fixed electrode to generate PD at lower pressure. Although it is a fine idea, it is not practicable and not recommendable especially for higher voltage VI. Besides the EMW spectrum measurement, there are ten presumed methods of vacuum measurement with the most relevant requirements and it ability indication summarized in table 1.3 [52].

1.2.3 CF_3I gas as a candidate to the replacement of potent greenhouse effect

CF_3I is one of the potential gases to substitute SF_6 gas because of its extremely low GWP, near-zero ODP, good long-term stability at ambient conditions, relatively low toxicity gas, colorless and nonflammable [53,54,55,56]. Fig. 1.9 shows the *V-t* characteristics of CF_3I gas at 0.1 MPa (abs) compared with SF_6 gas where the dashed lines indicate minimum sparkover voltages estimated by Schumanns' criterion [57]. It depicts that CF_3I gas has a high

dielectric strength 1.2 times greater than of SF_6 gas under 0.89 of field utilizing factor in atmospheric pressure. In the study of sphere-to-plane electrode configuration in pure CF_3I under AC applied voltage with 1 mm gap also depicted almost the similar magnitude of sparkover voltage with that of SF_6 gas at 0.1 MPa to 0.3 MPa [58] as shown in Fig. 1.10. However, the CF_3I has a weakness such as high point of boiling temperature -22.5℃ at ambient pressure. Fig. 1.11 shows the saturation vapor pressure curve in CF_3I compared with that SF_6 gas [9,57,59]. In practical GCB, the SF_6 gas is utilized at 0.5 to 0.6 MPa [9]. At these pressure level, SF_6 gas has lower boiling temperature point at about -30℃ while CF_3I gas is relatively high about 26℃. It is impossible to implement CF_3I gas at this pressure level due to its high boiling temperature yielding the liquefying of the gas. However, there are several ways to prevent CF_3I gas from liquefying by decreasing partial pressure and mixing with other gases such as N_2, air and CO_2.

As far as CF_3I is concerned, further research is necessary to understand their characteristics for the practical application. Beside the research on the dielectric strength of CF_3I and CF_3I gas mixture, the study on the fundamental properties of CF_3I under high-temperature conditions has been also conducted to find out the usefulness of CF_3I as an arc-quenching gas [60]. The study consists of the thermodynamics, the transport and the

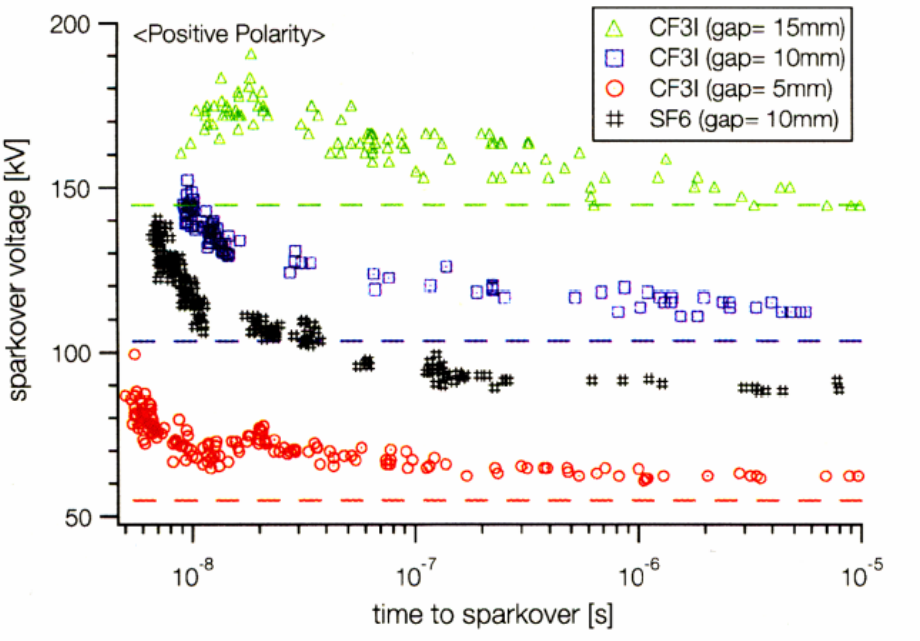

Fig. 1.9 Positive *V-t* characteristics of CF3I gas at 0.1 MPa (abs) [57]

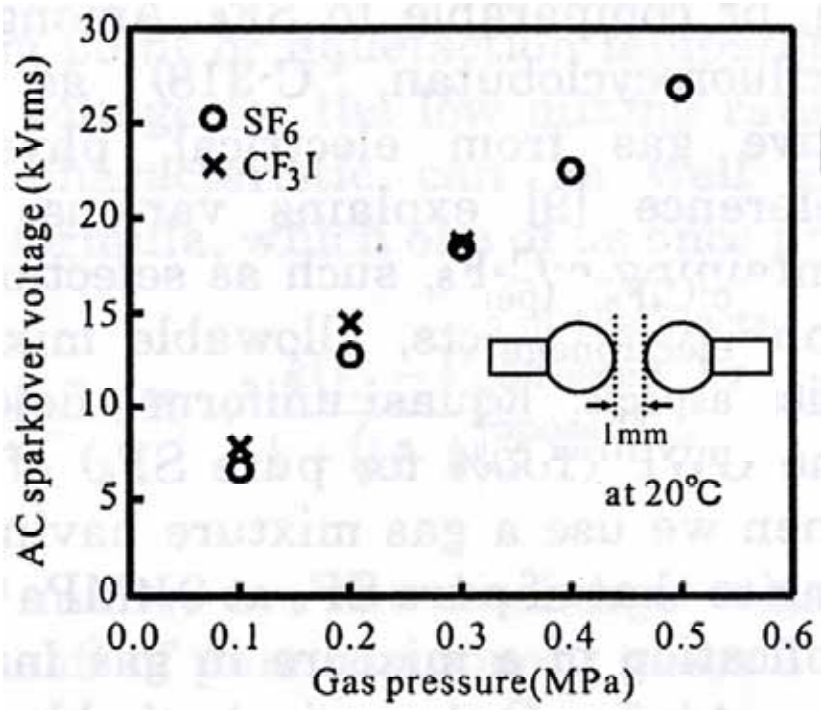

Fig. 1.10 Comparison of AC sparkover voltage between CF_3I and SF_6 gas [58]

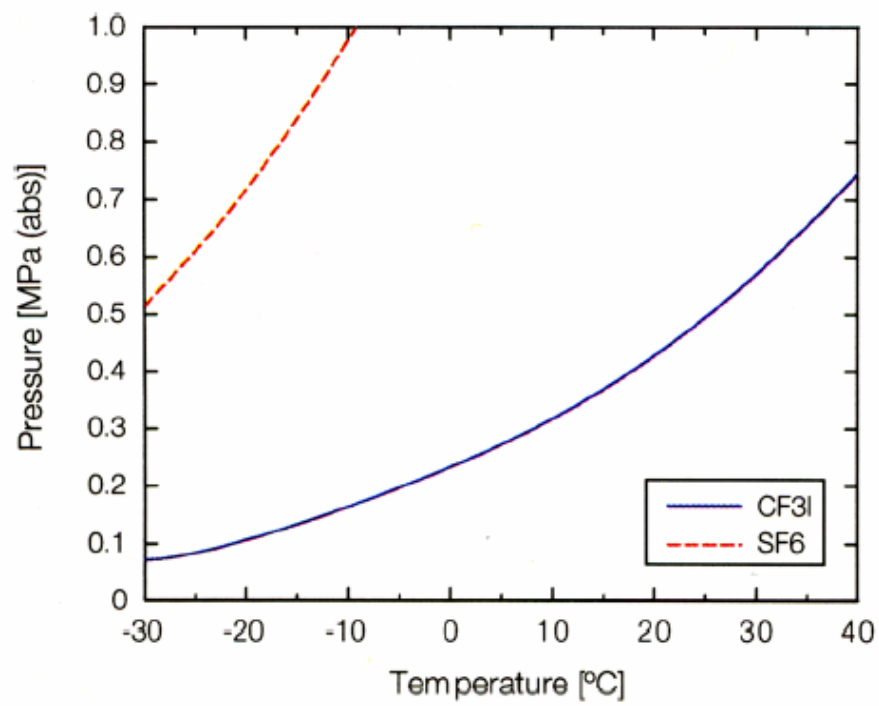

Fig. 1.11 Saturation vapor pressure curve in CF_3I and SF_6 gas [9,57,59]

radiation properties in the temperature from 300 ~ 1000 K at 0.1~1.0 MPa. The results revealed that CF_3I has higher arc extinguishing capability than other gases such as CO_2, N_2 and air. There are many other studies on CF_3I such as the dielectric strength and the fabrication process which involves the etching of silicon surfaces with a mixture of energetic neutrals, ions and electrons [61]. However, there still many unknown remain on the insulating performance in AC applied voltage under non-uniform field. Moreover, influences of the gas by-products on the environment and on the electrical insulation properties of solid insulating material are still remain to be investigated. PD measurement and by-product analysis are necessary to be clarified by changing parameter such as pressure, electric field utilization factor and water content. Thus, to obtain the full understanding on the uncertain item, extensive research is needed in order to apply the CF_3I gas to high voltage apparatus. Consequently, these lead to providing a design guideline for using CF_3I gas as insulating medium of environmental friendly gas insulated power apparatus in future.

1.3 Objectives and Outline of the Dissertation

1.3.1 The objectives of the research

As stated in the previous sections, it is understood that the environmental friendly aspect was the main criteria in a future development of electric power apparatus. Vacuum and CF_3I gas are the environmental friendly gas media that gives an impact to many researchers for switching and insulation purpose.

This dissertation dealt with the PD properties and diagnostic technique on vacuum performance in practical VI, and decomposition by-products analysis of CF_3I gas. Thus the following objectives were organized in order to achieve the targets of the study:

1) To investigate the PD properties in lower pressures of air and SF_6 gas of practical VI, which simulate the low performance of VI.
2) To clarify the position of PD occurrence in lower pressures of air and SF_6 gas of VI
3) To investigate the diagnostic technique of vacuum performance in VI based on partial discharge.
4) To investigate the sparkover voltage and PD inception voltage properties in CF_3I gas under AC applied voltage of non-uniform electric field.
5) To clarify the gas decomposition by-products of CF_3I gas under PD occurrence.

1.3.2 Outline of the dissertation

The dissertation is classified into 6 chapters. The outline of the dissertation can be composed as follows;

In chapter 2, it is mainly describes the experimental setup used in this research study for VI and CF_3I gas. For the investigation related to the VI, constructions of systems were performed to measure the PD current pulses and light pulses, and to observe the optical images. The PD current pulse was measured using radio frequency (RF) current transformer (CT) as a detecting device connected to the oscilloscope while the PD light intensity was measured using photomultiplier tube (PMT) connected to the oscilloscope. The optical images were observed by intensifier charge coupled device (ICCD) camera connected to the personal computer. The systems enable to obtain the relationship between the pressure variances and the rise time of the PD. For the investigation related to the CF_3I, the systems were constructed to measure all the PD charge quantity with cumulative charge and analyzed gaseous by-products of CF_3I gas suffering PD. Gas-Chromatography / Mass spectroscopy (GC/MS) device was used to analyze by-products of CF_3I gas after PD test. The sparkover voltage and PDIV also can be measured with the constructions systems performance.

In chapter 3, the ceramic type VI with 12 kV rated voltage which exactly similar to VI that applied in actual C-GIS was utilized to investigate the PD properties and the electromagnetic wave spectrum (EMW) emitted by PD. The circuit that simulates the real condition of VI used in C-GIS was constructed. The experiment was conducted in two conditions, closed contact and open contact conditions. The PD current pulses and the EMW spectrum emitted by PD in VI were measured with CT and antenna, respectively. The relationship between PD against the product and gap spacing (*pd*) was discussed. The flow of PD current paths inside the VI was also has been considered for both conditions.

In chapter 4, deals with the PD properties in low vacuum region of practical vacuum interrupter filled with air and SF_6 gas. The glass vessel of VI was used for a better understanding of the optical PD properties in the low vacuum region and to know the location of PD occurrence as the pressure varies at constant applied voltage. In this experiment, the pressures were set at 1 Pa to 1 kPa order to simulate the leakage. The measurement of PD occurring inside the vacuum interrupter was performed with CT, PMT, ICCD camera and PD measurement device. The PD properties was discussed on the basis of the rise time, peak intensity and width of the discharge light pulse. Meanwhile, the estimation of gas pressure in VI was performed based on phase-resolved discharge characteristics utilizing back propagation neural network.

In chapter 5, the investigation was performed on quantitative relation between cumulative charge of PD and by-products of CF_3I gas suffering PD. The cumulative charge of PD at 0.1 MPa was obtained using a PD measuring system for a given time

under the non-uniform electric field configuration. After the test, the amount of gaseous by-products of CF_3I gas was measured with a GC/MS detector for a given cumulative charge q_c to discuss the quantitative relation between q_c and the amount of the by-products. Meanwhile the AC sparkover voltage V_s and PD inception voltage V_{PDI+} and V_{PDI-} were also obtained for the pressure of 0.1 MPa to 0.2 MPa.

In chapter 6, the composition of this dissertation was summarized and the scope for the future research was also given.

References

[1] High GWP gases and climate change, US environmental protection Agency, 2006.

[2] Working group I: The scientific basis; Intergovernmental panel on climate change (2007-03-31). (http://www.grida.no/climate/ipcc_tar/wg1/248-htmT)

[3] US greenhouse gas inventory report and sinks: 1990-2005, pp.1-393, April 2007.

[4] T. Kawamura, M. Meguro, H. Hama and T. Yamagiwa, "Industrial Outlook: How to reduce SF_6 use and emission-Various aggressive approaches to realize less SF6 environment", Gaseous Dielectric X, pp. 475-484, 2004.

[5] J. Wang, Z. Liu, S. Xiu, Z. Wang, S. Yuan, L. Jin, H. Zhou and R. Yang, "Development of high voltage vacuum circuit breakers in China", XXIInd Int. Symp. on Discharges and Electrical Insulation in Vacuum, Matsue, Japan, pp. 247-252, 2006.

[6] Y. Matsui, K. Nagatake, M. Takeshita, K. Katsumata, A. Sano, H. Ichikawa, H. Saitoh and M. Sakaki, "Development and Technology of High Voltage VCBs; Breaf History and State of Art", XXIInd Int. Symp. on Discharges and Electrical Insulation in Vacuum, Matsue, Japan , pp. 253-256. 2006

[7] R. Renz, " High Voltage Vacuum Interrupters-Technical and Physical Feasibility versus Economical Efficiency", XXIInd Int. Symp. on Discharges and Electrical Insulation in Vacuum, Matsue, Japan, pp. 257-262, 2006

[8] Hans Schellekens and Georges Gaudart, "High-Voltage Vacuum Circuit Breaker a Feasibility Study", XXIInd Int. Symp. on Discharges and Electrical Insulation in Vacuum, Matsue, Japan, pp. 263-266, 2006

[9] M. Taki, D. Maekawa, H. Odaka, H. Mizoguchi and S. Yanabu, "Interruption Capability of CF_3I Gas as a Sunstitution Candidate for SF_6 Gas", IEEE Trans. on Dielectric and Electrical Insulation, Vol. 14, No. 2, April 2007.

[10] M. Kimura, Y. Morokuma and Y. Nakamura, "A Measurement of Ionization Coefficient in Pure Trifluoroiodo-methane", Papers or Technical Meetings on Electrical Discharge (in Japanese), IEE Japan, ED-02-98, pp. 13-18, 2002.

[11] Ayrton H., "The Electric Arc", D. Van Norstrand, New York, 1902.

[12] R. W. Sorensen and H. E. Mendenhall, "Vacuum Switching Experiments at the California Institute of Technology", Trans. AIEE, 45, pp. 1102-1105, 1926

[13] A. L. Streater, R. H. Miller and J. C. Sofianek, "Heavy Duty Vacuum Recloser", Trans. AIEE, 81, pp. 356-363, 1962.

[14] M. Homma, M. Sakaki, E. Kaneko and S. Yanabu, "History of Vacuum Circuit

Breakers and Recent Developments in Japan", IEEE Trans. on Dielectric and Electrical Insualtion", Vol. 13, No. 1, Feb. 2006.

[15] H. Ohashi, N. Masaki, I. Ohshima, E. Kaneko and S. Yanabu, "Application of Vacuum interrupters to Cubicle-Type Gas Insulated Switchgear (C-GIS)",International Conference on Electrical Contacts, Arcs, Apparatus and their Applications", 1989

[16] AE power systems corporation broacher.

[17] K. Nagatake, S. Akiyama, H. Ichikawa, M. Sakaki, T. Fukai and M. Honma, "Development of Environmentally Benign Type 72/84 kV Vacuum Circuit Breaker", Proceeding 14th Annual Conference Power & Energy Society, IEE Japan, No. 6-237, 2003.

[18] H. Saitou, H. Ichikawa, A. Nishijima, Y. Mataui, M. Sakai, M. Honma and H. Okubo, "Research and Development on 145 kV/40 kA One Break Vacuum Circuit Breaker", IEEE T/D Conference, Yokohama, pp.1465-1468, 2002.

[19] S. Yanabu, S. Arai, Y. Kawaguchi and T. Kawamura, "New Concept of Switchgear for Replacing SF_6 Gas or Gas Mixture", Gaseous Dielectrics IX, pp. 497-504, 2001.

[20] Philippe Picot "www.merlin-gerin.com.tr/ftp/literature/publications/".

[21] Guenter Leonhardt, Mauro Marchi and Giandomenico Rivetti, "Choosing the right MV circuit breaker –SF_6 or vacuum", ABB review, April 2004

[22] Hitoshi Okubo, "Development of electrical insulation techniques in vacuum for higher voltage vacuum interrupters", XXIInd Int. Symp. on Discharges and Electrical Insulation in Vacuum, Vol. 1, pp. 7- 12, 2006

[23] K. Kato and H. Okubo, "Optimization of electrode contour for improvement of insulation performance of high voltage vacuum circuit breaker", XXIInd Int. Symp. on Discharges and Electrical Insulation in Vacuum, Vol. 1, pp. 21- 24, 2006

[24] L. T. Falkingham, "Fifty years of vacuum interrupter development in the UK", XXth Int. Symp. on Discharges and Electrical Insulation in Vacuum, pp. 1- 8, 2002

[25] H. Okubo, "Technical trend of environmental-friendly high voltage vacuum circuit breaker (VCB)", Trans. IEE Japan, Vol. 123-B, No. 2, pp. 129-132, 2003

[26] H. Okubo and S. Yanabu, "Feasibility study on application of high voltage and high power vacuum circuit breaker", XXth Int. Symp. on Discharges and Electrical Insulation in Vacuum, pp. 275-278, 2002

[27] L. T. Falkingham, "A brief history showing trends in vacuum interrupter technology", XVIIIth Int. Symp. on Discharges and Electrical Insulation in Vacuum, pp. 407-413, 1998

[28] G.. A. Farall, “Electrical breakdown in vacuum ”, IEEE Trans. on Electrical Insulation, Vol. EI-20, No. 5, pp. 815-841, 1985

[29] H. C. Miller, “Electrical discharge in vacuum”, IEEE Trans. on Electrical Insulation, Vol. 26, No. 5, pp. 949-1043, 1991

[30] W. P. Dyke and J. K. Trolan, “The field emission initiated vacuum arc II: The resistively heated emitter”, Phy., Rev., Vol. 91, pp. 54-1057, 1953

[31] D. Alpert, D. A. Lee, E. M. Lyman and H. E. Tomaschke, “Initiation of electrical breakdown in ultrahigh vacuum”, J. Va. Sci and Techrol, Vol. 1, pp. 35-50, 1964

[32] Nevrovsky V. A, “Clump hypothesis and mechanisms of breakdown initiation in centimeter vacuum gaps”, XXIInd Int. Symp. on Discharges and Electrical Insulation in Vacuum, Vol. 1, pp. 45-47, 2006

[33] L. Cranberg, “The initiation of electric breakdown in vacuum”, J. Applied Phys., Vol. 23, pp. 516, 1952

[34] Gabriela Sandolache and Stephen William Rowe, “Vacuum breakdown between molten metal electrodes”, XXIInd Int. Symp. on Discharges and Electrical Insulation in Vacuum, Vol. 1, pp. 13-16, 2006

[35] H. Schellekens, M. B. Schulman, “Contact temperature and erosion in high current diffuse vacuum arcs on axial magnetic field contacts”, IEEE Trans. on Plasma Science, Vol. 29, No. 3, pp. 452-461, 2001

[36] S. W. Rowe, “Polarity effects in vacuum circuit breakers”, XIIth Int. Conf. on Gas Discharges and Their Applications, 1997

[37] D. Kopejtkova, H. P. Ott, H. Röhsler, F. Salamanca, J. J. Smit, A. Strand and P. Wester, “Strategy for condition based maintenance and updating of substations”, CIGRE 23-105, 1996

[38] C. Jones, “CIGRE working group 13.09- Monitoring and diagnostic technique for switching equipment”, IEEE/PES Transmission and Distribution Conference and Exposition, Vol. 2, pp. 1083-1087, 2001

[39] P. Wester and R. D Damstra, “The impact of a condition based maintenance strategy on network system operations”, CIGRE Session 2000, Paper No. P1-13, 2000.

[40] M. Okawa, T. Tsutsumi, and T. Aiyoshi, “Reliability and field experience of vacuum interrupter”, IEEE Trans. on Power Delivery, Vol. PWRD-2, No. 3, pp.799-804, 1987.

[41] W. F. H. Merck, G. C. Damstra, C. E. Bouwmeester and R. J. B. Gruntjes, “Methods for estimation of the vacuum status in vacuum circuit breakers”, IEEE Trans. on Dielectrics and Electrical Insulation, Vol. 6, No. 4, pp.400-404, 1999.

[42] John R. Lucek, Pittsfield, Mass and Willard J. Pearce, "Apparatus and method for measuring the pressure inside vacuum circuit interrupter", US-Patent No. 3263162, 26th July 1966.

[43] W. W. Watrous Jr.,"Methods and apparatus for measuring in vacuum circuit interrupter", US-Patent No. 3575656, 20th April 1971.

[44] Wilfried Kuhl and Klemens Wiehl, "Devices for measuring the internal pressure of vacuum interrupter", Siemens review XLV, No. 2, pp.87-89, 1978.

[45] Zhao Ziyu, Jiang Xiuchen, Jin Zhijian, Zou Jiyan and Shijing, "Study on internal pressure measurement of vacuum interrupter", 19th International Symposium on Discharge and Electrical Insulation in Vacuum-X'ian, pp.775-778, 2000.

[46] Patent publication bulletin 1-301136

[47] A. Ohta, Hiroaki Sano, Nobuaki Tamaki and Masayuki Sakaki, 'The development of detector that find leak of vacuum interrupter', HV-01-125, 2001

[48] Guan Yonggang, Xu Guozheng, Huang Yulong and Liu Weidong, "On-line monitoring the vacuum degree of vacuum interrupter by partial discharge", 12th Asian Conference on Electrical Discharge, Shenzhen, China, pp.195-197, Nov. 19-22, 2004

[49] M. Kamarol, S. Ohtsuka, H. Saitoh, M. Sakaki and M. Hikita, "Discharge phenomena in low vacuum region of glass tube vacuum interrupter under ac applied voltage", International Symposium on Electrical Insulating Material (ISEIM), pp.36-39, 2005.

[50] D. L. Schweickart, D. F. Grosjean, D. G. Kasten, X. Liu, and A. Sebo, "Partial discharge measurement at low pressures with and without a dielectric barrier", Annual Report on Electrical Insulation and Dielectric Phenomena, pp.462-465, 2004.

[51] Sergey V. Sydorenkov, Andrey S. Baturin, Eugeny P. Sheshin, "Field emission method of pressure dynamics registration in vacuum interrupters", 20th International Symposium on Discharge and Electrical Insulation in Vacuum-France, pp.568-571, 2002.

[52] G.. C. Damstra, W.F.H Merck, P.J Bos and C.E Bouwmeester, "Diagnostic methods for vacuum state estimation", 18th International Symposium on Discharge and Electrical Insulation in Vacuum-Eindhoven, pp.443-446, 1998.

[53] Susan Solomon, James B. Burkholder, A. R. Ravishankara and Rolando R. Garcia, "Ozone depletion and global warming potentials of CF_3I", Journal of Geophysical Research, Vol. 99, No. D10, pp.20,929-20,936, 1994.

[54] D. E. Dodd, H.F. Leahy, M.L. Feldmann, J.H. English, A. Vinegar, "Reproductive

toxicity screen of trifluoroiodomethane (CF_3I) in sprague-dawley rats ", Inhalation Toxicology, Vol. 11, Issue 11, pp.1041-1055, 1999

[55] Nozomi Nakayama, Elizabeth E. Ferrenz, Denise R. Ostling, Andrea S. Nichols, Janelle F. Faulk and Christopher R. Arumainayagam, "Surface chemistry and radiation chemistry of trifluoroiodomethane (CF_3I) on Mo(110)", Journal of Phys. Chem. B, 108 (13), pp.4080-4085, 2004.

[56] New Energy and Industrial Technology Development Organization (NEDO) report, "Feasibility study on application of SF_6 alternative gas (CF_3I) to the market of electric equipment for power transmission, transformation and substation system (FY2004) final report", 2005 (in Japanese).

[57] Hiroyuki Toyota, Shigeyasu Matsuoka and Kunihiko Hidaka, "Measurement of sparkover voltage and time lag characteristics in CF_3I-N_2 and CF_3I-Air gas mixtures by using steep-front square voltage", Journal of Electrical Engineering in Japan, Vol. 157, No. 2, pp.1-7, 2006

[58] Tadasu Takuma, Osamu Yamamoto and Shoji Hamada, "Gases as dielectric", Gaseous Dielectric X, pp.195-204, 2004

[59] Y. Y. Duan, M.S Zhu and L.Z. Han, "Experimental vapor pressure data and a vapor pressure equation for trifluoroiodomethane (CF_3I)", Fluid Phase Equilibria, Vol. 121, pp.227-234, 1996

[60] Yasunobu Yokomizu, Masato Suzuki and Toshiro Matsumura, "Thermodynamic, transport and radiation properties of high-temperature CF_3I and transient conductance of residual arc sustained in axial CF_3I flow", Transactions on Electrical and Electronic Engineering of Japan (IEEJ) , Vol. 1, No. 3, pp.268-275, 2006.

[61] Jason E. Sanabia, John H. Moore and John A. Tossell, "CF_3I on a silicon surface: Adsorption, temperature-programmed desorption, and electron-stimulated desorption", Journal of Chemical Physics, Vol. 116, No. 23, pp.10,402-10,410, 2002.

Chapter 2

Experimental Setup

2.1 Introduction

This chapter mainly describes the experimental setup used in this research study for vacuum interrupter (VI) and trifluoroiodomethane (CF_3I) gas. The constructions of partial discharge (PD) measuring systems related to VI and CF_3I were introduced and described in this chapter.

2.2 Experimental setup and apparatus for vacuum interrupter

2.2.1 Construction of partial discharge measurement systems

The closed contact condition is the basic practical situation of VI under normal operation while interrupted (open contact) one when over-current flows into the systems. Due to this reason, the closed contact condition of VI was implemented in this experiment. Fig. 2.1 shows the structure of VI [(1)]. It consists of insulating envelope, fixed and movable electrodes, an arc shield surrounding the electrodes, and a metal bellows to support the movable electrode. In practical, the pressure of VI is 10^{-6} Pa order. In this experiment, the pressures were variable. The pressures were set at 1 Pa to 1 kPa order to simulate the leakage. The VI was made from glass vessel to identify the location of PD occurrence easily and to have a better understanding of the optical properties as the pressure varies at constant applied voltage. The optical measurement may give accurate information because it has a high sensitivity and cannot be influenced by the external circuit.

Fig. 2.2 depicts the equivalent circuit for the closed contact condition used in the measurement of PD that simulates an actual configuration condition in cubicle-gas insulated switchgear (C-GIS). Fig. 2.3 shows the photograph of the experimental setup. A capacitance C_1 was connected to the high voltage side of a transformer in parallel with VI. C_1 has a value of 3000 pF to demonstrate the capacitance of an actual cable used in the field where cable length was 15 m. Note, that the cable has a capacitance of

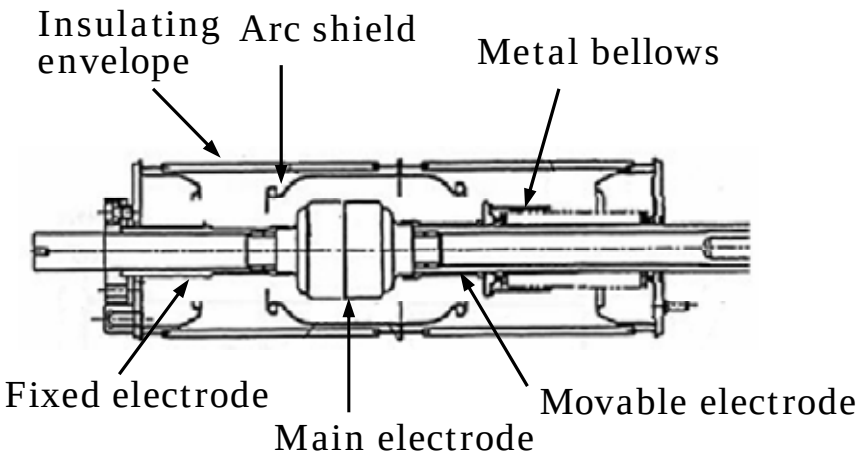

Fig. 2.1 Structure of vacuum interrupter [1].

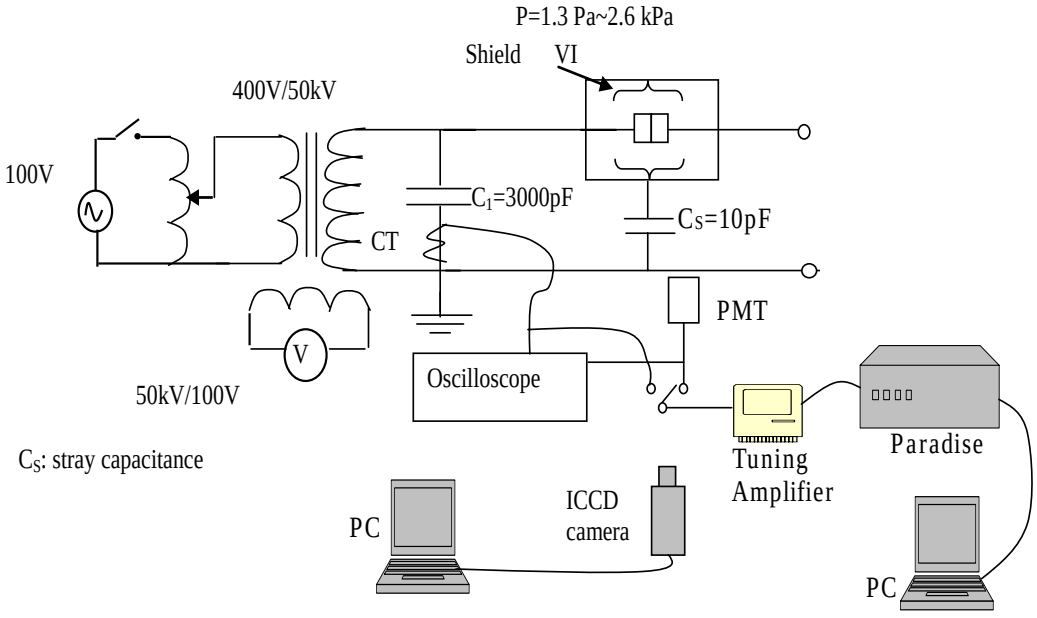

Fig. 2.2 Equivalent circuit diagram of experimental setup.

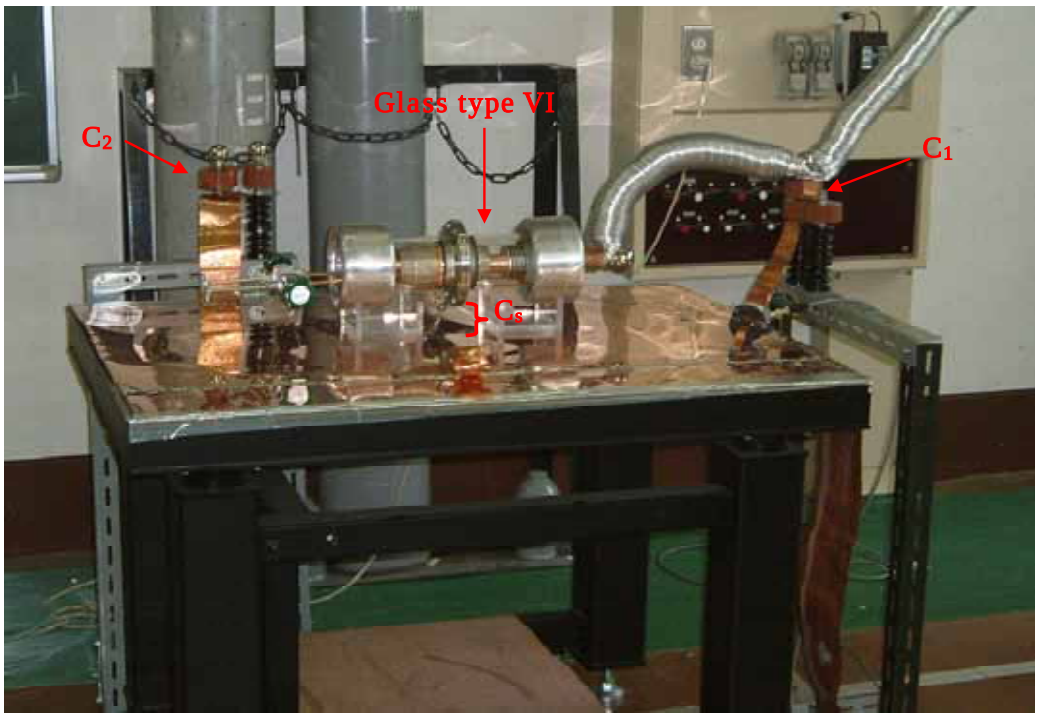

Fig. 2.3 Photograph of experimental setup for VI

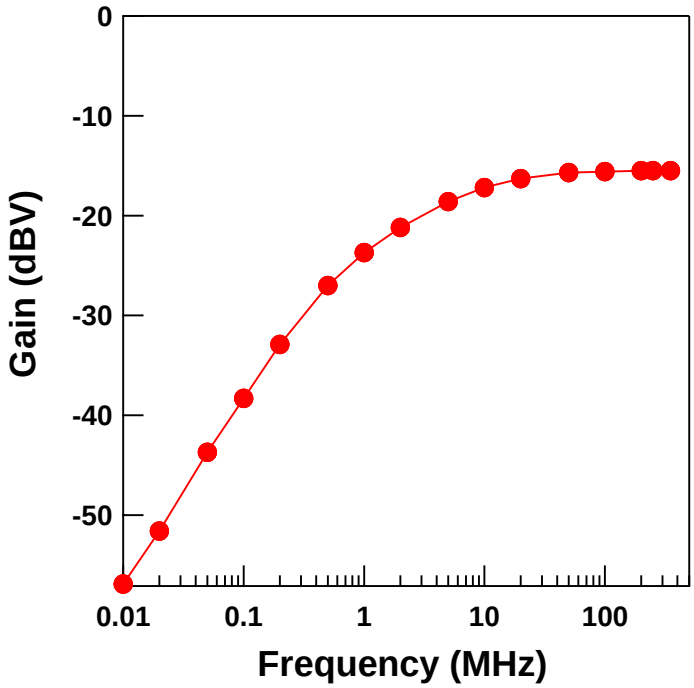

Fig. 2.4 Frequency response of CT

0.2μF/km. C_S is the stray capacitance between the shield and the tank wall of actual C-GIS. The value of the C_S was estimated to be around 10 pF. The distance between the ground plate and shield is fixed at 27 mm in order to maintain the value of C_S. The gap distance was obtained at the value of 10 pF with the electric field calculation. The experiment was performed under an AC applied voltage. A transformer of 400 V/50 kV with 75 kVA capacity was used as the power source and the applied voltage was measured at the third winding of the transformer.

The measurement of PD occurring inside VI was performed with a current transformer (CT), intensified charge coupled device (ICCD) camera and photomultiplier tube (PMT). The frequency response of the CT covering from 10 kHz to 250 MHz was clamped at the bottom side of C_1. The CT was found to have a flat frequency response from 3 MHz to 250 MHz as shown in Fig. 2.4. The output of CT was connected to an oscilloscope (LeCroy 9362, 1.5 GHz) to measure PD current occurring inside VI. The light emission of PD was measured with an ICCD camera (Hamamatsu model C5909). The ICCD camera with a UV filter from 240 to 370 nm of the spectrum range was fixed 1.5 m from VI. The PMT having a spectrum range from 300 to 850 nm was located 11 cm from VI at the movable electrode side near the bellows to measure the light intensity of PD.

The ϕ-q-n pattern of PD occurring in the low vacuum region of VI was measured using a partial discharge measurement device (PARADISE: Shoei Electronics). The output of the CT and PMT were connected to a tuning amplifier. Then the output of the tuning amplifier was processed into digital data using PARADISE and a computer.

2.2.2 Vacuum evacuation system

The internal pressure and the type of gas in glass vessel of VI can be fixed according to the research requirement. The pressures and the type of residual gas inside the VI can be decided by pumping out the gas inside the VI and replaced with the selected gas at low vacuum region. The process of pumping out gas to low vacuum region is called vacuum evacuation. The level of the internal pressure of VI can be monitored with a suitable vacuum gauge. This section would describe the construction of vacuum evacuation system.

2.2.2.1 Vacuum evacuation setup

Fig. 2.5 shows the schematic diagram of vacuum evacuation system. The VI has two valve terminals indicated as V_{TA} and V_{TB}. The terminal valve V_{TA} is connected to an ULVAC ceramic capacitance manometer gauge (model CCMH-100A) with the controller (model GM-1000) and ionization vacuum gauge (model GI-TL3) to monitor

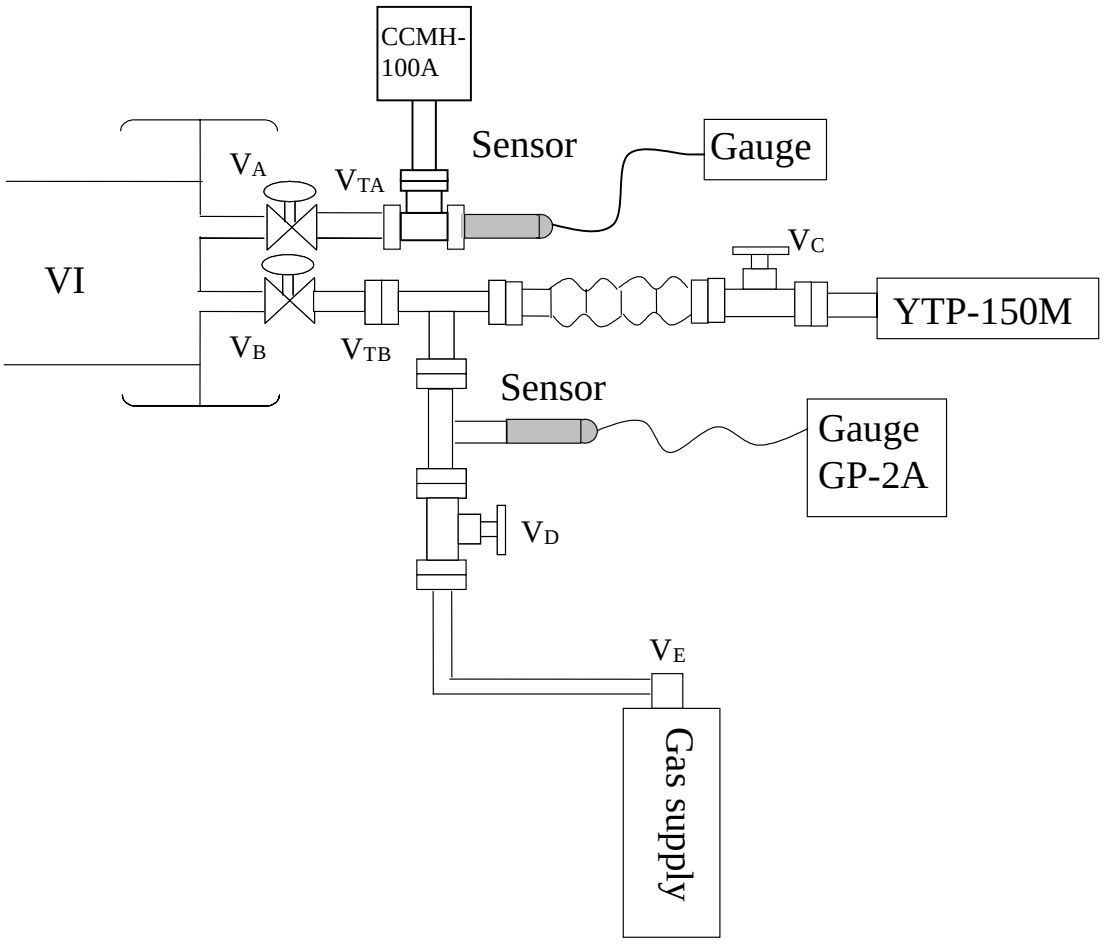

Fig. 2.5 Schematic diagram of vacuum evacuation system

the internal pressure of VI. The ceramic capacitance manometer and the vacuum ionization gauge were fixed to measure the pressure from 1.3 Pa to 13 kPa order and 10^{-5} Pa to 1 Pa order, respectively. The terminal V_{TB} is connected to turbo-molecular pump evacuation unit (model ULVAC: YTP-150M) and gas supply. The YTP-150M consists of rotary vacuum pump (model ULVAC: GVD-100A), turbo molecular pump (model ULVAC: UTM-150) and pirani gauge (model ULVAC: GP-1S). The turbo-molecular pump evacuation unit is able to pump out the gas from VI to high vacuum. Valves V_C and V_D were fixed at the same conduit of YTP pump and gas supply, respectively, for opening and closing purpose. To observe the internal pressure of the vacuum conduit system, a pirani gauge (model ULVAC: GP-2A) was installed between the YTP pump and the gas supply system.

2.2.2.2 Operating system of vacuum evacuation

Valve V_A, V_B, V_C, V_D and V_E was inherently kept at closed position. Switch on the YTP vacuum pump and turn all valves except V_E to open position. The internal pressure of the conducting must be ensured achieving 10 Pa with vacuum gauge (GP-2A and GP-1S) before switch on the YTP turbo molecular pump. At this pressure it is considered that no more foreign particle exists inside the conduit and the specimen. This is for avoiding the blade of turbo molecular from damage due to foreign particle during high speed spinning. When the pressure achieve at low region below than 1 Pa, turn valve V_C and V_D to close position and switch off the turbo molecular pump. Note the normal vacuum pump should be remained operating. Then turn valve V_E to open position and turn the needle valve V_D slowly to supply gas until the pressure inside the VI achieving the require pressure level. When the internal pressure of VI was determined, turn valve V_A, V_B and V_E to close position. Then turn valve V_C to open position to evacuate gas remaining inside the conduit. Then turn valve V_C to close position and switch off the YTP vacuum pump. Finally, the vacuum evacuation system will be disconnected from the terminal V_{TA} and V_{TB} to avoid from sparkover when high voltage is applied to VI. Fig. 2.6 depicts the flowchart of the vacuum evacuation operation for better understanding.

2.3 Experimental setup and apparatus for CF_3I gas study

Construction of system was performed to measure partial discharge inception voltage (PDIV), sparkover voltage (V_s), all PD charge quantity with cumulative charge q_c and to analyze gaseous by-products of CF_3I suffering PD. The system enables to obtain the Vs and PDIV characteristics. It also enables to determine quantitative relation between q_c and the amount of the by-product of CF_3I suffering PD.

2.3.1 Construction of partial discharge measurement systems

A transformer with a 400 V/50 kV and capacity of 75 kVA was used as AC power source. The simplified equivalent circuit of the experiment is shown in Fig. 2.7. A container of 450 cc made from acrylic was filled with pure CF_3I gas at a given pressure and placed into a chamber. The chamber was filled with SF_6 gas at 0.1 MPa to avoid PD or V_s occurring between the container and the chamber. Photograph of the 450 cc container and the chamber are shown in Fig. 2.8. PD current pulse and the charge quantity q were measured with a long-memory oscilloscope (model Tektronix TDS 7154 DPO) and specially designed PD measuring device (a high speed A/D converter-PARADISE). The oscilloscope has a capability to measure the PD current pulses of real-time sampling rate up to 20 GS/s for frequency up to 1.5 GHz. The PD signal was detected with an impedance matching circuit (IMC) via a tuning amplifier

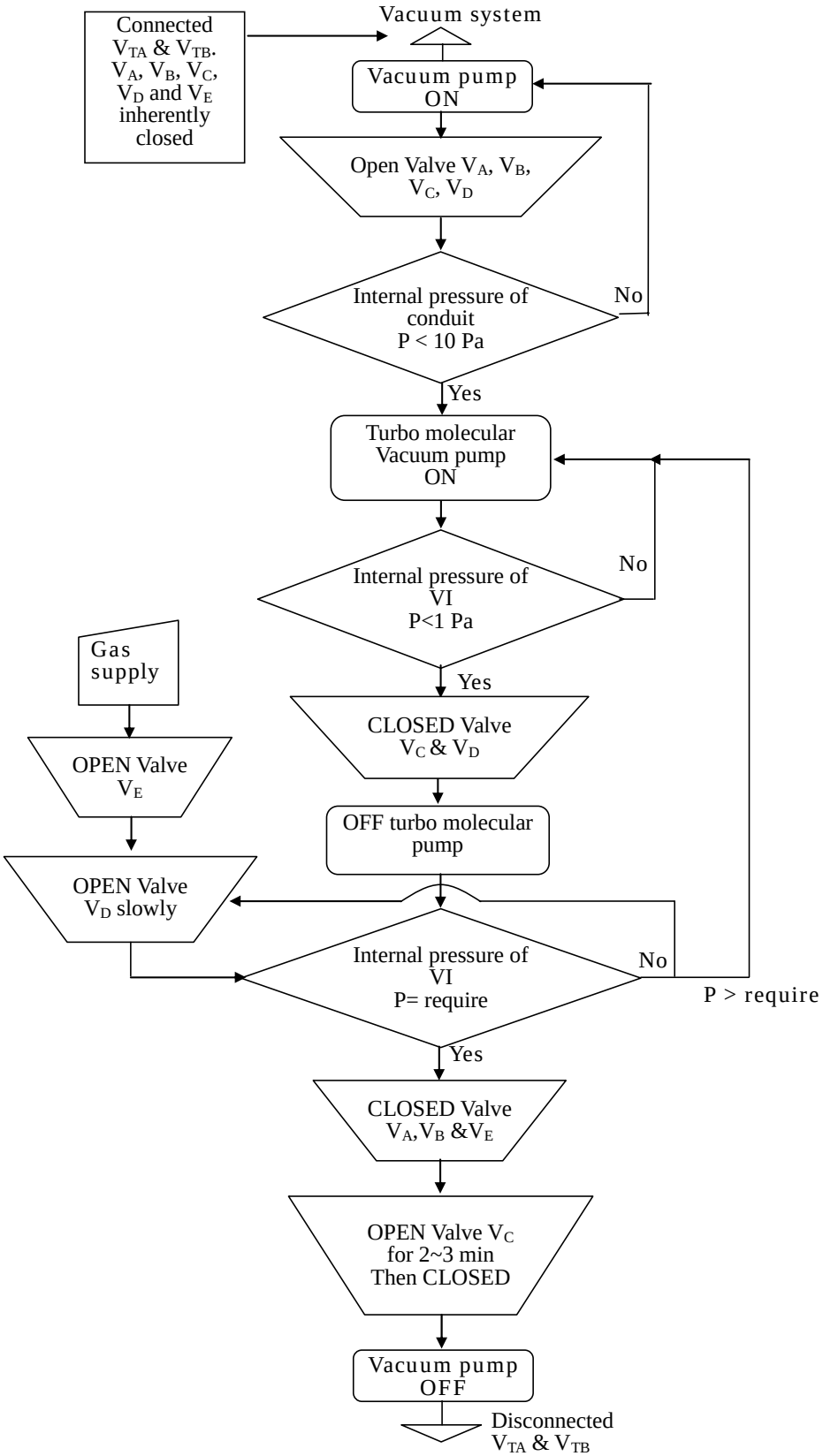

Fig. 2.6 Flowchart of vacuum evacuation system operation

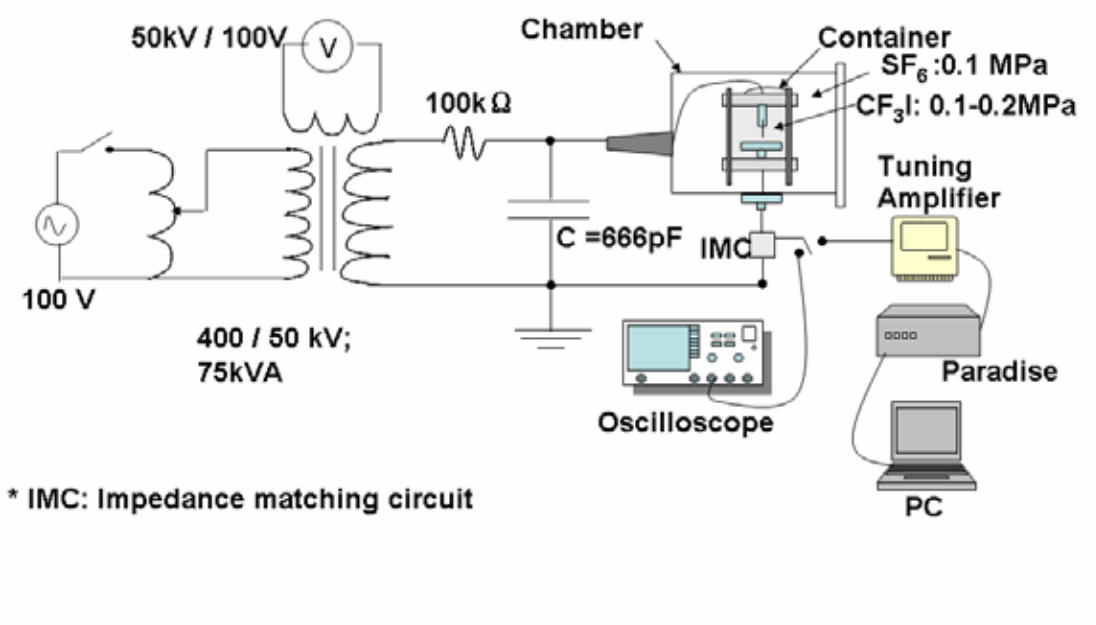

Fig. 2.7 Equivalent circuit of experimental setup

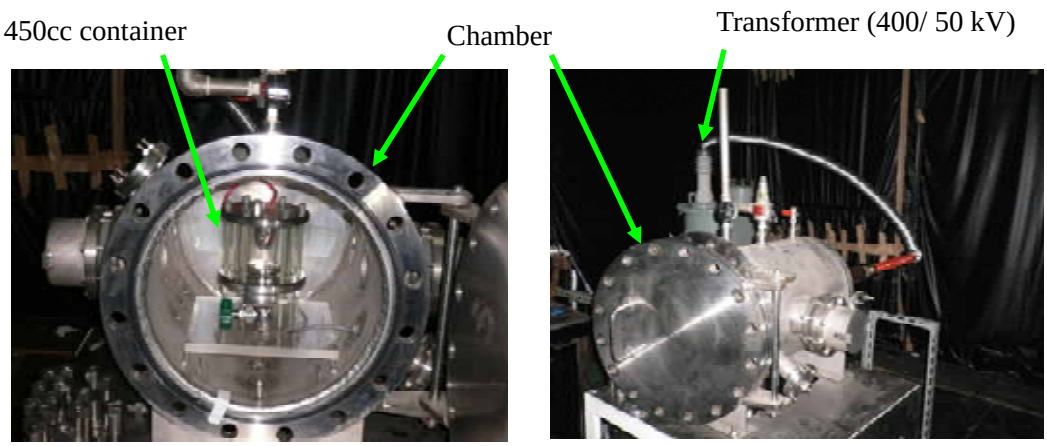

Fig. 2.8 Photograph of experimental setup consisting 450cc container and chamber

which enables to detect a high frequency signal up to 400 MHz. The V_s and PDIV characteristics inside CF_3I was measured with IMC to a long-memory oscilloscope (model Tektronix TDS 7154 DPO).

2.3.2 Electrode configuration

To analyze the gas by-product of CF_3I suffering PD for a given time under non-uniform electric field, an ideal electrode configuration producing maximum PD was obtained. The needle-plane electrode system consisted of the needle electrode in hemispherical shape with radius tip of 0.5mm and gap of 10mm. The electrode gave an optimum cumulative charge of PD occurrence in CF_3I. The plane electrode with a diameter of 68mm was connected to the ground. The field utilization factor, average strength of electric field divided by maximal strength of electric field, was 0.06.

2.3.3 Gas evacuation and filling system

Fix the container of 450cc at the gas evacuation conduit. Valve V_1, V_2, V_3, V_4, V_5 and V_6 were inherently kept at closed position. Switch on an oil rotary vacuum pump and turn valve V_1, V_2 and V_4 at open position to evacuate all gas inside the container. The evacuation process would take for at least 2.5 hours and above to ensure all water vapor existing in the container and conduit has been totally evacuated. Then close valve

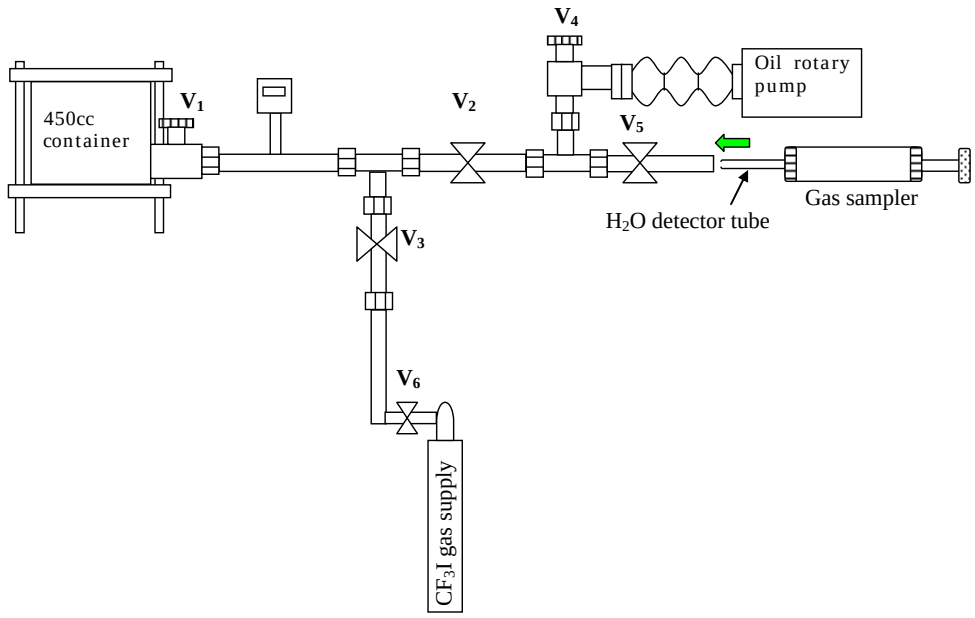

Fig. 2.9 CF_3I gas evacuation and filling system

V_2 and V_3. Turn valve V_6 to open position and slowly open needle valve V_3 to supply CF_3I gas into the container. When the required gas pressure was determined, valve V_3 and V_1 were closed. Then valve V_2 was opened to evacuate all CF_3I gas remaining inside the conduit. After the remained gas was evacuated, the water content measurement was made.

Water content confirmation can be measured with a H_2O detector tube with the gas sampler. The H_2O detector tube was fixed at the terminal near valve V_5. When the detector was fixed, valve V_5 can be turned to open position to evacuate all water vapor existing inside the conduit near valve V_5 for 2~3 min. Then close valve V_4. After V_4 has been closed, open valve V_1, and the knob of gas sampler syringe (Gastec No.6L) should be pull out to let CF_3I gas go from the container through the H_2O detector to measure the water content. Fig. 2.9 shows the schematic diagram of CF_3I gas evacuation and filling system.

2.3.4 Gaseous decomposition analysis system

Gaseous by-products formed after PD test was analyzed with a gas chromatography (GC-Agilent 6890N) and mass spectroscopy detector (MSD-Agilent 5975B). The GC consists of capillary column with 27m in length and 0.32mm of internal diameter. The analyzed gas by-products of CF_3I suffering PD was transported and separated by carrier gas of helium flowing at the rate of 3mℓ/min. The output gas of GC will be deposited into MSD ion source with interface temperature of 200℃ to analyze the gas decomposition. The scanning range of the MSD is m/z 35~300, where m and z represent mass number and charge number, respectively. Figs. 2.10 and 2.11 show the schematic diagram of GC-MSD systems with the draft chamber and the photograph of GC-MSD with the draft chamber, respectively. The draft chamber was utilized to dispel all gases released from the GC-MSD analysis to the outsider through the scrubber (filter) fixed at the top of draft chamber for safety purpose. The process of collecting the gas by-products of CF_3I for analysis was done manually by a syringe initially at the draft chamber and finally by injecting into the entrance of GC device. Only 0.5 ml of gas by-products is required for the analysis. The analysis would take for 40 minute and the result is printed automatically.

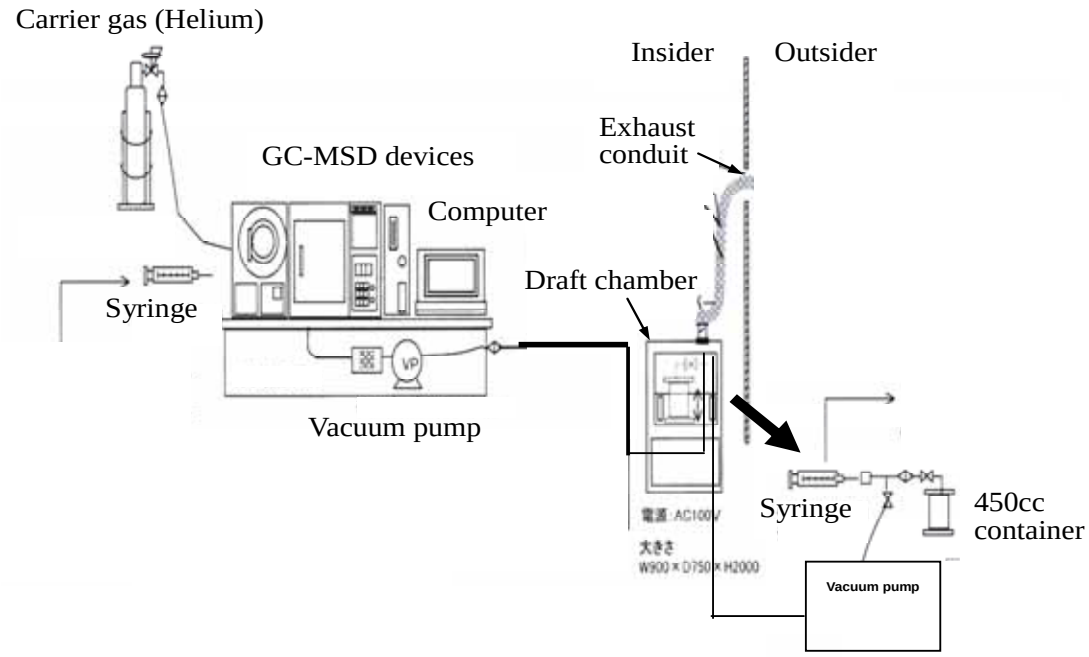

Fig. 2.10 Schematic diagram of GC-MSD systems with the draft chamber

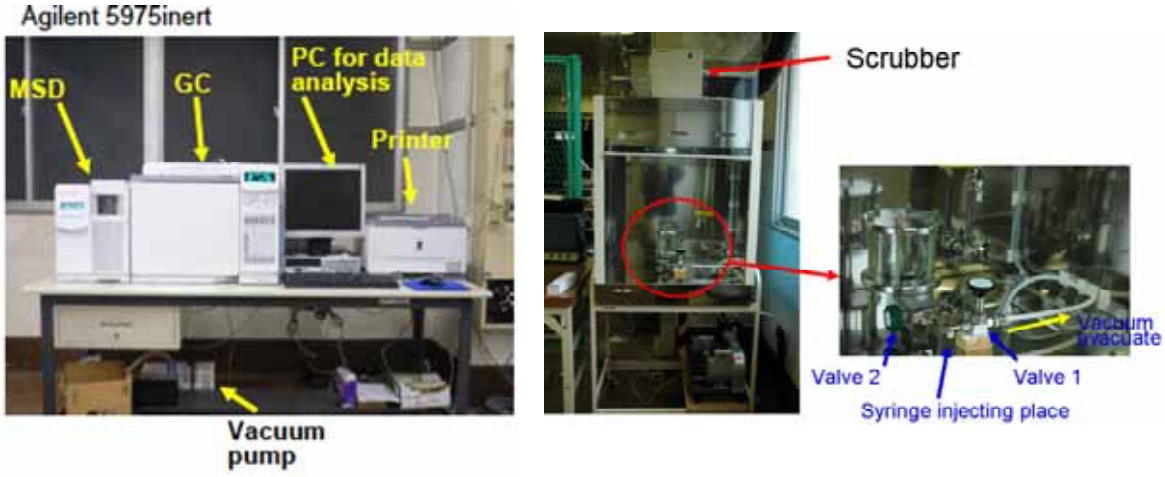

Fig. 2.11 Photograph of GC-MSD devices and draft chamber

Reference

[1] Mohamad Kamarol, “Fundamental study on diagnosis technique of environmental friendly type next generation switchgear for electric power distribution”, Master Thesis, pp. 30, 2005.

Chapter 3

Discharge Properties and Emitted Electromagnetic Wave Spectrum in Low Vacuum Region of Vacuum Interrupter

3.1 Introduction

Many types of ac circuit breaker (CB) have been used widely such as oil circuit breaker (OCB), air circuit breaker (ACB), gas circuit breaker (GCB), vacuum circuit breaker (VCB) and magnetic circuit breaker (MCB). Each type of CBs has their own rated voltage. One of the circuit breaker we are focusing now is VCB. A VCB of 168kV rated voltage has been reported to be in service since 1979 [(1)]. VCB has an alternative to contribute to reduction of usage of SF_6 gas insulated devices in future. One of the examples of VCB used in environmental friendly switchgear is cubicle-type gas insulated switchgear (C-GIS) where VCB is surrounded by SF_6 gas.

VCB consists of a vacuum interrupter (VI) and mechanical part. VI is structured by cylindrical shape called insulating envelop filled with high vacuum at the order of 10^{-8} ~ 10^{-7} Torr. VI consists of a fixed and a movable electrode, an arc shield surrounding the main electrode, and metal bellows to support the movable electrode. An example of the VI structure is shown in Fig. 3.1.

VCB is widely used in electric power distribution. Therefore the performance of VI should be maintained in order to have a stable and reliable electric power transmission and distribution. Most of causes leading to low performance of VI are gas permeation, gas evolution or slow leak of vacuum [(2)]. When the slow leak occurs, the surrounding gases or air may invade the VI and increase the internal pressure. The level of vacuum will deteriorate and the insulation performance will decrease. As a result partial discharges (PD) will take place and late action might lead to breakdown of VI. Therefore early detection of the slow leakage is essential for preventing breakdown, and for maintenance and labor cost saving.

Study to enhance reliability of VI such as detection method of the slow leak has been extensively carried out [(2)], while study on discharge properties in low vacuum of VI is still insufficient. In this chapter, a ceramic type VCB with 12 kV rated voltage similar to VCB applied in actual C-GIS was used. An electrical circuit was constructed

that simulates the actual condition of VCB used in C-GIS. Discharge properties inside VI were experimentally investigated at closed and open contacts of the main electrodes. Two VI with pressure level at 1 (133 Pa) and 5 Torr (665 Pa) each were used to simulate the leakage of VI. EMW spectrum emitted by discharge in low vacuum of VI was also studied.

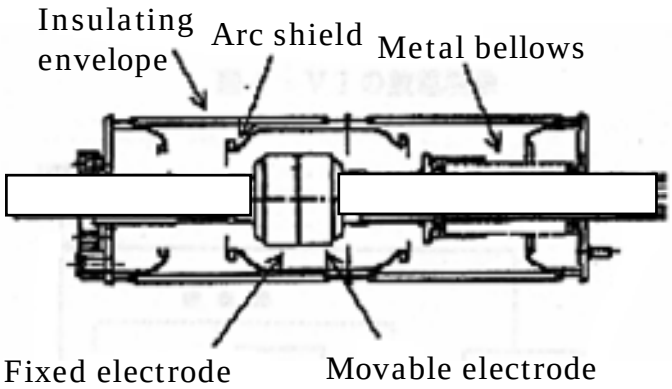

Fig. 3.1 Structure of vacuum interrupter

3.1.1 Diagnosis Technique of Vacuum Interrupter

One of the methods to measure the internal pressure of VI is magnetron method. This method was developed by J.R. Lucek et al [3] and W. W. Watrous jr et al [4]. Thereafter, similar measuring methods were developed by Wilfried Kuhl et al [5] and M. Okawa et al [2]. These traditional methods cannot be measured on-line; the VCB must be detached and set into a solenoid coil to measure vacuum level.

Later, Zhao Ziyu et al [6] developed an on-line pressure detection of VI by using a magnetron method with a Pockels electric fields sensor. In this method, Pockels sensor needs to be attached at the middle of VI envelope at the place where the shield is allocated. To connect the sensor to the monitoring system by an optical cable, a hole at the wall of the tank is required. Due to this reason, the possibility of vacuum leakage from a tank is high.

Therefore it is essential to have high sensitivity, reliable and good cost performance of detecting device that capable of detecting low performance of VI.

3.2 Experimental setup

Two equivalent circuits are used in measurement of discharges to simulate actual conditions used in C-GIS: closed and open contact condition of the main electrodes. Figures 3.2 (a) and (b) show the equivalent circuits for closed and open contacts of the main electrodes.

A capacitance C_1 is connected to the high voltage side of transformer in parallel with VI for both closed and open contact conditions. C_1 has value of 3000pF to simulate the capacitance of an actual cable used in the field which has 0.2μF/km. Therefore the cable length is 15m. C_s is a stray capacitance between the shield and the tank wall used in actual C-GIS. The value of C_s is estimated around 10pF. In order to keep the value of C_s, a grounded metal plate is fixed vertically parallel to the VI at intervals of 27mm. The gap distance was calculated by using an electric field software (Coulomb 3D electrostatic design software).

For open contact condition, a capacitance C_2 is connected at the load side to simulate an actual load in field. The value of C_2 is 3000pF to keep the potential of the load side nearly at 0 Volt for high frequency components of discharge. Furthermore this capacitance acts as a limiting impedance to suppress a leakage current flowing between the two electrodes when discharge occurs. For closed contact condition, C_2 is removed. The reason is that if the capacitance C_2 is connected to the load side of VI, the flow of discharge current would be divided and the value measured by a current transformer (CT) would fluctuate.

A CT, having frequency range from 10 kHz to 250 MHz, is clamped at the bottom side of C_1 for both closed and open contact conditions. The output of CT is connected to an oscilloscope (TDS 220, 100MHz, 1 GS/s) to measure current waveform of discharge occurring inside VI. In addition, a loop antenna with a frequency band from 10 kHz to 30 MHz is used to measure electromagnetic wave (EMW) spectrum emitted by discharge occurring inside VI. The loop antenna is fixed at intervals of 2m from VI and is connected to a spectrum analyzer (Advantest-R3162) with a 9 kHz to 8 GHz frequency band.

A transformer with 400V/50kV and 75kVA capacity is used as a power source and an applied voltage is measured at the third winding of the transformer.

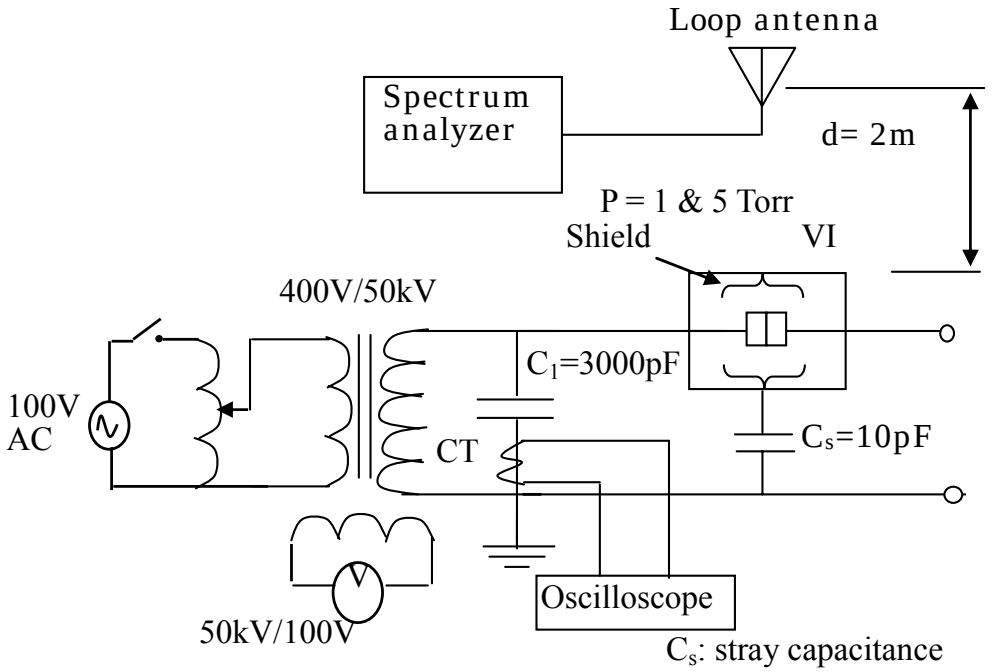

a) Closed contact condition

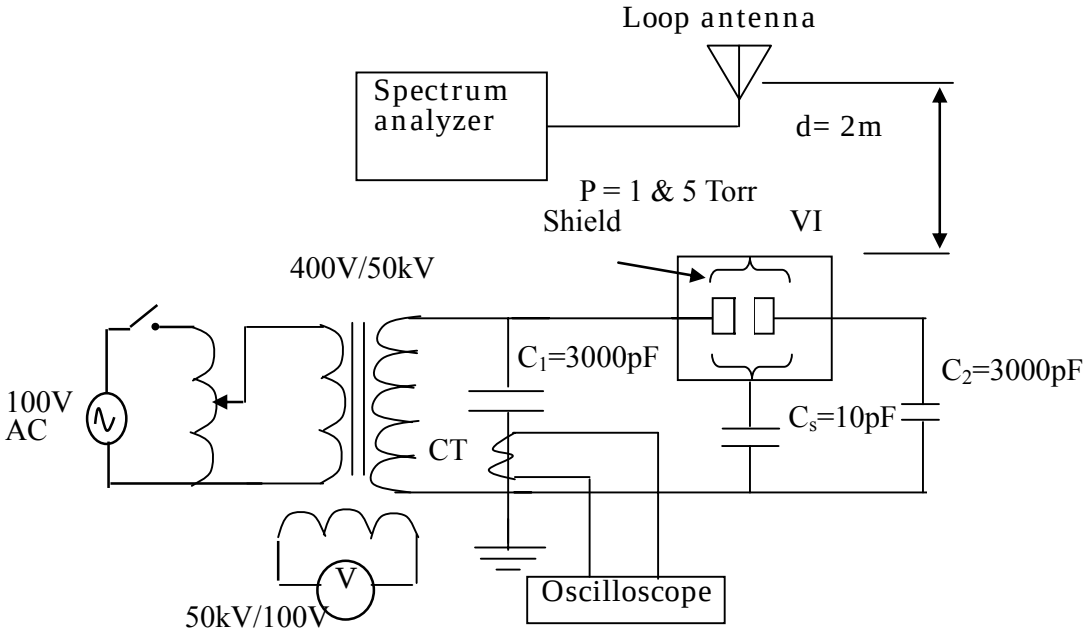

b) Open contact condition

Figs. 3.2: Equivalent circuit of discharge measurement for ceramic type VI

3.3 Experimental results and discussions

3.3.1 Discharges under closed contact condition

Fig. 3.3 shows the relationship between partial discharge inception voltage (PDIV) and the pressure at closed contact condition. The graph indicates that PDIV increases with increase of the pressure. PDIV at 1 Torr is lower than that at 5 Torr.

Figs. 3.4 (a) and (b) show typical current waveforms of discharge at 1 and 5 Torr during the PDIV measurement. The waveforms indicate that discharge current pulse at 5 Torr is much larger than that at 1 Torr. As can be seen in the current waveforms, the same pattern at both pressures indicates that the same discharge phenomena occur in the low vacuum of VI. At the same time we measured EMW spectrum emitted by the discharges during the PDIV measurement. Fig. 3.5 shows the EMW spectrum intensity emitted by discharges at 1 and 5 Torr. The spectrum intensity at 1 Torr is weaker than that at 5 Torr. This is attributed to the small magnitude of discharge current occurring in VI, as shown in Figs. 3.4. The results of measured spectra shown in Fig. 3.5 indicate that two peaks of spectrum intensity appear at f_l 6 MHz and f_h 24 MHz. The 6 MHz frequency components are attributed to LC resonance of the external circuit as seen in the current waveforms shown in Figs. 3.4 (a) and (b).

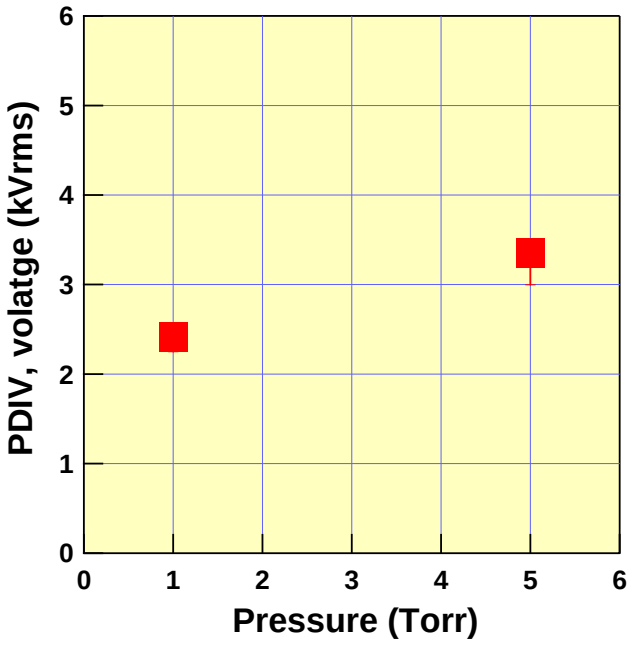

Fig. 3.3 PDIV against pressure at closed contact condition

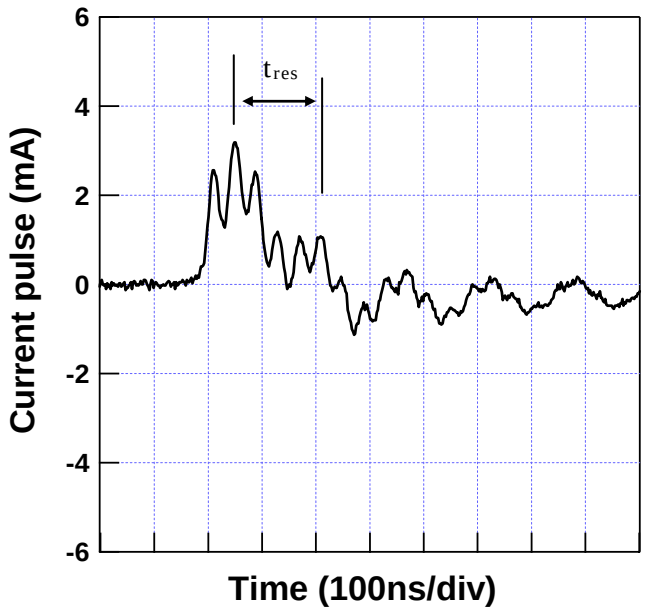

(a) Pressure = 1 Torr

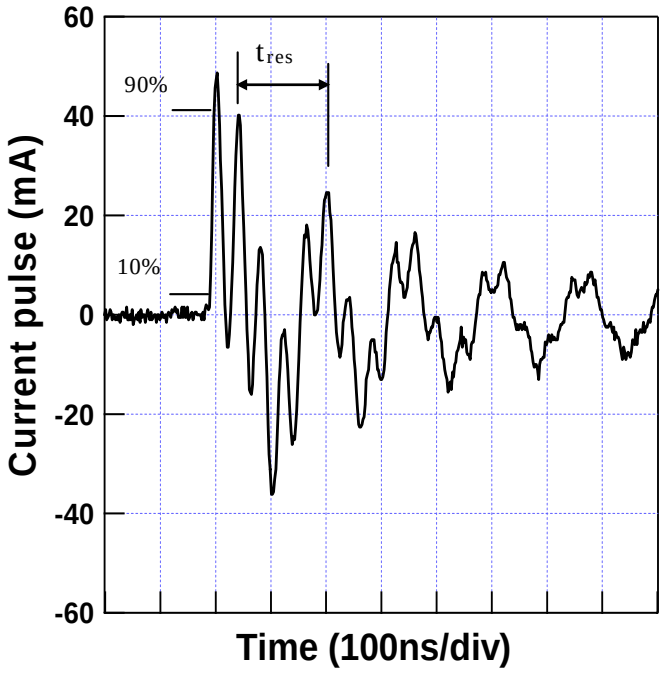

(b) Pressure= 5 Torr

Figs. 3.4 Typical current waveform measured with CT at PDIV for closed contact

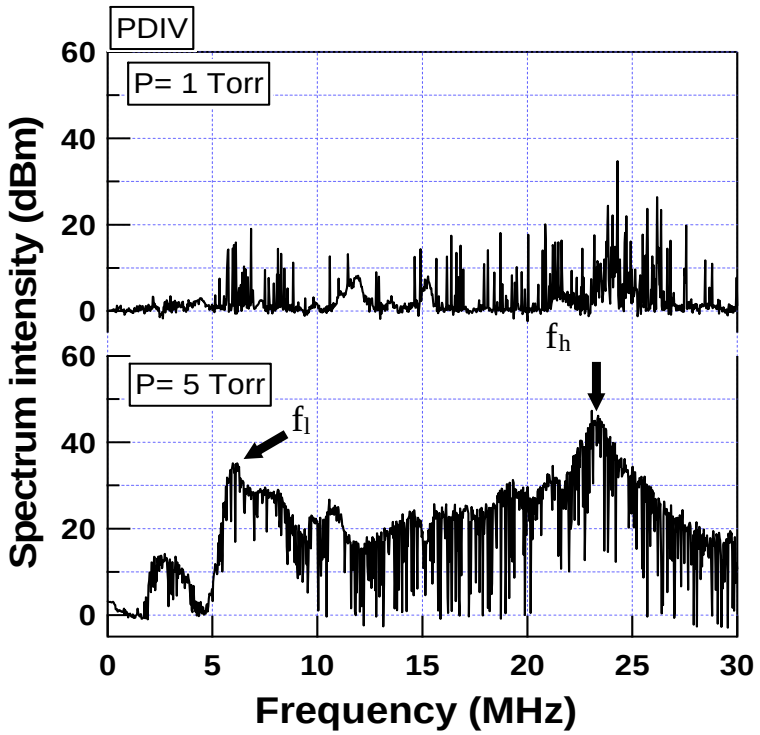

Fig. 3.5 EMW spectrum intensity measured by loop antenna at PDIV for closed contact condition

In the following let us give a reason of this consideration: The resonance frequency is determined by an inductance and capacitance of the circuit through which the discharge current flows. The inductance L, of a cable of length *l*, located at height *h* from a ground is expressed by the following equation.

$$L_0 = \frac{\mu_0}{2\pi} \ln \frac{2h}{r} \quad (H/m) \qquad (3.1)$$

where μ_0 is the permeability of free space, L_0 is the inductance per unit length of an aluminum hose with a radius r placed at height h (m) from the ground. In the present experiment, l = 1 m and r = 0.02 m so that L= L_0 l is estimated to be 0.25μH. Since the resonance frequency f_{res} is expressed as equation (3.2), f_{res} is estimated to be 6 MHz with capacitance of 3000pF. It should be noted that estimated f_{res} agrees well with f_l 6 MHz at which one of spectrum intensity peak appears.

$$f_{res} = \frac{1}{2\pi\sqrt{LC}} \qquad (3.2)$$

On the other hand, the 24 MHz frequency component is considered to arise from the nature of discharge itself occurring in VI. This consideration is supported by calculating a rise time t_r of discharge current pulse at 10% to 90% values of the magnitude of the current pulse as shown in Fig. 3.4 (b) by using the following equation

$$f_h = 0.35 / t_r \tag{3.3}$$

Namely, t_r=14.4 ns of the waveform in Fig. 3.4 (b) gives f_h 24.3 MHz which gives rise to the 24 MHz frequency component of the spectrum intensity.

Further investigation to verify the relationship between the frequency component of discharges and the applied voltage Va was carried out by increasing Va at 5, 10 and 15 kVrms. The results of the discharge current and spectrum intensity against applied voltage are shown in Figs. 3.6 and 3.7, respectively. It is obvious in Fig. 3.6 that the current intensity increases with increasing the applied voltage up to 5 kVrms, and then abruptly decreases as Va increases further up to 15 kVrms. The same situations also happen at about 24 MHz frequency band of peak intensity of EMW spectrum as shown in Fig. 3.7. This phenomena can be explained by results of phase angle dependence of discharge pulses accumulated in 15 cycles of different ac applied voltages as shown in Figs. 3.8. It is found from Fig. 3.8 (a) that discharge pulses start to occur in negative half cycle of the applied voltage at PDIV. It is also found from the other figures in Figs. 3.8 that as the magnitude of ac voltage increases, the phase angle where discharge pulses occur shifts to earlier phase (i.e to the left direction in the phase angle region), acrossing the zero phase angle. Note that the peak current of discharge pulses shown in Figs. 3.8 correspond to those shown in Fig. 3.6 at 5 Torr.

Although at the present situation it is a little bit difficult to identify where the discharge occur under the closed contact condition, the following consideration can be done from the phase dependence of the discharges shown in Fig. 3.8. At PDIV, discharges start to occur between the edge of the shield and the main electrode. Above 5 to 15 kVrms the phase where negative PD pulses occur in the positive half cycle indicates the possibility that surface discharges might occur on the ceramic wall insulator surrounding the shield electrode. These considerations have to be confirmed by observing light emission inside a vacuum interrupter using a transparent glass wall insulator. This will be performed and discussed in chapter 4.

In additions Fig. 3.9 shows results of f_h against the applied voltage measured with CT, antenna and calculated from the measured discharge waveform. The result indicates that the frequency f_h obtained from the calculation gives a good agreement to the measured ones. The frequency band 24 MHz remains constant even though Va is increased.

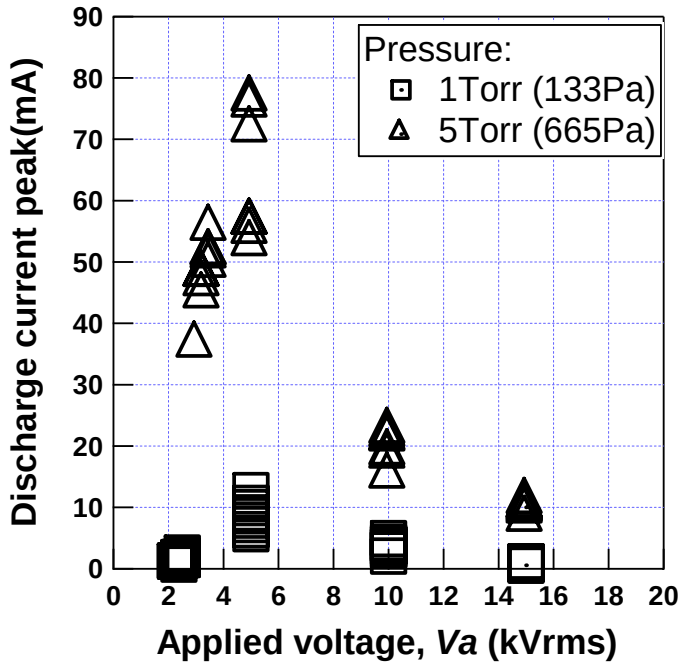

Fig. 3.6 Discharge current intensity against applied voltage for closed contact condition

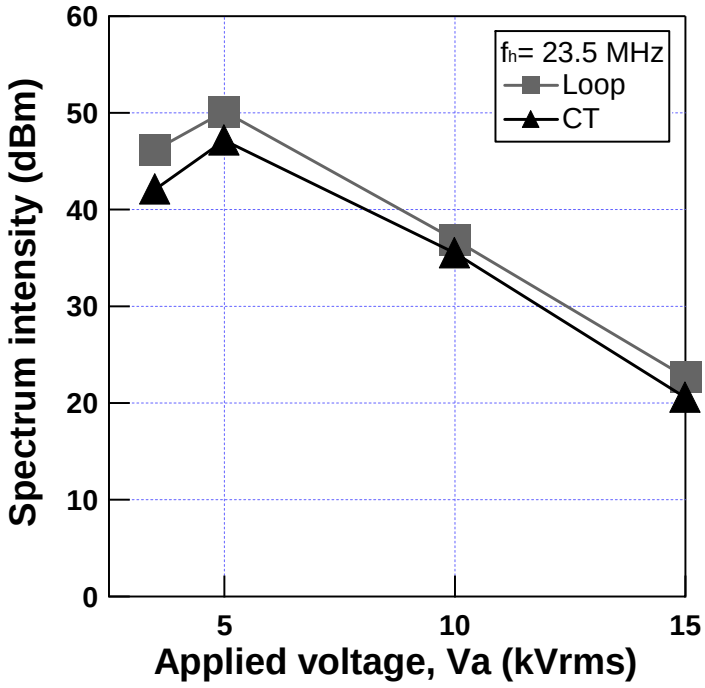

Fig. 3.7 EMW spectrum intensity against applied voltage measured by CT and loop antenna at 23.5 MHz for closed contact condition (p= 5 Torr)

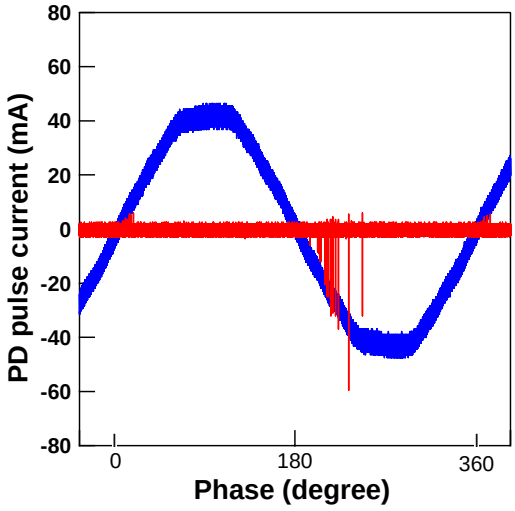

a) Va = 3.5 kVrms (PDIV)

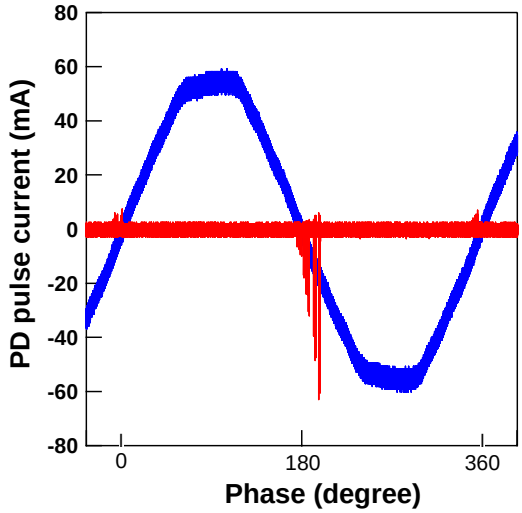

b) Va = 5 kVrms

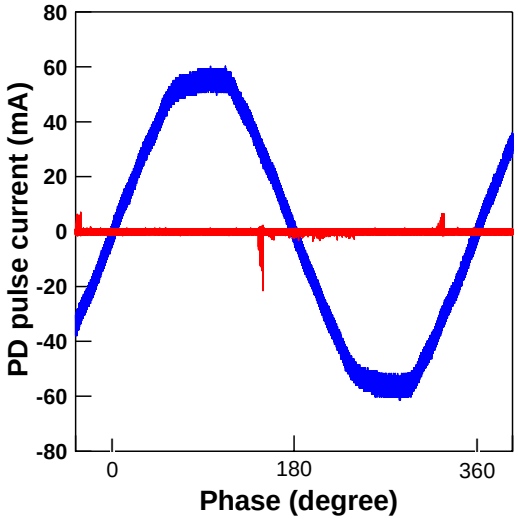

c) Va = 10 kVrms

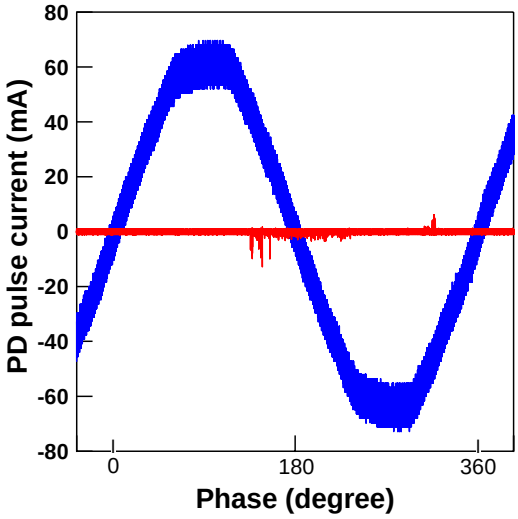

d) Va = 15 kVrms

Figs. 3.8 Phase angle dependence of discharge pulses accumulated for 15 cycles of different ac applied voltages at pressure 5 Torr under closed contact condition

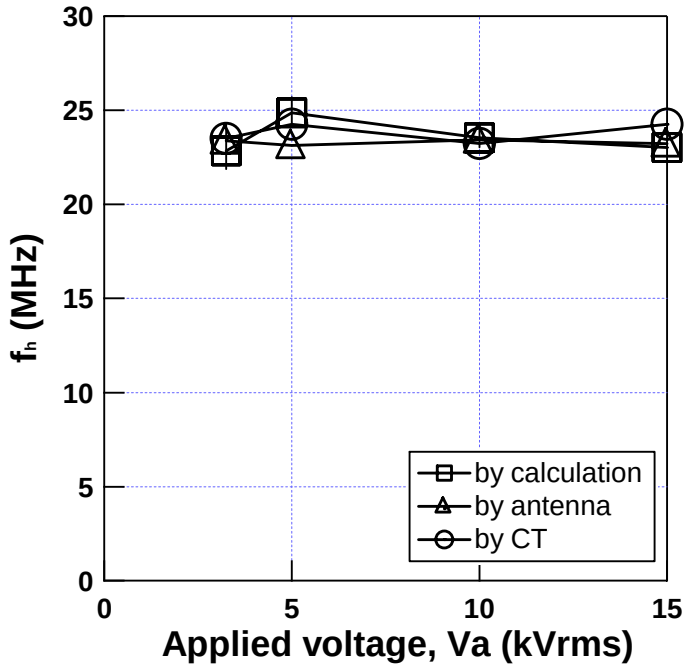

Fig. 3.9 f_h against applied voltage for closed contact condition at 5 Torr

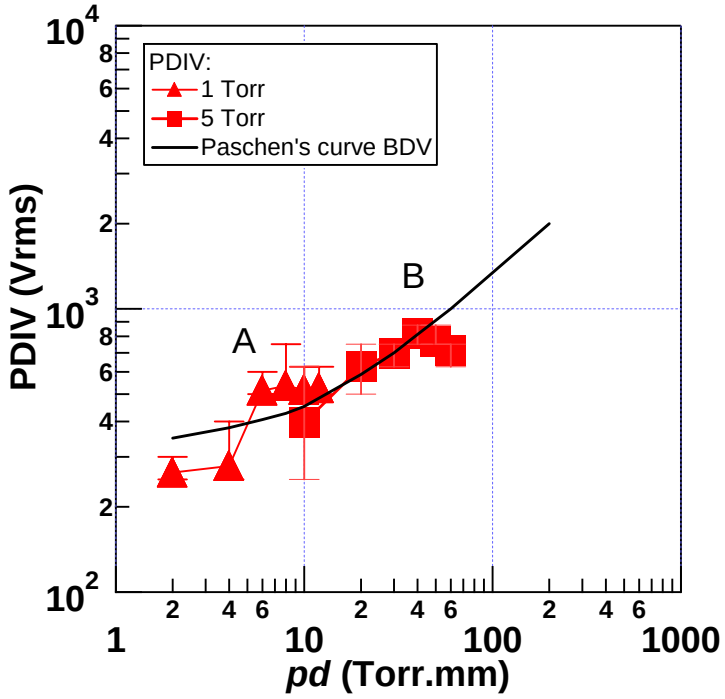

Fig. 3.10 PDIV against product of pressure spacing, pd at open contact condition

3.3.2 Discharges under open contact condition

Fig. 3.10 shows the relationship between PDIV and the product of the pressure and the gap distance (pd). The graph indicates that PDIV increases with increasing of pd. The result gives a good agreement with Paschen's curve of breakdown voltage of air in uniform field [7].

Figs. 3.11 (a) and (b) show typical discharge waveforms occurring at low vacuum of VI as a product of pd increases. The discharge current waveforms for pd ≤ 20 Torr·mm and pd ≥ 20 Torr·mm shown in Fig. 3.11 (a) and (b) represent region A and B, respectively. It is clear that different patterns of the current waveforms between region A and B are observed. The results indicate that different discharge phenomena would occur inside VI. Fig. 3.12 shows a plot of the current peak against inter-electrode distance d at E/p equal to 7kV/Torr·cm. The gap distance dependence of the discharge current in region 'A 'seems to obey an exponential growth with the gap length. So we try to estimate the ionization coefficient α by assuming Townsend criterion where the current of ln I is proportional to the effective primary ionization coefficient, α. The Townsend criterion can be expressed as follows

$$I = I_0 e^{\alpha d} \qquad (3.4)$$

.

where I_0 is constant. From Fig. 3.12 and the above equation, α is estimated to be 5.14/cm, which gives a good agreement with α of air obtained experimentally in reference [8]. Thus, the discharge criteria supports the consideration of discharge occurring between the fixed and the movable electrode since the current intensity increases in exponential manner with increasing pd up to 20 Torr・mm. Accordingly, a probable discharge current path is illustrated as I in Fig. 3.13.

The current peak in region B decreases abruptly to 30 ~ 50 mA as pd increases from 20 to 60 Torr・mm. Based on the current waveforms shown in Fig. 3.11 (b), we can say that the discharge occurs between the electrode and the shield, since the current intensity in this region is almost the same irrespective of pd; the distance between the shield and electrode is fixed while the gap length between the contact electrodes varies. Thus it is considered that the discharge current flows through the path II illustrated in Fig. 3.13.

Fig. 3.14 shows EMW spectra measured at PDIV for open contact condition for different gap distances. Several peaks of the spectrum intensity appear at more than one frequency band. In order to verify the frequency band of discharges, we have calculated the rise time t_r of discharge current pulse of Figs. 3.11 (a) and (b) by using equation

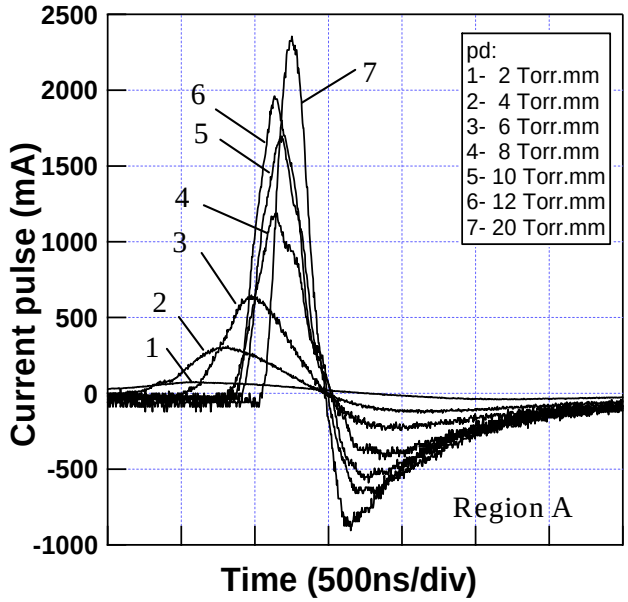

(a) pd ≦ 20 Torr・mm

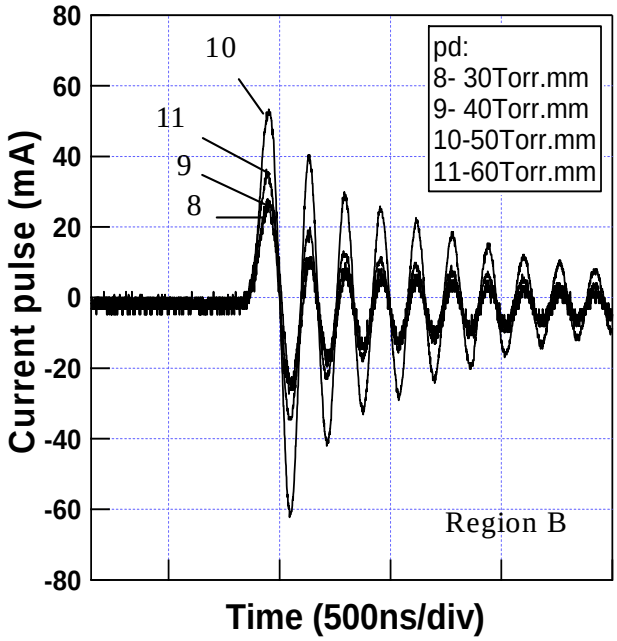

(b) 20 Torr・mm ≦ pd ≦ 100 Torr・mm

Fig. 3.11 PDIV current waveform measured by CT for open contact condition

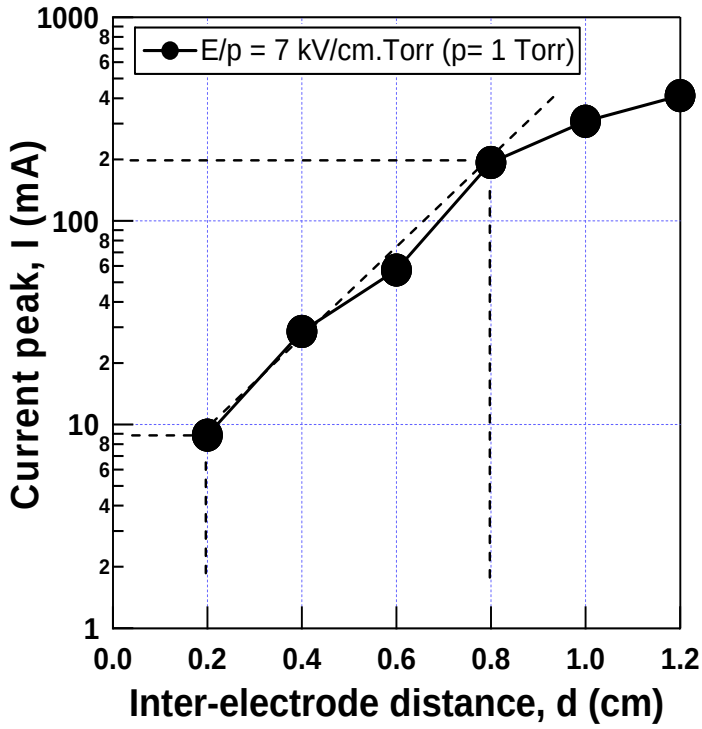

Fig. 3.12 PDIV current intensity against pd product for open contact condition

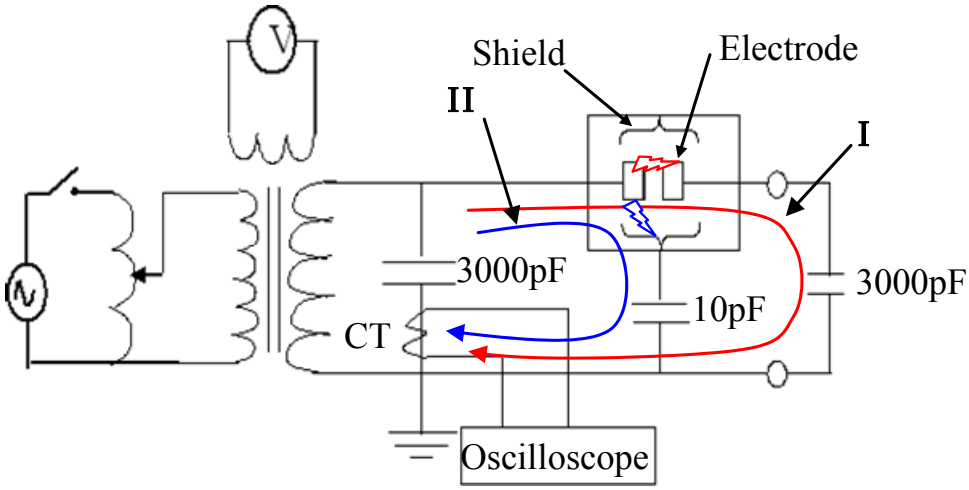

Fig. 3.13 Diagram of discharge current path for open contact condition

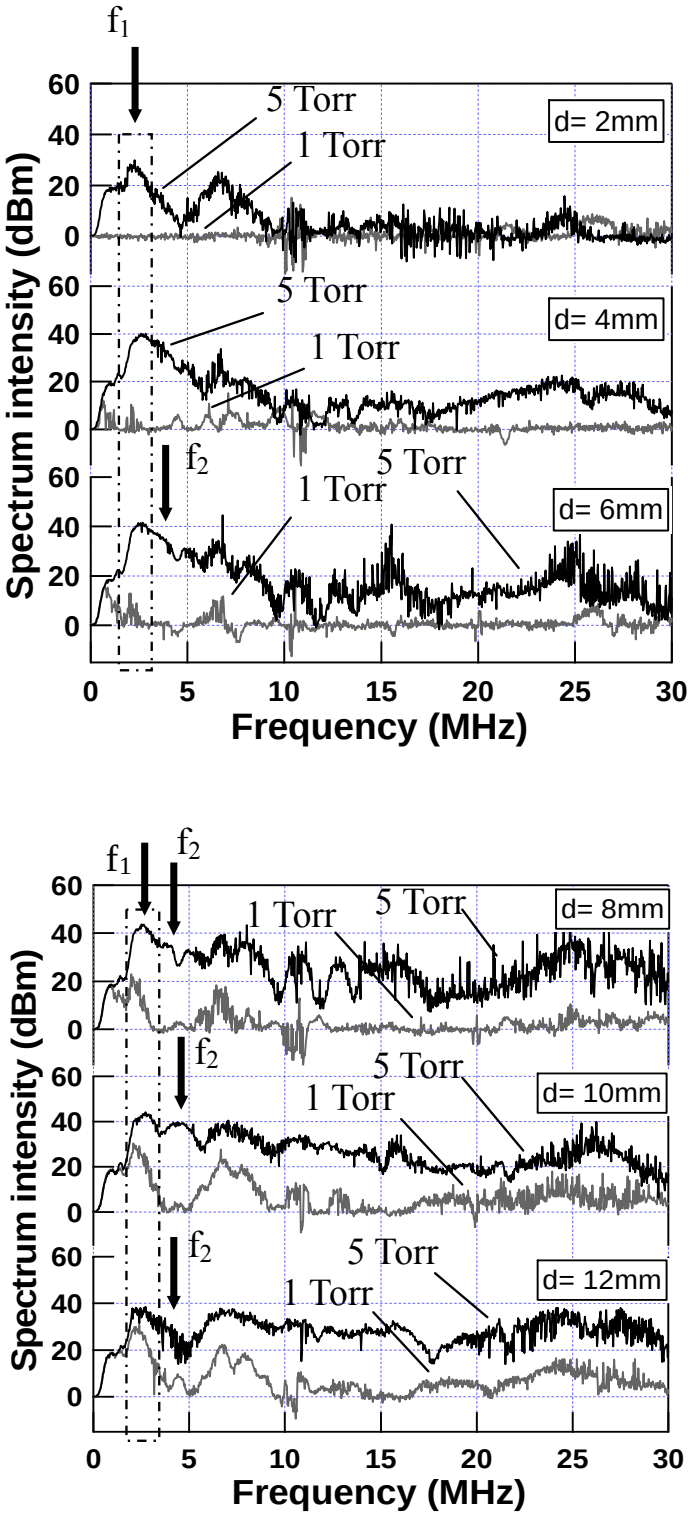

Fig. 3.14 EMW spectrum measured with loop antenna at PDIV for open contact condition

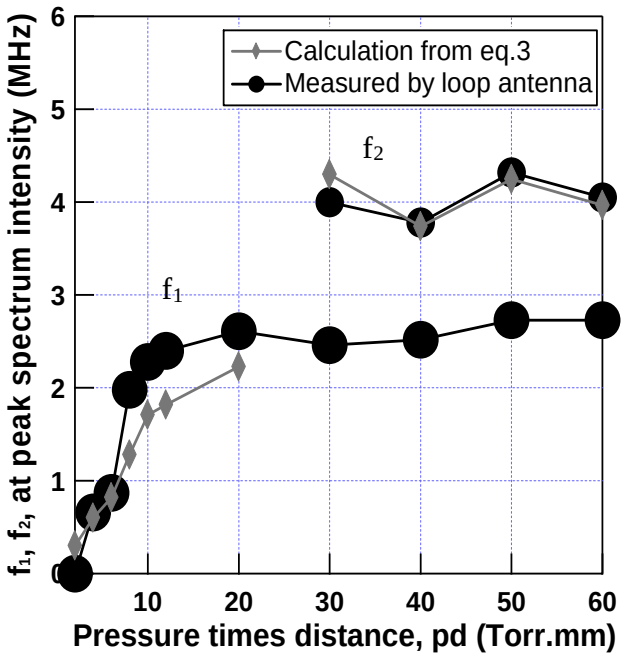

Fig. 3.15: Frequency giving maxima in spectra and f_A, f_B estimated from current waveforms given in Fig. 3.11 as a function of pd for open contact condition

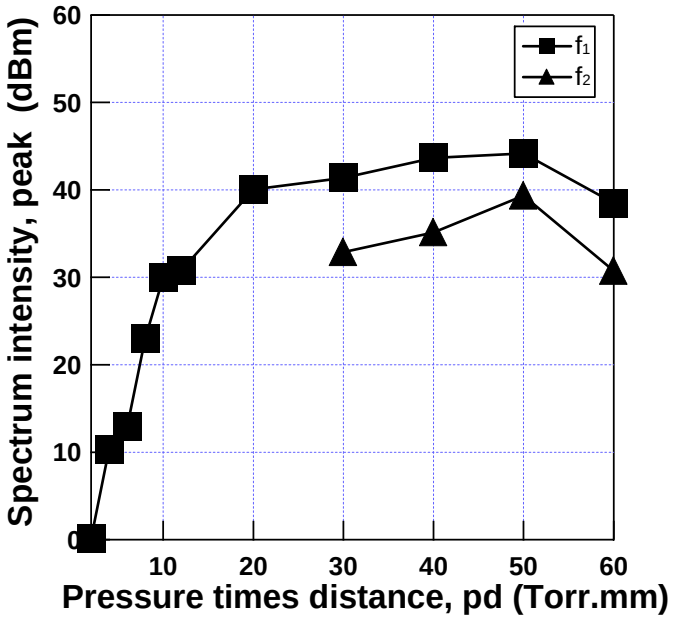

Fig. 3.16: Spectrum intensity dependence on pd for open contact condition

(3.3). Fig. 3.15 shows the results of the calculation together with the frequency at peak spectrum intensity. It is found that the discharges occurring in region A and B have dominant frequency bands f_A from 0.3 to 2.8 MHz and f_B from 3.7 to 4.5 MHz, respectively. These frequency bands f_A and f_B estimated from the current waveforms shown in Figs. 3.11 (a) and (b) respectively correspond to f_1 and f_2 measured in EMW spectrum. Namely, two different types of discharges phenomena are considered to occur with pd of 30 Torr・mm as boundary. Note that the loop antenna can detect both frequency band at 0.3 to 2.8 MHz and 3.7 to 4.5 MHz, while the CT detecting the discharge with main frequency band of 3.7 to 4.5 MHz owing to the low trigger level set in the oscilloscope.

Fig. 3.16 shows results of the spectrum intensity at f_1 and f_2 as a function of pd. Fig. 3.16 indicates that the spectrum intensity of discharges in region A (pd ≤ 20 Torr·mm), i.e. f_1 (f_A) component seems to obey an exponential growth with the gap length, being consistent with the current increasing with pd in exponential manner.

3.4 Conclusions

We have measured discharge current waveforms and spectrum of EMW emitted by the discharges in VI with CT and loop antenna, respectively. In closed contact condition, the results of measured spectra revealed that two peaks of spectrum intensity appeared at 6 MHz and 24 MHz. The 6 MHz frequency components are attributed to LC resonance of the external circuit. On the other hand, the 24 MHz frequency component is considered to arise from the nature of discharge itself occurring in VI. The discharge is considered to occur between the electrode and the shield of VI since the reflections appearing in the waveform might be due to large impedance of the stray capacitance C_s, resulting in an impedance mismatching in the external circuit.

In open contact conditions, the gap distance dependence of the discharge current in region A (pd ≤ 20 Torr·mm) was found to obey an exponential growth with the gap length. Therefore the discharges are considered to occur between the fixed and the movable electrode. The current intensity in region B decreased abruptly to 30 ~ 50 mA as pd increases from 20 to 60 Torr・mm. Based on the measured current waveforms, we can say that the discharge occurs between the electrode and the shield, since the current intensity in region B is almost same irrespective of pd. Furthermore, we found that the discharges occurring in region A and B have dominant frequency bands f_A from 0.3 to 2.8MHz and f_B from 3.7 to 4.5MHz, respectively.

The experiment utilized the actual ceramic type VI with the construction of the measurement circuit is the first one ever proposed. The results of discharge current properties and EMW spectrum emitted by PD in the closed and open contact conditions are very useful and essential for the basic idea on the diagnostic technique of VI performance.

References

[1] T. Kawamura, M. Meguro, H. Hama and T. Yamagiwa, "Industrial outlook: How to reduce SF_6 use and emission-various aggressive approaches to realize less SF_6 environment", Tenth International Symposium on Gaseous Dielectric, chapter 74, 2004

[2] M. Okawa, T. Tsutsumi, T. Aiyoshi, "Reliability and field experience of vacuum interrupters", IEEE Trans. on PWRD-2, No.3, pp.799-804, July 1987

[3] John R. Lucek, Pittsfield, Mass., and Willard J. Pearce, "Apparatus and method for measuring the pressure inside vacuum circuit interrupter", US-Patent No.3263162, 26.7. 1966

[4] W. W. Watrous jr., "Method and apparatus for measuring in vacuum circuit interrupter", US-Patent No.3575656, 20.4.1971

[5] Wilfried Kuhl and Klemens Wiehl, "Devices for measuring the internal pressure of vacuum interrupter", Siemens review XLV, No.2, pp. 87-89, 1978

[6] Zhao Ziyu, Jiang Xiuchen, Jin Zhijian, Zou Jiyan, Shijing, "Study on internal pressure measurement of vacuum interrupter", 19th International Symposium on Discharge and Electrical Insulation in Vacuum-Xi'an, pp. 775-778, 2000

[7] T. W. Dakin, G. Luxa, G. Oppermann, J. Vigreux, G. Wind, H. Winkelnkemper, 'Breakdown of gases in uniform fields Paschen's curves for nitrogen, air and sulfur hexafluoride', Electra N32, pp.61~82, 1974

[8] A. Von Engel, "Ionized gasses", Oxford University press, pp. 347, 1965

Chapter 4

Partial Discharge Properties and Determination of Gas Pressure in Vacuum Interrupter Based on Partial Discharge

4.1 Introduction

A vacuum circuit breaker (VCB) is an alternative device that may be employed to contribute to reducing usage of SF_6 gas insulated apparatus in the future [(1), (2)]. There are several classes of VCBs used in power systems such as medium voltage (MV) and high voltage (HV). The improvement with increasing the rated voltage of VCB has been the subject of numerous studies [(3),(4)]. The trend of research conducted on the improvement of vacuum technology to the higher rated voltage indicates that the use of a VCB in power distribution and transmission will expand. Today, VCB is widely used in electrical power distribution, such as cubicle-type insulated switchgear (C-GIS) and air insulated switchgear (AIS), to control and protect power lines and equipment under conditions of overload, short-circuit, over-current and other faults. Since the application of vacuum technology is increasing, the performance of the vacuum interrupter (VI) should be maintained in order to have stable and reliable system operation. The stability and reliability of the system can be ensured by detecting and improving the performance of the VCB. Detecting the gas pressure is one of the suggested ways to monitor the VCB performance, prevent serious faults, and reduce maintenance costs.

VCB in C-GIS and AIS are surrounded by SF_6 gas and air, respectively. VI is the key part of the VCB. Knowing the gas pressure in VI after long periods of operation is important for both manufacturers and users. The gas pressure of VI may increase gradually after long periods of operation. During the operation, when the gas pressure of VI exceeds the order of 10 Pa, partial discharge (PD) may occur and lead to an interruption failure. If no measures are taken, this phenomenon is not detected and it could lead to a serious failure to the VI as well as the operation system. A serious fault to the operation system due to interruption failure brings heavy losses to both manufacturers and consumers.

The estimation of the gas pressure in the VI after a long period of service is of interest to users. Numerous diagnostic apparatus have existed in the market with a simple indication such as good-bad indicators. The Magnetron method is impracticable to use in the field

because detaching of the vessel would be necessary. Such an operation should be performed only by a well trained operator under guidance of the manufacturer of the device. The diagnostic devices used in the field should be simple to operate and to interpret results. Many studies have been devoted to investigation of gas pressure and the ability of practical application [6],[7]. Although the diagnosis technique for detecting the gas pressure of VI based on PD has been studied recently [8], there have been no adequate studies on discharge characteristics and electromagnetic wave spectrum (EMW) in low vacuum of practical VI. The goal of this study is to develop a reliable diagnostic technique for gas pressure in the VI based on detection of PD. To acquire good knowledge to develop a gas pressure estimation based on PD, an understanding of PD properties in a practical VI is necessary. For this reason, investigation of PD properties and EMW spectrum in practical VI were conducted previously [9-11]. With continuing from previous work this chapter deals with the characteristics of PD in the low vacuum region of a practical VI filled with air and SF_6 gas under the rated voltage. The relation between the phase-resolved PD pattern and the gas pressure is also investigated. Eventually the phase-resolved PD characteristics (ϕ-q-n) are used to estimate the gas pressure of VI with a back propagation neural network (BPNN).

4.2 Experimental setup

In a practical situation, VI is basically operated under a closed contact condition and the contacts of VI are opened during current interruption due to over-current flow. Thus, study of the detection of gas pressure based on PD is more important for a closed contact condition rather than an open contact condition. In this experiment the glass vessel of VI was used for a better understanding of the optical PD properties in the low vacuum region and to know the location of PD occurrence as the pressure varies at constant applied voltage. In addition, since the optical measurement has a high sensitivity and cannot be influenced by the external circuit structure, it gives an accurate and fundamental knowledge of the PD phenomena and gas pressure estimation based on the PD. This can be as a reference for the measurement technique based on PD. Moreover before starting the experiment, the outgassing influences were confirmed. The internal gas of VI was evacuated to the specified pressure and kept for a longer time to observe the changes of the internal pressure. The residual pressure was maintained for 6 h and the measurement was conducted within this period.

The detail of the experimental setup were already explained in chapter 2, section 2.2.

4.3 Experimental results and discussions

4.3.1 Partial discharge and light emission in low pressure of air at various applied voltages

Fig. 4.1 shows the partial discharge inception voltage (PDIV) verses the internal pressure of VI in air. The PDIV of VI filled with air was measured using CT and PMT in the pressure range 1.3 Pa – 6.6 kPa. The measurement result indicates that PDIV increases with the increase of the internal pressure. Thus, the pressure dependence of the PDIV is considered. The measurement of PDIV in air with CT was only detectable in the pressure range of 260 Pa – 6.6 kPa due to the low sensitivity of the measurement device. The PD current measured at 130 Pa had a very small magnitude below the noise level of the measuring device even though the applied voltage was increased to 7 kVrms. The occurrence of the PD at 130, 660, 1300 and 2300 Pa at 7 kVrms obviously can be seen with an ICCD camera as shown in Fig. 4.2. The light emissions of PD seem to scatter on the surface of the glass envelope at both the movable (bellows side) and fixed side of the electrodes. The luminosity of PD captured by the ICCD camera especially at 130 Pa indicates that the PD is still occurring at this level of pressure though it cannot be detected with CT. The PD at 660 Pa and above seems to occur at the edge of the bellows and the shield of VI. Thus, two different types of PD can be considered for the pressure below and above 660 Pa. These results will be explained in section 4.3.2.

Fig. 4.3 shows the PDIV verses the number of experiments in 1 Pa order measured with PMT. The voltages were applied 20 times until PDIV appeared. Then this process was repeated 2 to 3 times by re-evacuating the VI to the same vacuum level and refilling the VI with air to the pressure of 1 Pa order. It is apparent from the results depicted in Fig. 4.3 that the occurrence of PD at 1 Pa order would result in the immediate increase of the internal pressure of VI to pressure giving the minimum PD inception voltage. The immediate increase of the internal pressure may be related to the out-gassing or gas evolution due to PDIV. This information indicates that the measurement of PD is more applicable to estimating the gas pressure and feasibility at the pressure giving the minimum of PD inception voltage.

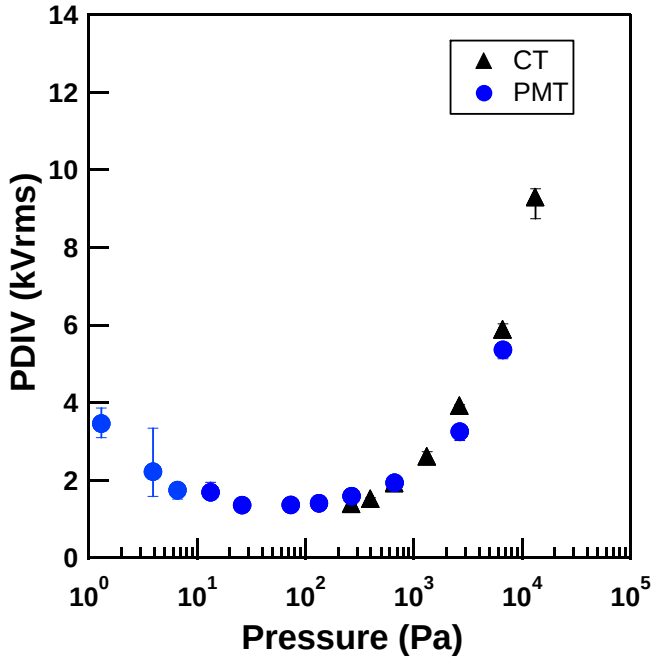

Fig. 4.1 PDIV as a function of internal pressure.

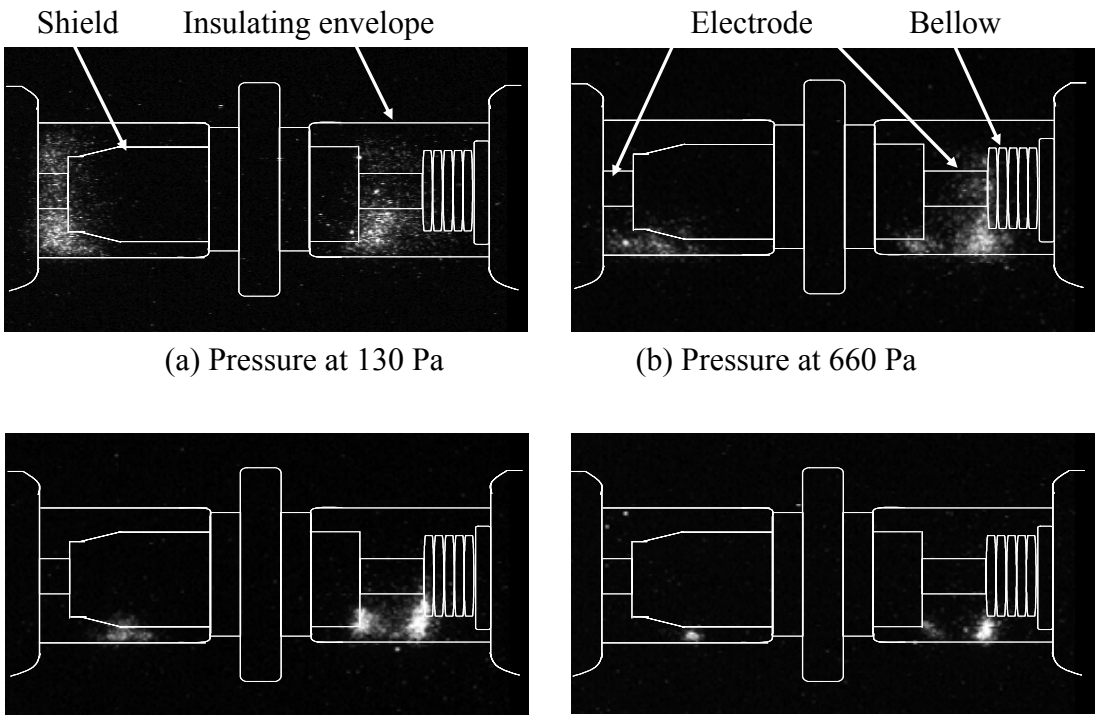

(a) Pressure at 130 Pa (b) Pressure at 660 Pa

(c) Pressure at 1.3 kPa (d) Pressure at 2.6 kPa

Figs. 4.2 Partial discharge light emission captured by ICCD camera at 7 kVrms.

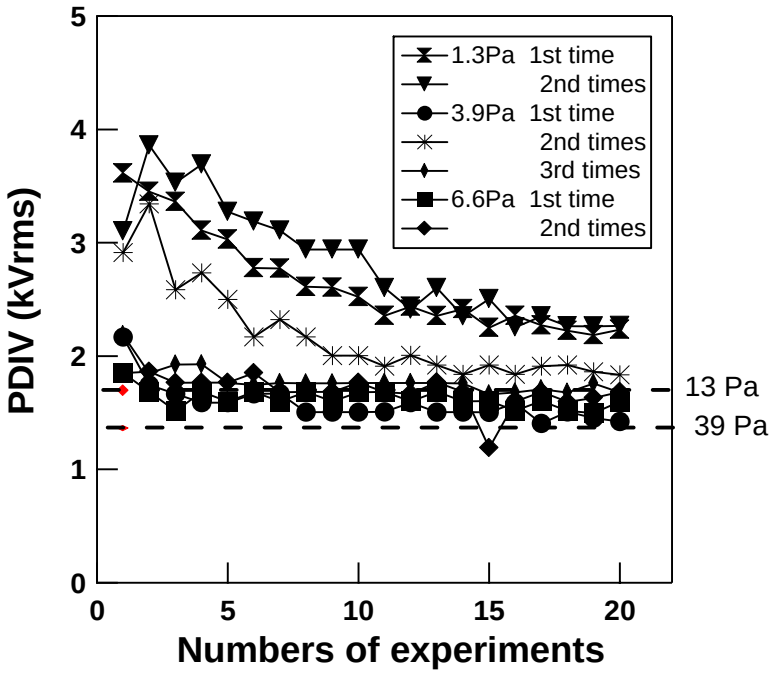

Fig. 4.3 PDIV detected with PMT verses the number of experiments.

4.3.2 Partial discharge light intensity in low pressure of air at various pressures

At a given pressure and applied voltage, PD light pulses appearing at any phase angles were found to have a similar waveform. The results also revealed that the phase distribution of PD light pulses strongly depended on the phase angle of the applied voltage. These results indicate that one can estimate gas pressure based on the phase angle dependence of PD light pulse characteristics.

Fig. 4.4 depicts the summarized plot of the PD pulse rise time as a function of the internal pressure of VI at 2, 5 and 7 kVrms. At the bottom side of the graph are shown typical waveforms of single PD light pulses triggered at the phase where the maximum number of pulses appeared. It is found from the results that two distinct types of PD pulses appear with their own characteristic features. The characterization of PD light pulses was done on the basis of the rise time and peak intensity [(12),(13)]. The rise time t_r measured in this experiment corresponds to 10% to 90% of the peak amplitude of the light intensity. The results reveal that the PD pulses observed at 13 Pa to 130 Pa of air have a relatively larger rise time (1 μs order) and smaller magnitude (less than 0.5 mA), while at pressures of 660 Pa and above they exhibit a shorter rise time (10 ns order) and larger magnitude (greater than 1 mA). The pulses with the larger rise time and smaller

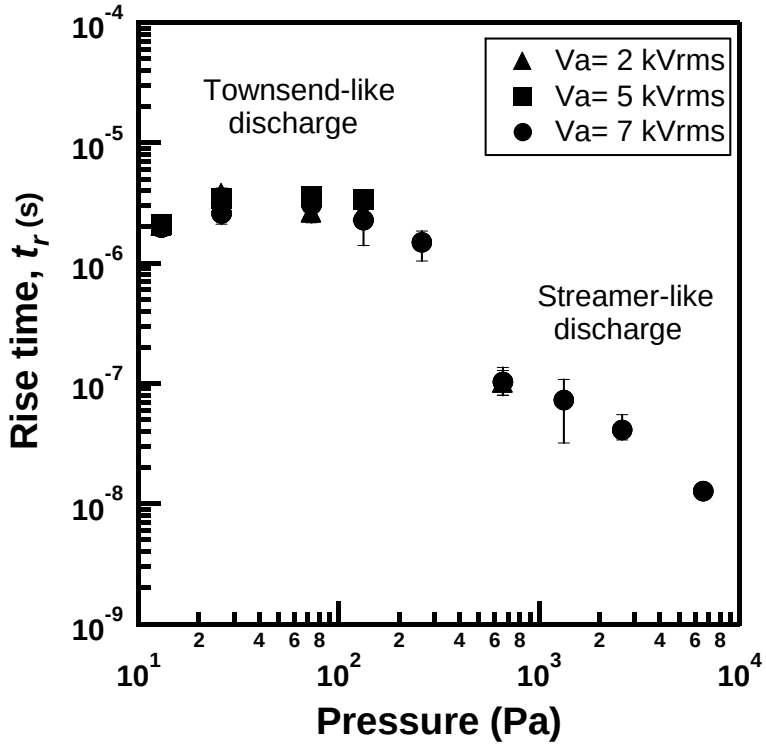

(a) Rise time of PD light pulses as a function of internal pressure of VI.

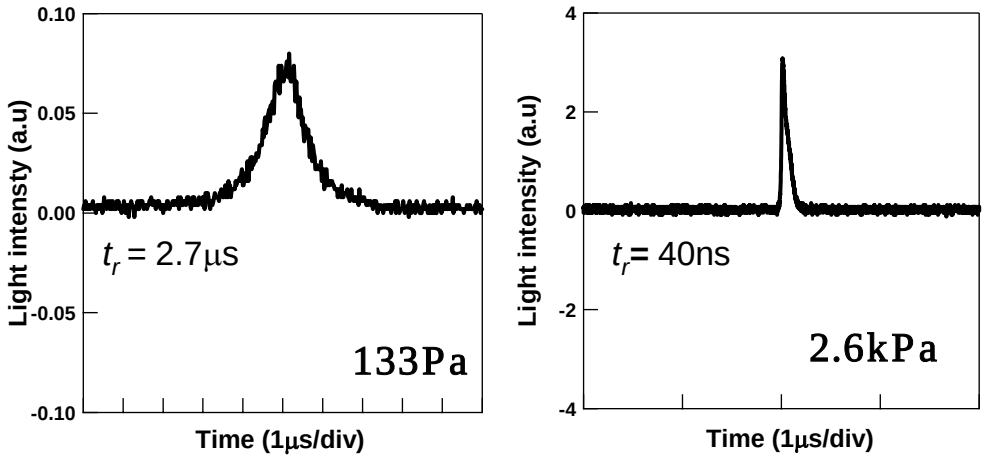

(b) PD light waveform at 133Pa and 2.6kPa

Figs. 4.4 Rise time of PD light pulse as a function of internal pressure of VI measured with PMT and typical waveforms.

peak value can be attributed to a Townsend-like discharge while those with the sharper rise time and larger peak value are characterized as streamer-like discharge. As depicted in Figs. 4.2 (a), the luminous area of PD in 130 Pa seems to scatter and spread over the glass wall of VI. This may be the consequence of many secondary avalanches in the Townsend-like discharge. Note that the gap between the electrode and the shield is 11 mm under the present experimental conditions. Von Engel [14] showed that the logarithm of the reduced current in air at constant reduced field (E/p) is a linear function of the distance up to 6 mm and then rises sharply due to the Townsend secondary effect. From this point of view, since the gap between the electrode and the shields is 11 mm under the present experimental conditions, the luminous PD is considered to arise from the secondary avalanches of the Townsend-like discharge which makes the PD spread out over the glass surface of VI.

On the other hand, as shown in Figs. 4.2 (b), 4.2(c) and 4.2(d), the luminous area of PD seems to be initiating from the edge of the bellows toward the edge of the shield, indicating a streamer-like discharge. The streamer mechanism of the inhomogeneous field in air occurs if the number of ions in the avalanche reaches 10^8 which can be expressed as follows [15].

$$\exp\left(\int_0^d \alpha \quad dx\right) \geq 10^8 \qquad (4.1)$$

Note that α is the first ionization coefficient. The distance between the edge of the bellows and the edge of the shield in VI is 25 mm. Thus, the streamer-like discharge can be explained by the following consideration; from the left side of equation (4.1), if α is about 8 ion pairs/cm [12] under a constant reduce field E/p of 1.32 V/cm-Pa, the number of the ions existing in avalanches will reach 4.8 x 10^8 which agrees with the right side of equation (4.1).

Moreover, Ramachandra et al [13] has interpreted that the Townsend-like discharge has a smaller magnitude (1 mA order) with a larger rise time (10-100 ns order) while the streamer-like discharge has a larger peak value (10mA order) with a shorter rise time (1 ns order). Their experiments were carried out at an inception voltage and room temperature for various artificial voids of three thin polypropylene films and pressures of 13.3, 26.6 and 53.2 kPa order. Although the test sample and the value of the rise time were different, the shapes of the discharge pulses obtained from their experiments are similar to those obtained in Fig. 4.4 (b).

Furthermore, F. H. Kreuger [15] reported that the rise time of the Townsend-like

discharge pulse in a virgin cavity is far slower than several tens of nanoseconds compared with the streamer-like discharge, which has a duration of one to three nanoseconds. They also noted that as a consequence of many secondary avalanches in the Townsend-like discharge, the discharge spread out over a broad surface area of the cavity.

4.3.3 Partial discharge light in low pressure of SF_6 at various pressures

The occurrence of the discharge inside VI was verified by the measurement of the discharge inception voltage. The result revealed that the discharge inception voltage varied depending on the gas pressure, depicting that the discharge was occurring inside VI.

The typical discharge light pulses measured with PMT at 7kVrms of 26Pa, 130Pa and 660Pa are shown in Figs. 4.5. Note that the discharge pulses measured with PMT has the same pulses measured with that current transformer (CT). From these results, two distinct pulse forms are produced as shown in Fig. 4.5(a), 4.5(b) and 4.5(c). Note that the discharge light pulse of 26 Pa has occasions of gradually decline of the fall times. It may consider due to the positive ions component which produced a photo-effect at the shield. However further investigation will be carried out in future. Fig. 4.6 portrays the summarized plots of discharge rise time and discharge width against the gas pressure of VI measured with PMT at applied voltage of 7kVrms. The rise time t_r corresponds to 10% to 90% of the peak amplitude of the light intensity [12]. The rise time and the width of the discharge in low vacuum of SF_6 gas are found to gradually reduce as the pressure going to exceed 50Pa and slightly reduce as the pressure exceeded 50Pa above. The result shows that two distinct types of discharge exist when the gas pressure of SF_6 varies from below 50Pa to above 50Pa. The result reveals that the discharge pulses below 50Pa have relatively larger rise time of 100ns and larger pulse width of 2μs order. When the gas pressure exceeded 50Pa above, the rise time depicts relatively smaller value of 10ns and pulse width of 0.1μs order.

Figs. 4.7 show a typical luminous area of the discharge in low vacuum of SF_6 captured with ICCD camera at 7 kVrms. The luminous areas of discharge are indicated in dashed circle line. In Figs. 4.7 (a), an extremely weak luminous area of discharge in 26 Pa seems to spread out from the both side of the shield and scatter over the glass wall of VI. The luminous area at this pressure corresponds to the discharge pulse shown in Fig. 4.5(a) and is believed to have a criterion of Townsend-like discharge which is discussed in section 4.3.4. When the gas pressure exceed 50Pa and above, a slightly

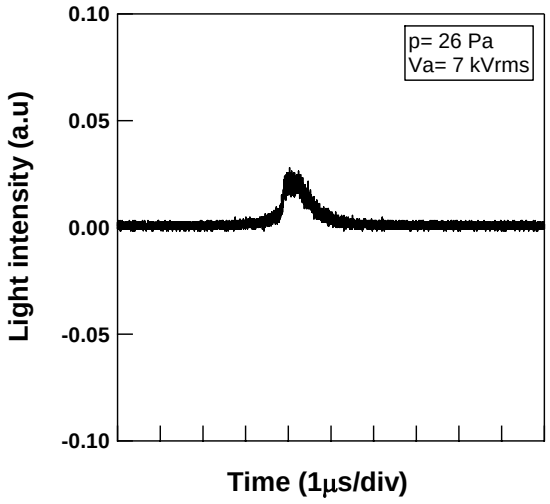

a) p = 26Pa

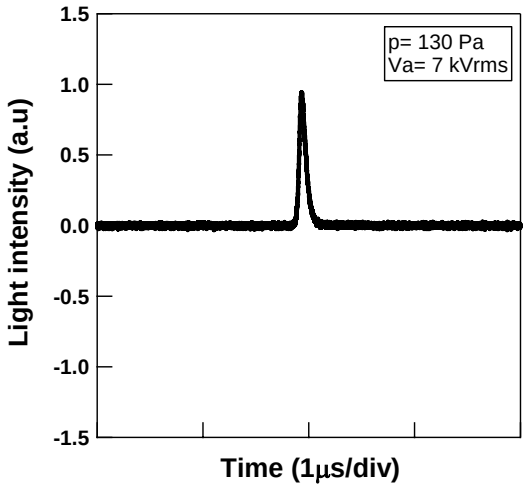

b) p = 130Pa

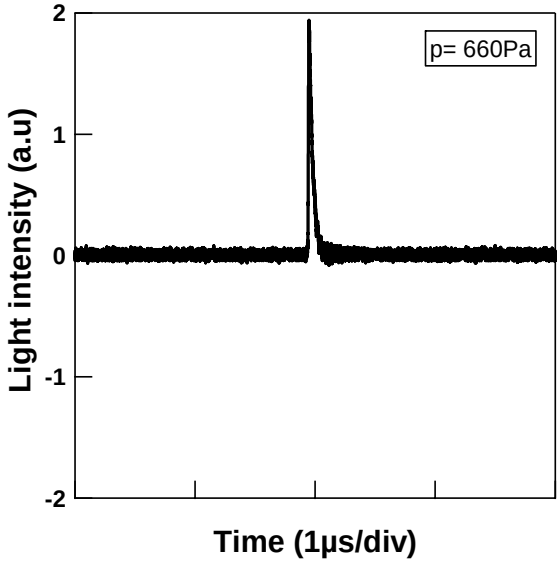

c) p = 660Pa

Figs 4.5 Typical discharge light pulses in vacuum interrupter filled with SF_6 at 7kVrms.

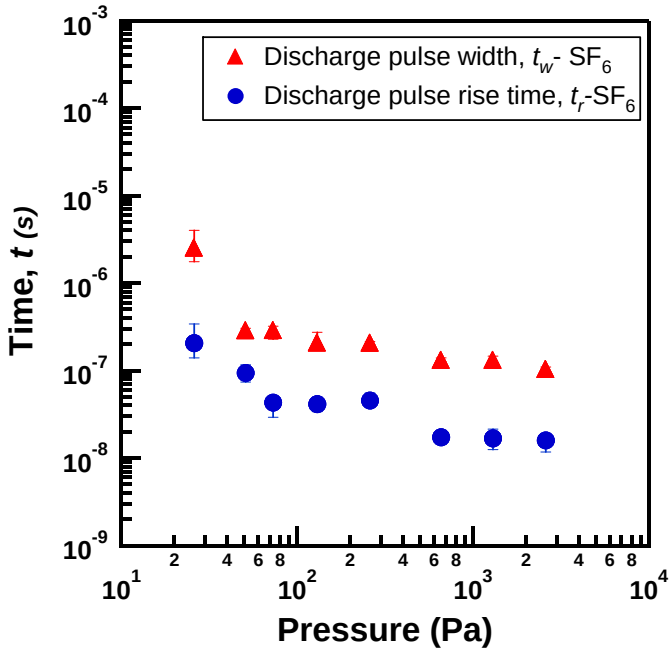

Fig. 4.6 Discharge pulse rise time and width against internal pressure of vacuum interrupter filled with SF_6 at 7kVrms.

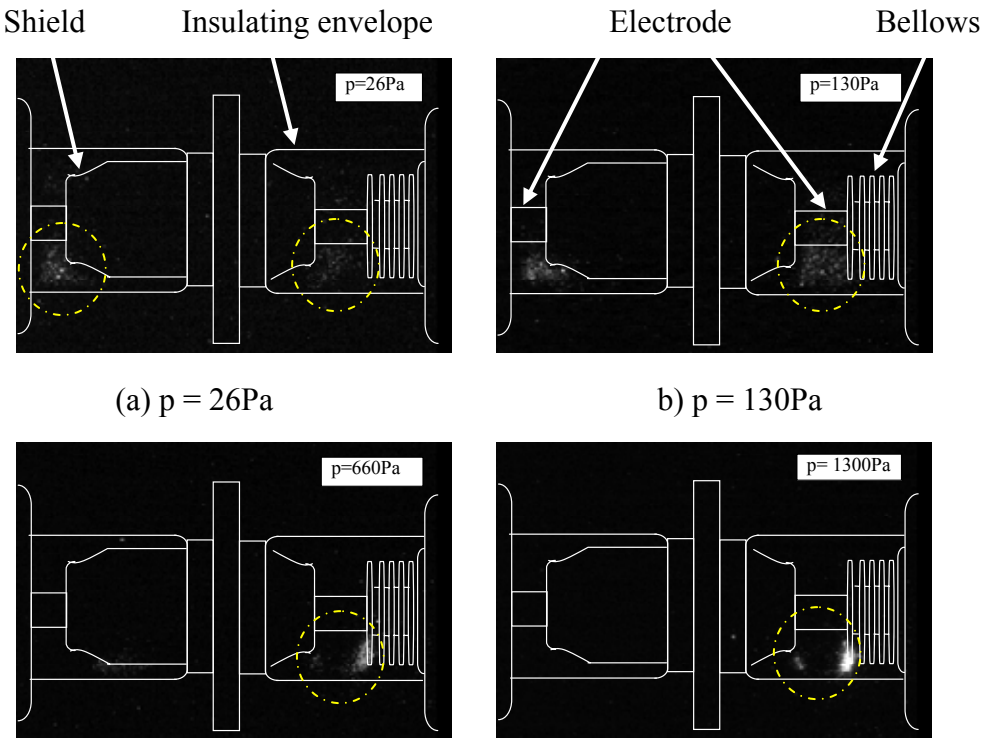

Figs. 4.7 Luminous area of discharge in vacuum interrupter filled with SF_6 at 7kVrms captured with ICCD camera.

clear sustaining luminous area of discharge can be observed at the right side of the shield and at the vicinity of edge of the bellows as shown in Figs. 4.7(b), 4.7 (c) and 4.7 (d). These luminous areas have relatively smaller discharge rise time and width as shown in Fig. 4.5(b) and 4.5(c), which are believed to be characterized by the criterion of streamer formation. Here the gap length at the occurrence of the luminous area between the bellows and the shield is taken into consideration to explain the streamer criterion in section 4.3.4. The luminous area and PD light pulses in low pressure of VI filled with SF_6 gas demonstrated similar characteristic with that in low pressure of air as explained in the previous section (4.3.2).

4.3.4 Partial discharge type in low pressure of vacuum interrupter

If number of electrons n_e with elementary charge ϵ moves with constant velocity υ_e across the gap d, a current flow during the transit time $T_e = d / \upsilon_e$ of electrons can be expressed as [16]

$$I_e(t) = \frac{\varepsilon\, n_e(t)}{T_e} \tag{4.2}$$

The number of electron growth can be written as

$$n_e = \exp(\alpha x) \tag{4.3}$$

where α is the ionization coefficient. If the number of electrons increases with growing distance x from the cathode by ionization, the electron current becomes function of time $t = x/\upsilon_e$ as follows

$$I_e(t) = \frac{\varepsilon}{T_e}\exp(\alpha \nu_e t) \qquad 0 \leqq t \leqq T_e \tag{4.4}$$

Therefore the time constant is

$$\frac{t}{\tau} = \alpha \nu_e t \qquad \therefore \tau = \frac{1}{\alpha \nu_e} \tag{4.5}$$

The time constant τ can be drawn from the tangent line as shown in Fig. 4.8. This is a basic idea that α can be obtained from the PD current pulse. However in this dissertation α is obtained from the PD light pulse. The rise time t_r of PD light pulses is assumed to has an approximation with time constant τ because the simultaneously measurement with PMT and CT given the same waveform between the PD light pulse and PD current pulse. Fig. 4.9 shows the measurement results of PD light pulse and PD current pulse measured simultaneously with PMT and CT, respectively at 26 Pa of SF_6

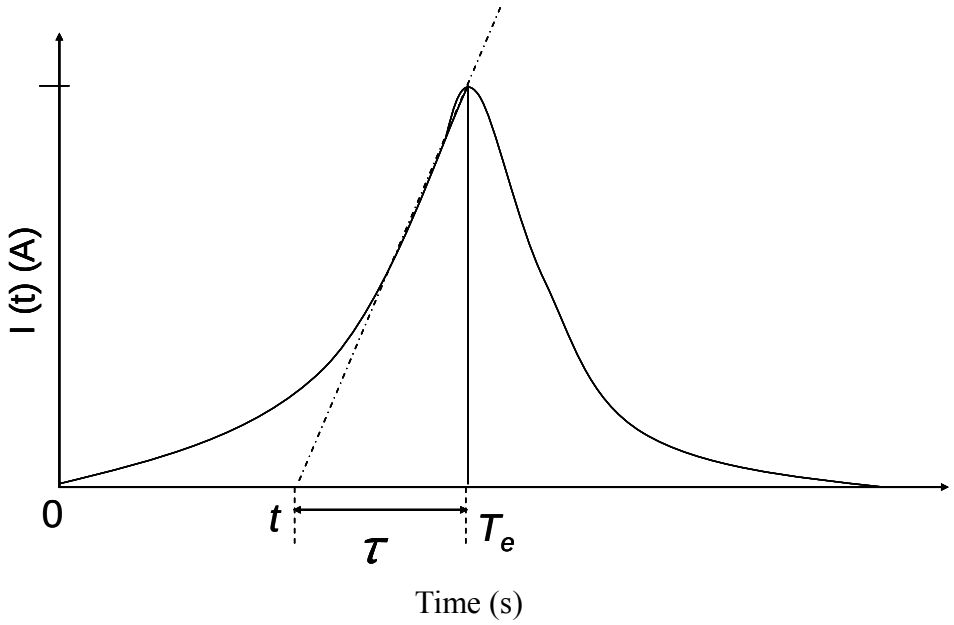

Fig. 4.8 Example time constant drawn from the tangent line [16]

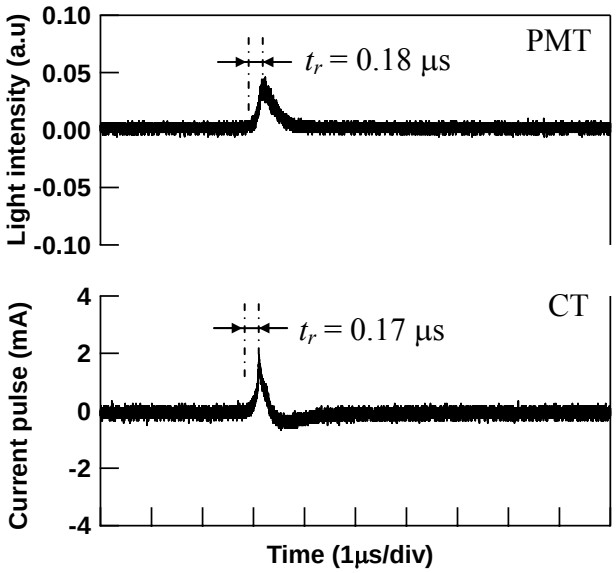

Fig. 4.9 PD pulse measured with PMT and CT at 26Pa of vacuum interrupter filled with SF_6 gas. (Va = 7 kVrms)

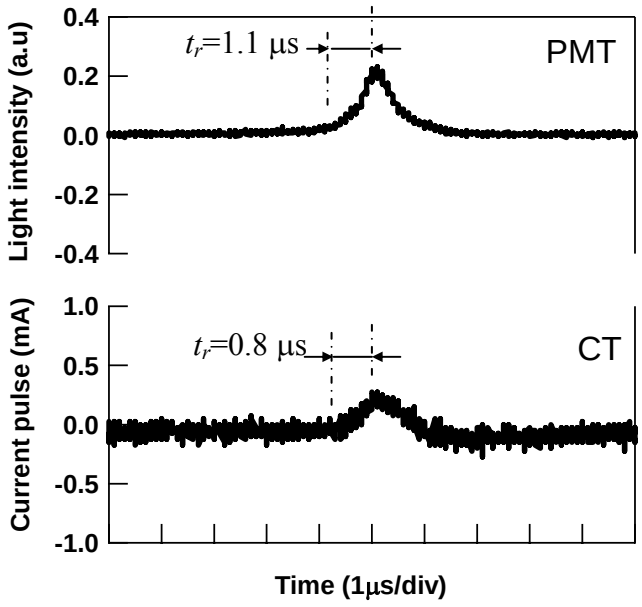

Fig. 4.10 PD pulse measured with PMT and CT at 260 Pa of vacuum interrupter filled with air. (Va = 7 kVrms)

gas. The rise time t_r of PD light pulse is 0.18 μs almost equal to that of PD current pulse which is 0.17 μs. While the fall time of PD light pulse is 0.38 μs which is 0.02 μs larger than PD current pulse. Note that the rise time of PD light pulse and PD current pulse also give approximate value of 47 and 44 ns respectively, at 130 Pa of SF_6 gas. In addition, VI filled with air at 260 Pa also depicts the same waveform between PD light and current pulse as shown in Fig. 4.10 where the rise time is 1.1 μs and 0.8μs, respectively. Thus, it is assumed that the number of photons $dp(t)$ created between t and $t + dt$ where $dp(t)$ is proportional to the number of drifting electrons n_e as follows[16],

$$d\,p(t) = \delta\, n_e(t)\, \upsilon_e\, dt \tag{4.6}$$

where δ is the number of photons produced by one electron per centimeter. The proportionality between $dp(t)$ and n_e mean that the life time of the excited states is even smaller compared to the time constant τ of the electron current growth. Consequently, the growth rate of electrons can be considered equal to that of photons in avalanches. In addition, the time constant of the photon growth and the electron growth in the same single avalanche are considered to be the same under the low pressure of SF_6 gas.

Therefore, the time constant τ was estimated from the measurement result of PD

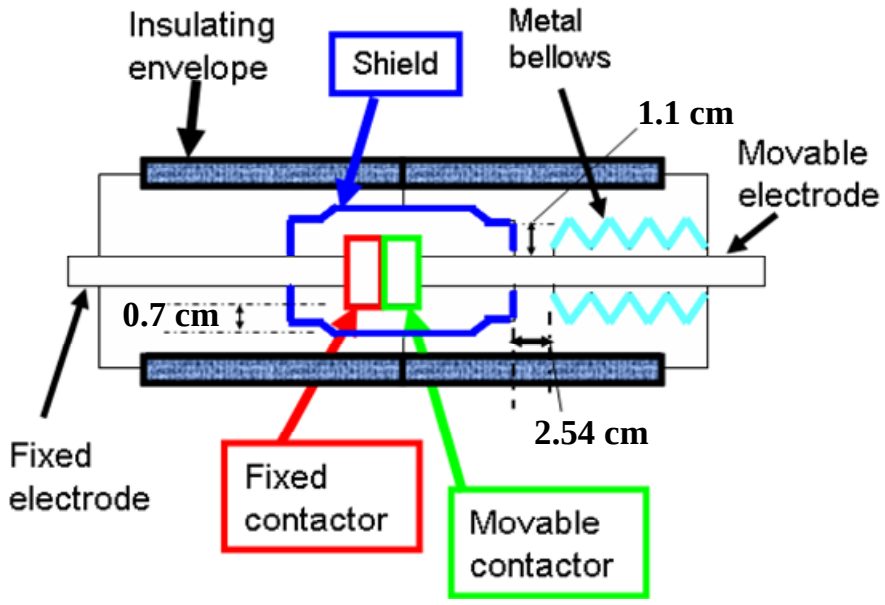

Fig. 4.11 Schematic diagram of vacuum interrupter.

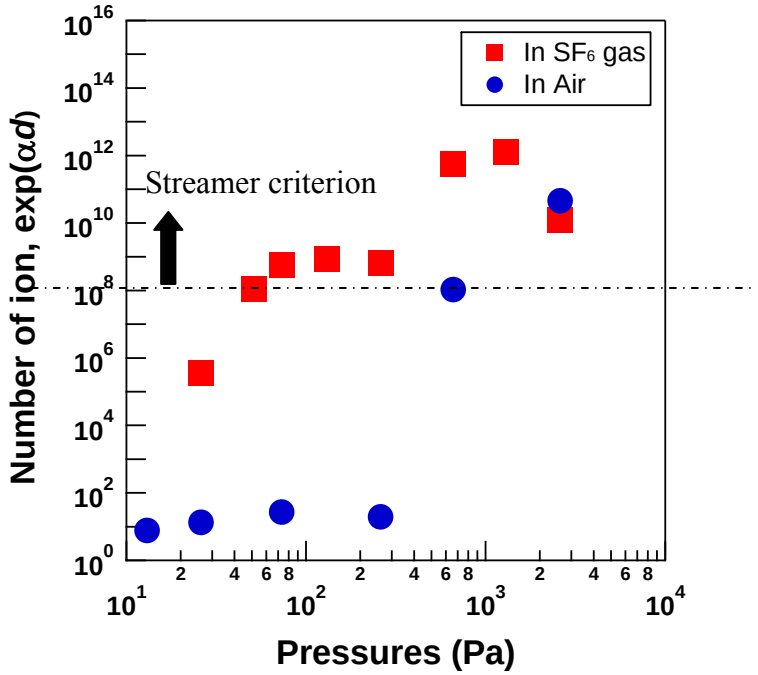

Fig. 4.12 Number of ions in avalanches as a function of pressures at 7 kVrms for low pressure of SF_6 gas and air in VI

light pulse by drawing the tangent line with the same methodology of that shown in Fig. 4.8. The value of τ was compared to the rise time t_r of PD light pulse obtained from the experiment. The estimation of τ from the measurement result gives an average percentage error of approximately 10 % to the rise t_r of PD light pulse. Therefore t_r of PD light pulse was assumed to has approximation with time constant τ as expressed in eq. 4.7 [16],[18]

$$t_r \approx \tau = \frac{1}{\alpha \upsilon_e} \tag{4.7}$$

From the experimental results shown in Fig. 4.7(a), the luminous area of the discharge in 26 Pa seems to spread out from the both sides of the shield and scatter over the glass wall near the shield. The gap length between the rods and the shield is 1.1cm while the gap length between the main contact and the shield is 0.7cm. The schematic diagram of VI with the indication of gap length is shown in Fig. 4.11. By utilizing the rise time t_r of PD light pulse as expressed in eq.(4.7), the ionization coefficient α was estimated. Note that υ_e is the electron drift velocity and t_r is the average rise time of the discharge obtained from the experiment. The υ_e is deduced from the measurement of the duration t_w of the PD light pulse together with the gap distance d as the following equation [16], [18]

$$v_e = \frac{d}{t_w} \quad \left(cm/s\right) \tag{4.8}$$

where d is the gap length between the main contact and the shield and t_w is the average of the discharge pulse width obtained from the experiment as shown in Fig. 4.6. The t_w is assumed as a transit time of electron in avalanches which occupy almost the whole gap distance. Thus the streamer criterion may take place at only very small distance near the bellows when critical numbers of ion in avalanches achieve more than 10^8 ion pairs. From this assumption and by using the data from the experiments, α is estimated.

The t_r and t_w have the value of 0.21μs and 2.51μs at 26 Pa of SF_6 gas, respectively. By substituting the value of t_r and t_w into eq. (4.7) and (4.8), α is estimated as about 11 ion pairs/cm. Therefore the number of ions in avalanche can be obtained by substituting the value of α and the gap length d,1.1cm into the eq. (4.9) [5], [16]

$$\exp(\alpha d) \geq 10^8 \tag{4.9}$$

Consequently, the number of ions in avalanche could not reach 10^8 which indicate that no criterions for streamer formation occur.

On the other hand, the luminous area of PDs in SF_6 gas are observed between the

edge of the shield and the edge of the bellows as shown in Figs. 4.7(b), 4.7(c) and 4.7(d). The gap length between the edge of the shield and the edge of the bellows is 2.54 cm. The average t_r obtained at 130, 660 and 1300 Pa are 41.2 ns, 17.2 ns and 16.7 ns, respectively. While the average t_w at pressures 130, 660 and 1300 Pa are 212 ns, 132 ns and 132 ns, respectively. By substituting the values of t_r and t_w into eq. (4.7) and (4.8) with d= 0.7cm, α is estimated as about 7.4, 10.9 and 11.3 ion pairs/cm for pressures 130, 660 and 1300 Pa, respectively. Therefore when d = 2.54 cm, by using the eq.(4.9), the number of ion pairs are 1.3 x10^8, 1.23x10^{12} and 2.9x10^{12} at 130, 660 and 1300 Pa, respectively. These results show that ions in avalanches reach 10^8 and 10^{12} which are at the lower limit of streamer criterion. This indicates that the number of ion in avalanches achieves 10^8 at very short distance which is near bellows. These are relevant to optical images of the discharge shown in Figs. 4.7(b), 4.7(c) and 4.7(d) which can be considered as streamer-like discharge.

Fig. 4.12 depicts the summarization of the number of ions in avalanches as a function of pressure at 7 kVrms for SF_6 gas compared with that in air. The result shows that the number of ions in avalanche has fulfilled the streamer criterion when pressure exceeding 50 Pa for SF_6 gas compared with 660 Pa for air.

Moreover, Penning [21] and Van Brunt [22] also mentioned that the criterion for the streamer is reached when $n_e \geq 10^8$ electrons per avalanche. Raether [16] also referred to Penning and claimed that the velocity for a streamer is 10^7 to 10^8 cm/s. Likewise, M. G. Danikas [23] claimed that the Townsend discharge has the number of electrons per avalanche less than 10^8 which agrees with the discussion above.

Consequently, the relatively larger rise time, larger width and smaller magnitude of the PD light pulse can be attributed to Townsend-like discharge while the relatively smaller rise time, smaller width and higher magnitude of discharge are characterized by streamer-like discharge. These results agree with the definition given by F. H. Kreuger [15] and Ramachandra et al [13].

4.3.5 Pattern corresponding to the gas pressure and the identification by neural network approach

The study on PD properties in vacuum interrupter in various low pressures of air and SF_6 gas was implemented in previous sections to acquire a good knowledge on determination of pressures based on PD. This section deals with fundamental technique of estimation for the gas pressure in VI based on phase-resolved discharge algorithm. The phase-resolved discharge patterns for each pressure were established with special

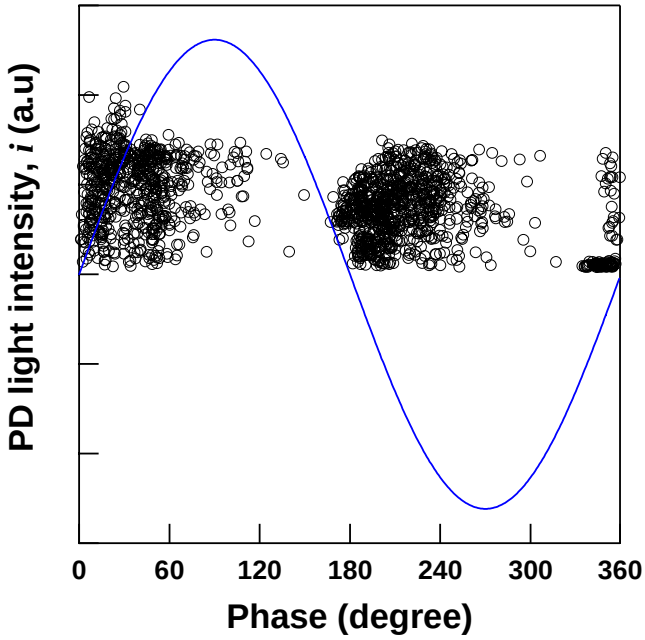

(a) Typical *ø-i-n* pattern

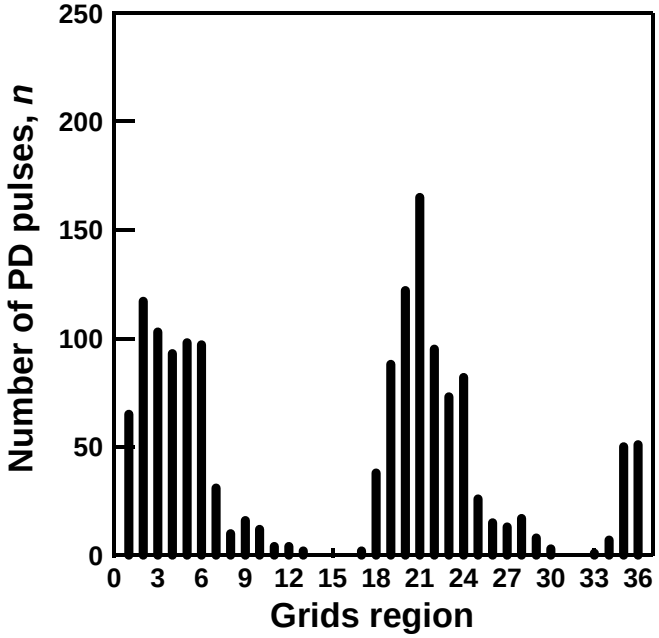

(b) Development of 36 grids

Figs. 4.13 (a) Typical *ø-i-n* pattern in air at 1.3kPa and 7kVrms measured with PMT. (b) Development of 36 grids.

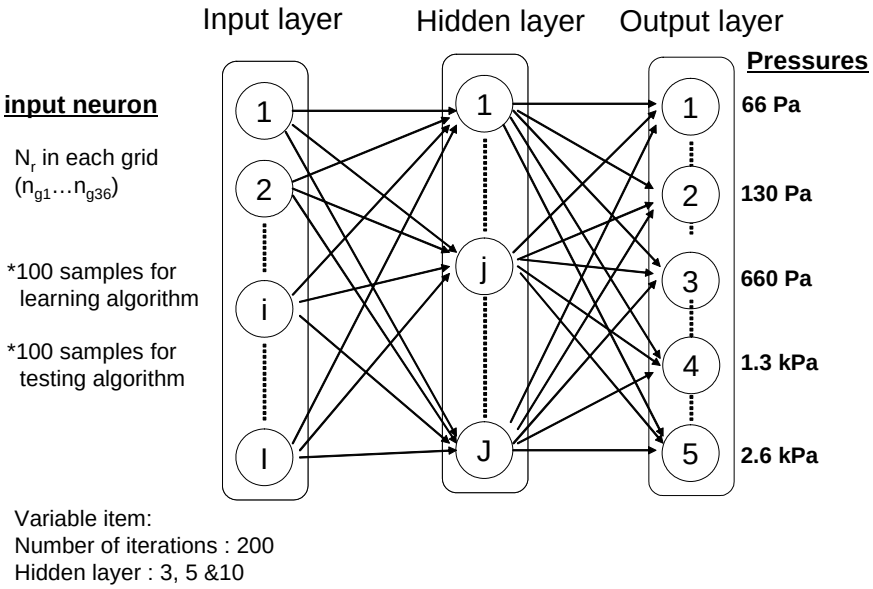

Fig. 4.14 Structure of back propagation neural network.

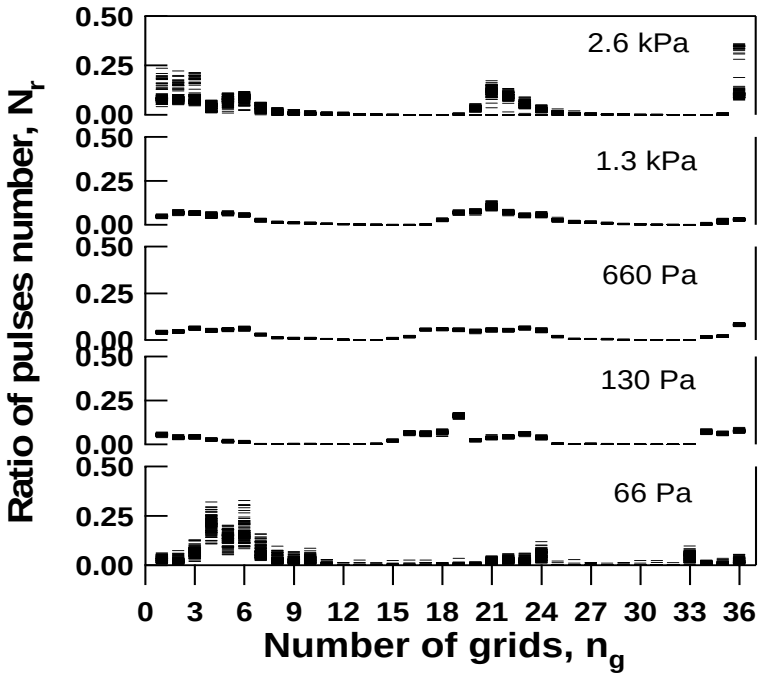

Fig. 4.15 The ratio of pulse number verses number of grids for five different pressures with 100 samples each.

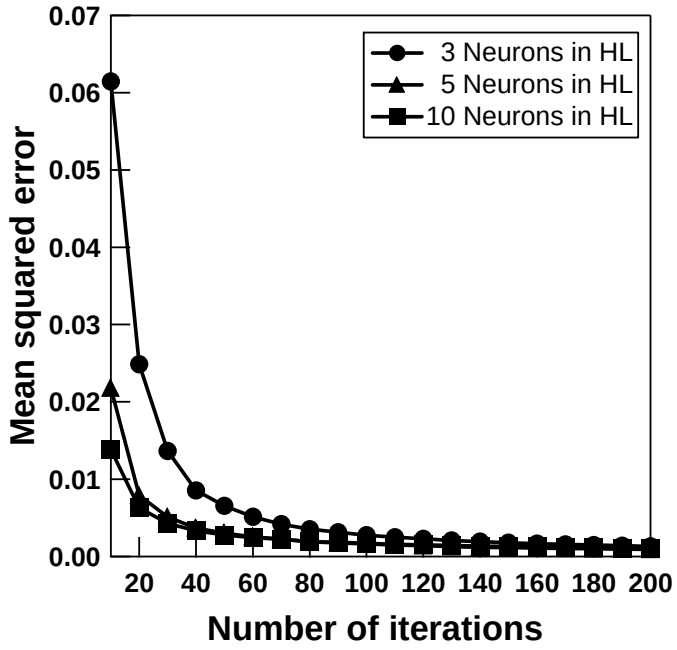

Fig. 4.16 Recognition error of the BP NN in discrimination of the gas pressure for 200 iterations.

Table 1 Summarization of average successful rate for 3 and 10 neurons of the hidden layer (HL) for 100 and 200 iterations.

Pressures (Pa)	3 neurons of HL		10 neurons of HL	
	100 iterations	200 iterations	100 iterations	200 iterations
66	90.4 %	93.1 %	90.6 %	92.6 %
130	92.7 %	94.9 %	92.8 %	94.7 %
660	90.7 %	94.2 %	96.5 %	97.7 %
1300	95.0 %	96.6 %	96.7 %	97.7 %
2600	94.5 %	96.6 %	97.0 %	97.9 %

design PD measuring device (PARADISE) and have been analyzed by utilizing artificial back propagation neural network (BPNN) methodology [24),(25),(26),(27)].

Fig. 4.13(a) shows the results represented by the ϕ-*i*-*n* patterns during 300 cycles of the applied voltage taken for the VI filled with air at 1.3 kPa and 7 kVrms using PMT. The ϕ-*i*-*n* pattern of PD occurrence in the low vacuum region of VI was measured using PARADISE. It is noted that ϕ is for the phase angle (horizontal axis), *i* is for the PD light pulse intensity (vertical axis) and *n* is for the number of PD pulses distributed during 300 cycles of the applied voltage (their distribution is marked by circles). The light intensity of the PD was neglected. Only the ϕ and *n* patterns were taken into consideration since the intensity of the PD light pulses varies with the distance of the PMT from the specimen (VI). Therefore, considering only the ϕ-*n* pattern from Fig. 4.13(a), the example of *n* against the developed grids was plotted in Fig. 4.13(b). The 36 grids were developed vertically where each grid represents 10 degrees of the phase angle. Using the data of the ϕ-*n* patterns, the neural network (NN) approach was employed to recognize the gas pressure in VI. The input algorithm was analyzed by the neural network assistant software (NNAS) with the back propagation technique which provided the desired response. Fig. 4.14 shows the structure of the BPNN. The normalized number of pulses N_r in each grid becomes a set of the input of BPNN. The N_r was determined by the ratio n_p to n_{tp} which can be expressed as follows

$$N_r = \frac{n_p}{n_{tp}} \tag{4.10}$$

Note that n_p is the number of discharges occurring in each grid region and n_{tp} is the total number of PD at all the phase angles (36 grids). The normalized number of pulses verses the number of grids for five different pressures with 100 samples each is plotted in Fig. 4.15. The N_r with 100 samples was assigned for a learning and testing algorithm for different pressure levels. The outputs of the BP network were 66 Pa, 130 Pa, 660 Pa, 1.3 kPa and 2.6 kPa. The hidden layer of the BPNN is considered as important part where appropriate number of neurons should be identified in order to have an accurate discrimination of pressures level in VI. The number of layers and neurons therein is altered by trial and error to optimize the performance of the BPNN in its recognition task required for the classification of gas pressure based on PD patterns. To obtain the accurate number of neurons the recognition error test should be carried out. The recognition error test proceeds through a series of iterations where for each iteration a comparison is made of its own output with that of the desired response and computation is carried out to determine whether there is a match [28), (29)].Thus, the number of neurons

in the hidden layer was varied to obtain the optimum successful rate of the NN.

Fig. 4.16 demonstrates the recognition error of the BP NN in discrimination of the gas pressure for 200 iterations of 3, 5 and 10 neurons in the hidden layer. The result shows that after 120 iterations, the recognition error of the NN is perceived to be negligibly small for 10 neurons of the hidden layer compared to 170 iterations for 3 neurons of hidden layer.

Table 1 summarizes the recognition success rate of the BP NN in the discrimination of gas pressure at 100 and 200 iterations for 3 and 10 neurons of the hidden layers. From the experiment results, 10 neurons of the hidden layer have a higher successful rate compared to that for 3 neurons of the hidden layer. Note that regarding the number of neurons in the hidden layer, more than 10 does not give much difference from that of 10 neurons. The average of the successful recognition rate of the vacuum degree from 93 to 98 % is obtained, indicating a cognitive ability of vacuum degree estimation based on PD pattern recognition using the BP NN approach.

4.4 Conclusions

The determination of gas pressure based on partial discharge was investigated. From these experimental results, the following conclusions were drawn:

1) The PD pulses in VI filled with air for a pressure below 260 Pa having a relatively larger rise time (2 μs) with a smaller magnitude (less than 0.5 mA) were attributed to a Townsend-like discharge, while those with a sharper rise time (10-100 ns order) and larger magnitude (greater than 1 mA) were characterized as a streamer-like discharge at pressures above 260 Pa.
2) The discharge pulses in SF_6 gas at below 50 Pa have relatively larger rise time of 100ns order, larger pulse width of 2 μs order and lower magnitude compared with those obtained above 50 Pa.
3) The Townsend-like discharge in SF_6 gas was characterized for pressures below 50 Pa while streamer-like discharge was characterized for pressures above 50 Pa.
4) The consideration on avalanche with discharge pulse rise time and width in air and SF_6 gas allowed discharge in VI to fulfill the streamer-like criterion formation for above 660 Pa and 50 Pa, respectively.
5) The estimation of gas pressure based on partial discharge phase-angle characteristics using the NN approach gave a recognition success rate from 93 to 98 %. Thus the neural network algorithm is applicable to the discrimination of gas pressure in VI using ϕ-n patterns.

In practical situations, it is expected that once the leakage of gas into the VI occurs, the gas pressure of VI will increase immediately so as to pass the pressure giving the minimum of PD inception voltage; i.e. reaching the 1 Pa-10 Pa order. In this sense, investigation of PD properties over 1 Pa is also meaningful and important to diagnose the pressure level of VI.

References

[1] H. Okubo and S. Yanabu, "Feasibility study on application of high voltage and high power vacuum circuit breaker", 20th International Symposium on Discharge and Electrical Insulation in Vacuum, Tours, France, pp.275-278, 2002

[2] T. Kawamura, M. Meguro, H. Hama and T. Yamagiwa, "Industrial outlook: How to reduce SF6 use and emission-Various aggressive approaches to realize less SF6 environment", Gaseous Dielectrics X, New York, pp.475-484, 2004.

[3] S.Giere, M.Kurrat and U. Schumann, "HV dielectric strength of shielding electrodes in vacuum circuit breakers", 20th International Symposium on Discharge and Electrical Insulation in Vacuum, Tours, France, 2002.

[4] H. Saitoh, H. Ichikawa, A. Nishijima, Y. Matsui, M. Sakaki, M. Honma and H. Okubo, "Research and development on 145 kV/40 kA one break vacuum circuit breaker", IEEE/PES T&D Asia Pasific, PN-13, 2002.

[5] N.H. Malik, A.A. Al-Arainy and M.I. Qureshi, "Electrical insulation in power system", Marcel Dekker, Inc., pp.204, 1998.

[6] W.W. Watrous jr., "Method and apparatus for measuring in vacuum circuit interrupter", US-Patent No. 3575656, 1971.

[7] Z. Ziyu, J. Xiuchen, J. Zhijian, Z. Jiyan and S. Jing, "Study on internal pressure measurement of vacuum interrupter", 19th International Symposium on Discharge and Electrical Insulation in Vacuum Xi'an, pp.775-778, 2000.

[8] G. Yonggang, X. Guozheng, H. Yulong and L. Weidong, "On-line monitoring the vacuum degree of vacuum interrupter by partial discharge", 12th Asian Conference on Electrical Discharge, Shenzhen, China, pp.195-197, Nov. 19-22, 2004

[9] M. Kamarol, S. Ohtsuka, H. Saitou, M. Sakaki and M. Hikita, "Discharge properties and emitted electromagnetic wave spectrum in low vacuum region of vacuum interrupter", IEEJ Trans. Power Energy, Vol. 125, pp.797-802, 2005.

[10] M. Kamarol, S. Ohtsuka, H. Saitou, M. Sakaki and M. Hikita, "Discharge phenomena in low vacuum region of glass tube vacuum interrupter under AC applied voltage", Intern.l Symposium on Electrical Insulating Materials (ISEIM), pp.36-39, 2005

[11] M. Kamarol, S. Ohtsuka, H. Saitou, M. Sakaki and M. Hikita, "Investigation of discharge characteristic for diagnosis of degree of vacuum in glass type vacuum interrupter", 14th Intern. Symposium on High Voltage Engineering (ISH), Beijing, pp.171, 2005.

[12] Donald G. Kasten, Xin Liu, Stephen A. Sebo, Dennis F. Grosjean and Daniel L. Schweickart, "Partial discharge measurement in air and argon at low pressures with and without a dielectric barrier", IEEE Transaction On Dielectric and Electrical Insulation, Vol. 12, No.2, pp.362-373, 2005.

[13] B. Ramachandra and R. S. Nema, "Discharge mechanism in voids at sub-atmospheric pressures", IEEE Intern. Sympos. Electr. Insul., USA, pp.165-168, 1998.

[14] A.Von Engel, "Ionized gases", Oxford University Press, Great Britain, 1965.

[15] F.H.Kreuger,"Industrial high voltage", Delft University Press, Netherlands, Vol.1, pp.117-133, 1995.

[16] H. Raether, "Electron avalenches and breakdown in gases", Butterworth, Washington, (1964)

[17] A. Haddad and D. Warne, "Advance in High Voltage Engineering", IEE Power and Energy,Vol. 40 (2004)

[18] Mazen Abdel-Salam, Hussein Anis, Ahdab El-Morshedy and Roshdy Radwan, "High-Voltage Engineering Theory and Practice", 2000

[19] H.Okubo and N.Hayakawa, "Electrical insulation diagnosis and breakdown prediction of gas insulated power apparatus based on partial discharge mechanism", Gaseous Dielectrics IX ,pp.199-204, New York, 2001.

[20] H.Okubo, T.Ishida, T.Yamada and N.Hayakawa, "Partial discharge mechanism and current waveforms in electronegative gases and gas mixtures", Gaseous Dielectric IX, pp. 307-312, 2001.

[21] F.M. Penning, "Electrical Discharges in Gases", The MacMillan Company, New York, 1957.

[22] R.J. van Brunt, "Stochastic properties of partial discharge phenomena", IEEE Trans. Elec. Insul., Vol. 26, pp. 902-948, 1991.

[23] Michael G. Danikas, "The definitions used for partial discharge phenomena", IEEE Trans. on Elec. Insul., Vol. 28, No. 6, pp. 1075-1081, 1993.

[24] R. Bartnikas, "Partial discharges their mechanism, detection and measurement", IEEE Transaction on Dielectric and Electrical Insulation, Vol. 9, No.5, pp.763-808, Oct, 2002.

[25] A. Kelen, "Trends in PD diagnostic: when new options proliferate, so do old and new problems", IEEE Trans. on Dielectric and Electrical Insulation, Vol. 2, pp.529-534, 1995.

[26] A. Kelen and M.G. Danikas, "Evidence and presumption in PD diagnostics", IEEE Trans. on Dielectric and Electrical Insulation, Vol. 2, pp.780-795, 1995.

[27] P.K Simpson, “Artificial neural systems; Foundations, paradigms, applications and implementations”, McGraw-Hill, New York, 1990.

[28] Amira A. Mazroua, R. Bartnikas and M. M. A. Salama, “Neural network system using the multi-layer perceptron technique for the recognition of PD pulse shapes due to cavities and electrical trees”, IEEE Trans. on Power Delivery, Vol. 10, pp.92-96, 1995.

[29] H. Gish, “A probabilistic approach to the understanding and training of neural network classifiers”, IEEE International Conference on Acoustics, Speech and Signal Processing, pp.1361-1364, 1990

Chapter 5

AC Sparkover Voltage Properties and Gas Decomposition By-Products Analysis of CF_3I under Non-Uniform Electric Field Configuration

5.1 Introduction

Sulfur hexafluoride (SF_6) is an organic compound extensively used as an insulator in gas circuit breaker (GCB) and gas insulated switchgear (GIS) because it has higher dielectric strength, excellent arc extinction properties, harmless and inactive. However, SF_6 gas is a potent greenhouse effect of 23,900 times that of CO_2 over 100 year period which was announced at COP3. The quest to reduce the emission or replace the greenhouse gas with the same or better dielectric strength with SF_6 gas has been conducted extensively [(1),(2)]. Recently, trifluro-iodo-methane (CF_3I) has been proposed as a potential replacement for SF_6 gas in the insulation of gas insulated electrical power apparatus because of their some better properties. The CF_3I gas is extremely low global warming potential, good long term stability at ambient conditions and relatively low toxicity [(3)]. Moreover, the critical electric field at α-η equal to zero under uniform configuration has relatively higher of 440Td compared to that SF_6 gas[(4)].

Although CF_3I gas has some advantages, there are still many uncertainty items that should be clarified and understood prior to implement to the electric power apparatus in future. So far there were some reports by S.M. Webb et al [(5)] and Gann R.G [(6)] that CF_3I when exposed to sunlight will has a photolysis reaction and produced hexafluoroethane (C_2F_6) gas and dissociation of atomic iodine (I_2). At the same time the reformation of CF_3I also happen which is almost twice as fast as the production of C_2F_6. The reported chemical reaction of CF_3I to the sunlight exposure is as follows,

$$2CF_3I \xrightarrow{h\nu} 2CF_3\bullet + 2I\bullet \longrightarrow \underset{2CF_3I}{C_2F_6 + I_2} \tag{5.1}$$

The analysis of decomposition by-products of CF_3I gas under PD stress is very important to be studied. It is because PD occurring in electric power apparatus

contribute to pre-breakdown phenomena prior to failure when various kinds of defects exist in the apparatus. Thus, the sparkover voltage, PD properties, and the gas decomposition by-products of CF_3I under non-uniform field of AC applied voltage has been investigated and reported in this chapter. The results is useful to provide a design guideline for using CF_3I gas as insulating medium of environmental friendly gas insulating power apparatus.

5.2 Experimental setup

Construction of experimental setup was performed to measure partial discharge, sparkover voltage and all the PD charge quantity with cumulative charge q_c and to be able to analyze gaseous by-products of CF_3I suffering PD. The system enables to obtain quantitative relation between the q_c and the amount of the by-products. The detail of the experimental setup was explained in chapter 2, section 2.3.

5.2.1 Electrode configuration

In order to analyze the gas by-product of CF_3I suffering PD for a given time under non-uniform electric, an ideal electrode configuration producing maximum PD was obtained. Considering PD in the power apparatus are generated from various kind of defects, optimum cumulative charge q_c was selected to verify the gaseous decomposition by-products of CF_3I gas. A set of experiment was conducted to ensure the condition inclusive pressure and electrode configuration giving the optimum q_c of PD. Fig. 5.1 shows the cumulative charge q_c as a function of time of PD occurrence t_{PD} at 80% of sparkover voltage. The needle-plane electrode system consisted of the needle electrode in hemispherical shape with diameter tip of 1 mm and 0.5 mm with the gap of 10mm. The test pressures were 0.1 and 0.2 MPa. It was found from the experiment results that the electrode configuration giving an optimum cumulative charge q_c was the needle-plane with the diameter tip of 1 mm and the gap of 10mm under 0.1 MPa. Thus, this configuration was selected for the gas decomposition by-products analysis. The plane electrode with a diameter of 68mm was connected to the ground. The field utilization factor, which is determined as average strength of electric field divided by maximal strength of electric field, was 0.06.

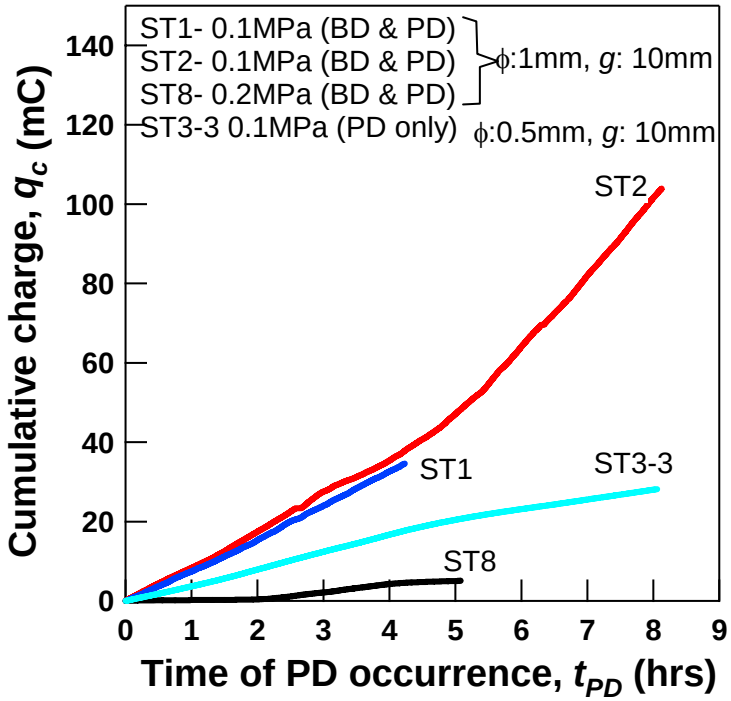

Fig. 5.1 Cumulative charge q_c as a function of time of PD occurrence t_{PD} at 80% of sparkover voltage for the selection of electrode configuration

5.3 Experimental results and discussions

5.3.1 Sparkover voltage and partial discharge inception voltage

Fig. 5.2 shows sparkover voltage (V_s) and partial discharge inception voltage (V_{PDI}) in CF_3I gas as a function of pressure compared to those of SF_6 gas in same size of the container used for CF_3I gas. V_s in CF_3I gas was relatively 70% of V_s in SF_6 gas at 0.1 MPa. V_s in SF_6 gas at 0.1 MPa of 450 cc container has been relatively same value with V_s in SF_6 gas at 0.1 MPa of a chamber previously obtained by Kiyama et al [7]. V_s of CF_3I decays to 40% at pressure 0.2 MPa different with the result of SF_6 gas obtained by Kiyama et al. The results show that V_s in CF_3I gas was significantly different from that of SF_6 gas under AC applied voltage. On the other hand, $V_{PDI(-)}$ in CF_3I is almost the same with $V_{PDI(-)}$ in SF_6 gas at 0.1 MPa. The result agrees with comparable same critical field between the two gases. $V_{PDI(+)}$ in CF_3I has 70% and 40% higher than $V_{PDI(+)}$ in SF_6 gas at 0.1 MPa and 0.15 MPa. $V_{PDI(+)}$ in CF_3I at 0.2 MPa was not detected with the applied voltage (V_a) at 80 % of V_s. The result obviously shows that CF_3I has different

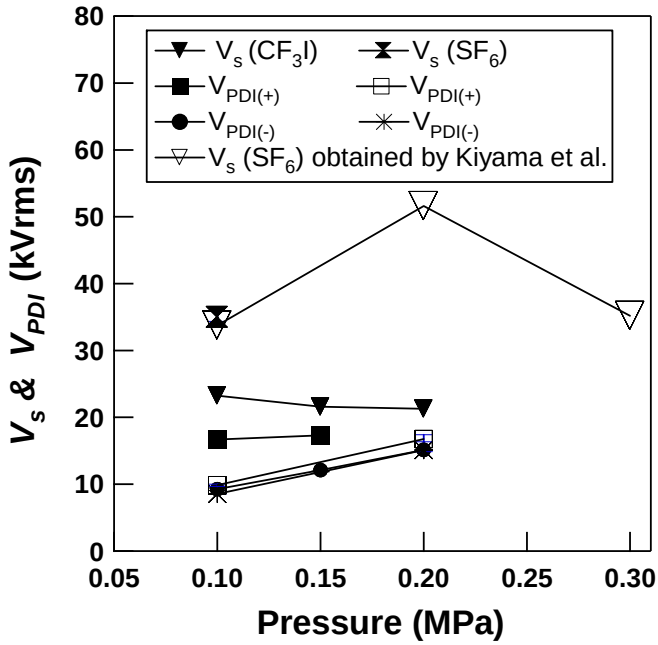

Fig. 5.2 Sparkover voltage and partial discharge inception voltage in CF_3I as a function of pressure compared to SF_6 gas

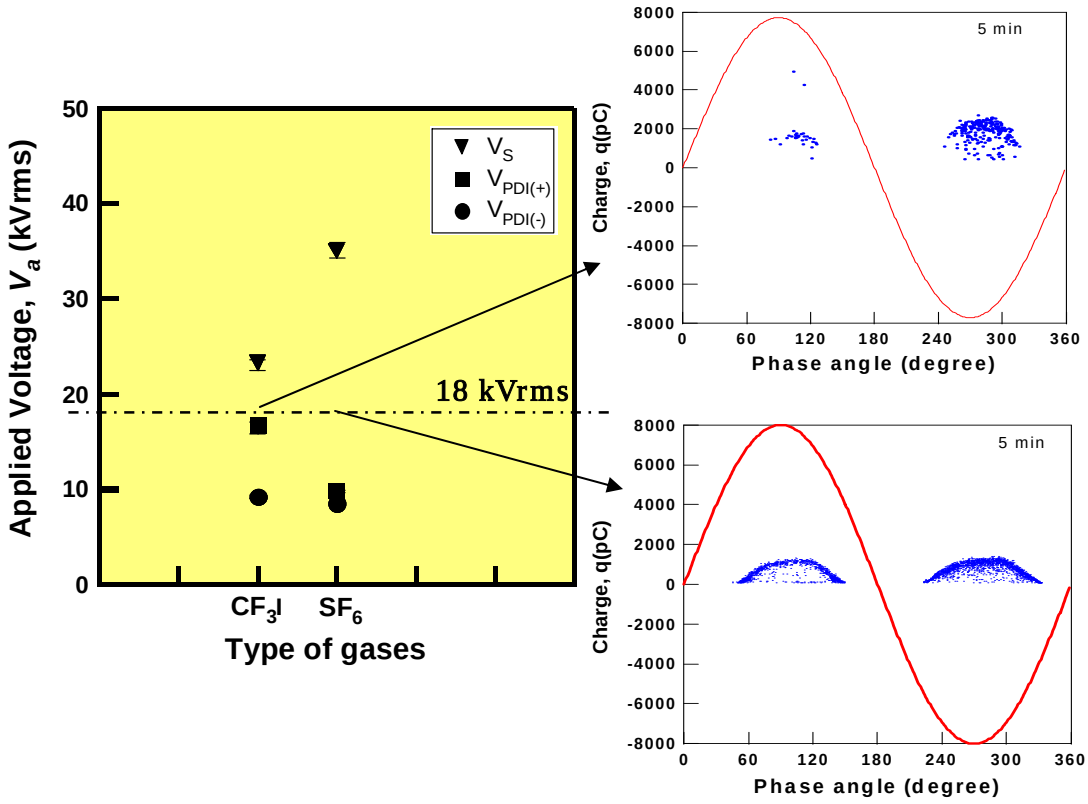

Fig. 5.3 Phase-resolved discharge at 18 kVrms of V_a comparing between CF_3I and SF_6 gas at 0.1 MPa

dielectric performance with SF_6 gas under non-uniform electric field of AC applied voltage. The difference of the pressure dependence of V_s in CF_3I gas and SF_6 gas may arise from the difference in corona stabilization effect. Namely, the corona stabilization effect of CF_3I gas may be smaller than that of SF_6 gas.

Fig. 5.3 shows the comparison of phase-resolved discharge between CF_3I and SF_6 gas at 0.1 MPa of 18 kVrms. The experimental result depicts that the generation of charge in positive half cycle of PD in CF_3I is approaching 6000 pC. The amount of charge in CF_3I is relatively higher compared with that in SF_6 gas which is below 2000 pC. It is suggested that the higher magnitude of charge in positive half cycle of CF_3I may yield to the lower triggering of sparkover voltage V_s.

5.3.2 Gaseous decomposition by-products of CF_3I suffering PD

Three samples SM1~SM3 with the same amount of water content were prepared to obtain three different cumulative charge of PD for the gas analysis purpose. PDs were generated for a given time at 18 kVrms V_a which is 80% of V_s. The amount of water content was from 250 to 400ppm. Fig. 5.4 shows the plot of cumulative charge q_c as a function of PD period t_{PD} in CF_3I at 0.1 MPa. The cumulative charge q_c seems to linearly increase with the increase of t_{PD}. The cumulative charge q_c for a given t_{PD} of 8, 12 and 20 hrs were 30, 67 and 161 mC, respectively.

Fig. 5.5 shows the photograph of a blotch substance on the surface of plane electrode after 20 hrs of the PDs occurrence. The reddish brown colour of dry blotch substance was obviously observed on the surface at the centre of the plane electrode. The similar blotch substance has been observed for the other two samples.

The gaseous by-products of CF_3I suffering PD with the variance of q_c in the presence of 250 to 400ppm of water contents were verified with the GC-MSD devices. Fig. 5.6 shows the gas decomposition fragment of CF_3I for various q_c after PD test analyzed with GC-MSD device for each sample and comparing with virgin gas as reference. The results revealed that hexafluoroethane (C_2F_6), tetrafluoroethane (C_2F_4), pentafluoroethyliodide (C_2F_5I), octafluoropropane (C_3F_8), trifluoromethane (CHF_3), hexafluoropropene (C_3F_6) and methyliodide (CH_3I) were the gaseous by-products of CF_3I under the PD stress. From the time fragmentation of CF_3I gas decomposition results obtained by GC-MSD, the mass spectroscopy fragmentation of dominant gaseous by-product was verified from the peak desorption of time fragments shown in Fig. 5.6. Desorption peaks for mass fragments of m/z = 69 (CF_3) and 119 (C_2F_5) were assigned to C_2F_6 as shown in Fig. 5.7. Desorption peak for mass fragments of m/z = 50

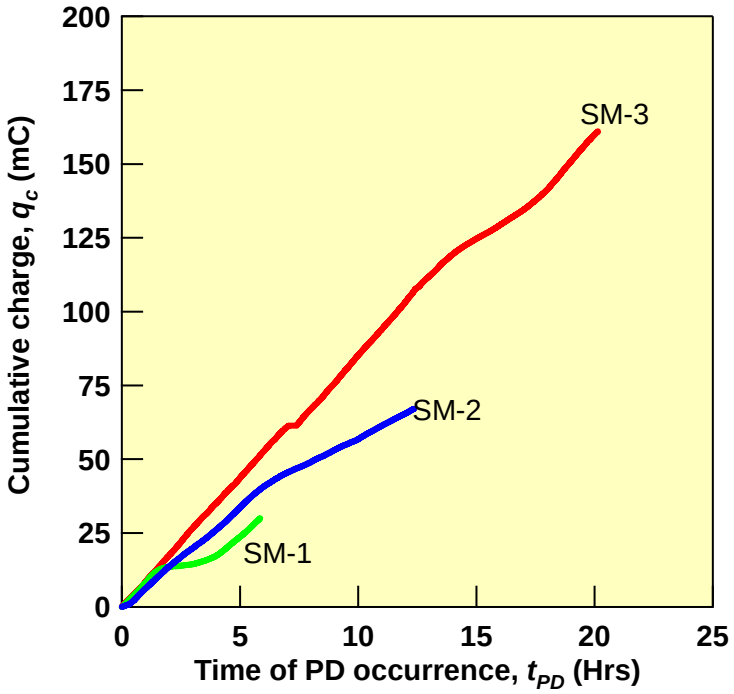

Fig. 5.4 Cumulative charge as a function of PD period in the presence of water content (Va = 18 kVrms, water content from 250 to 400 ppm)

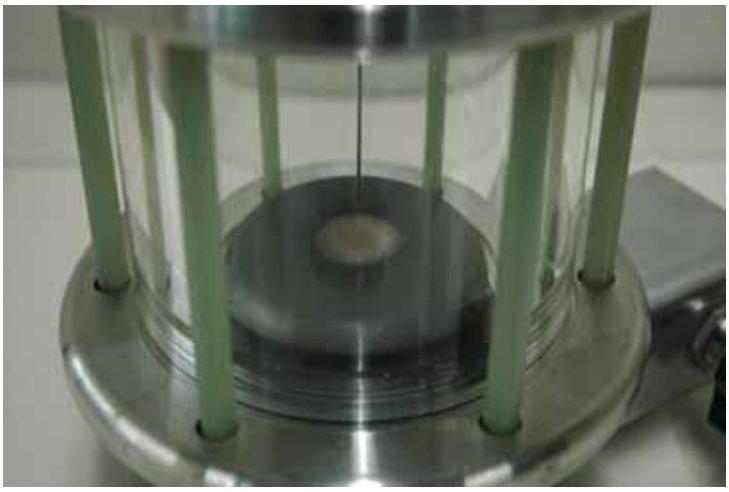

Fig. 5.5 Photograph of reddish brown colour of dry blotch substance on the surface of plane electrode after 20 hrs (SM3) of the PDs occurrence.

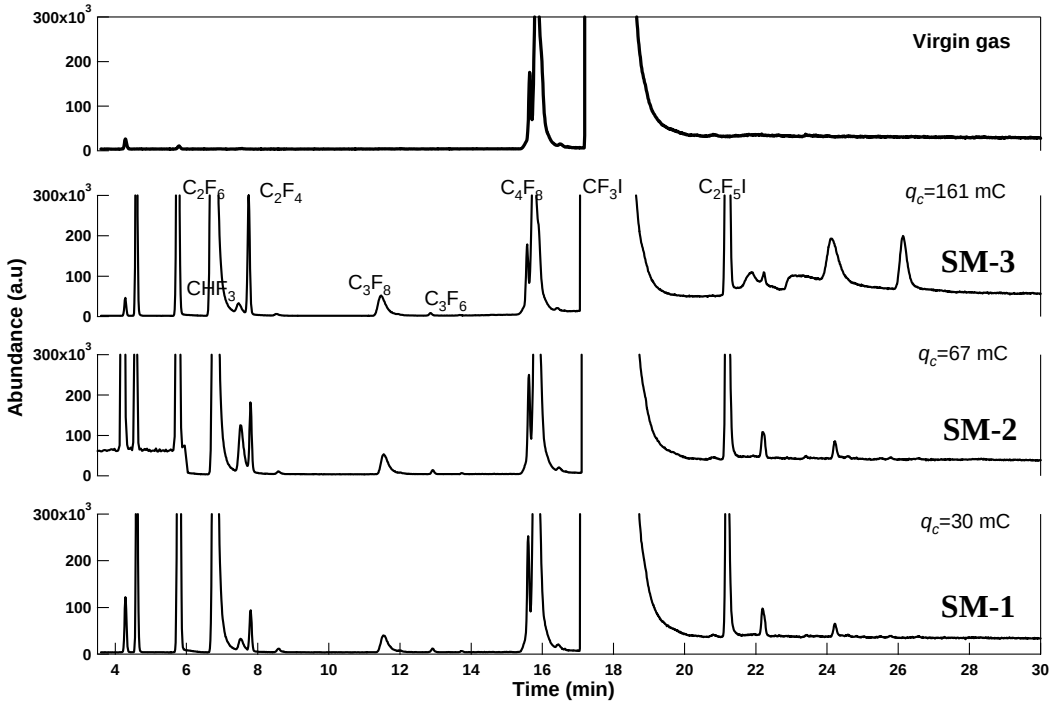

Fig. 5.6 Gaseous by-products result of GC-MSD analysis

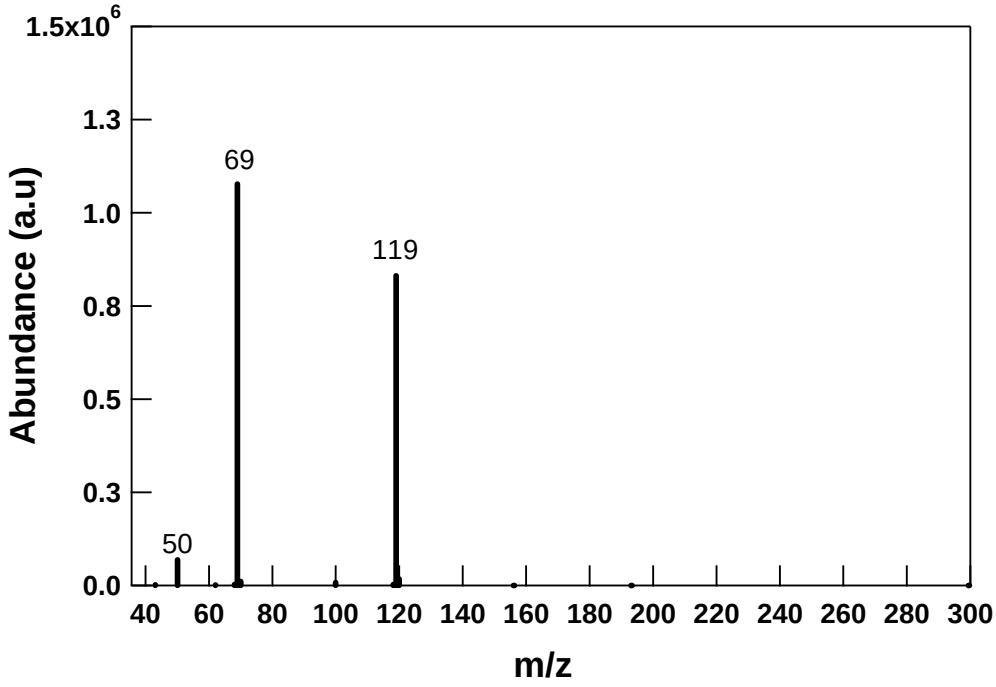

Fig. 5.7 Mass spectroscopy of C_2F_6 gas
(m: mass number, z: charge number)

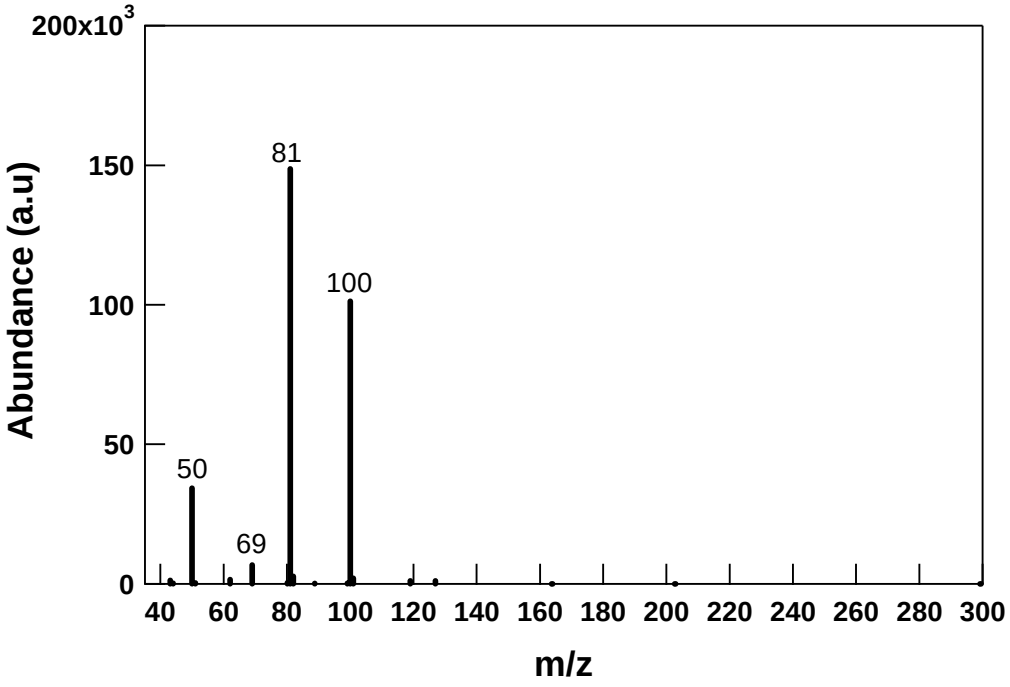

Fig. 5.8 Mass spectroscopy of C_2F_4 gas
(m: mass number, z: charge number)

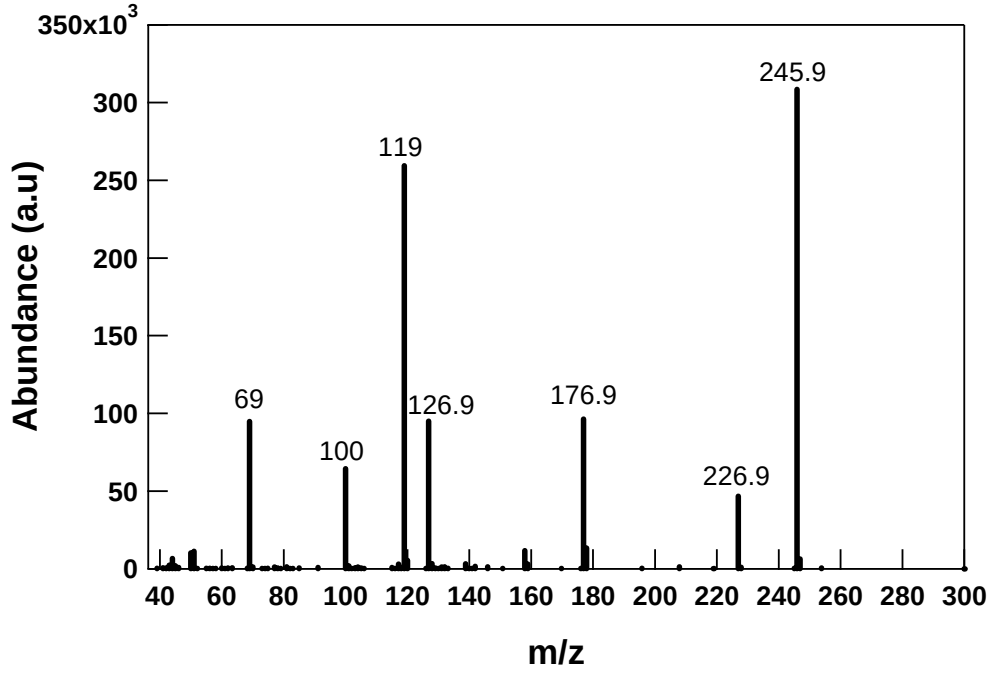

Fig. 5.9 Mass spectroscopy of C_2F_5I gas
(m: mass number, z: charge number)

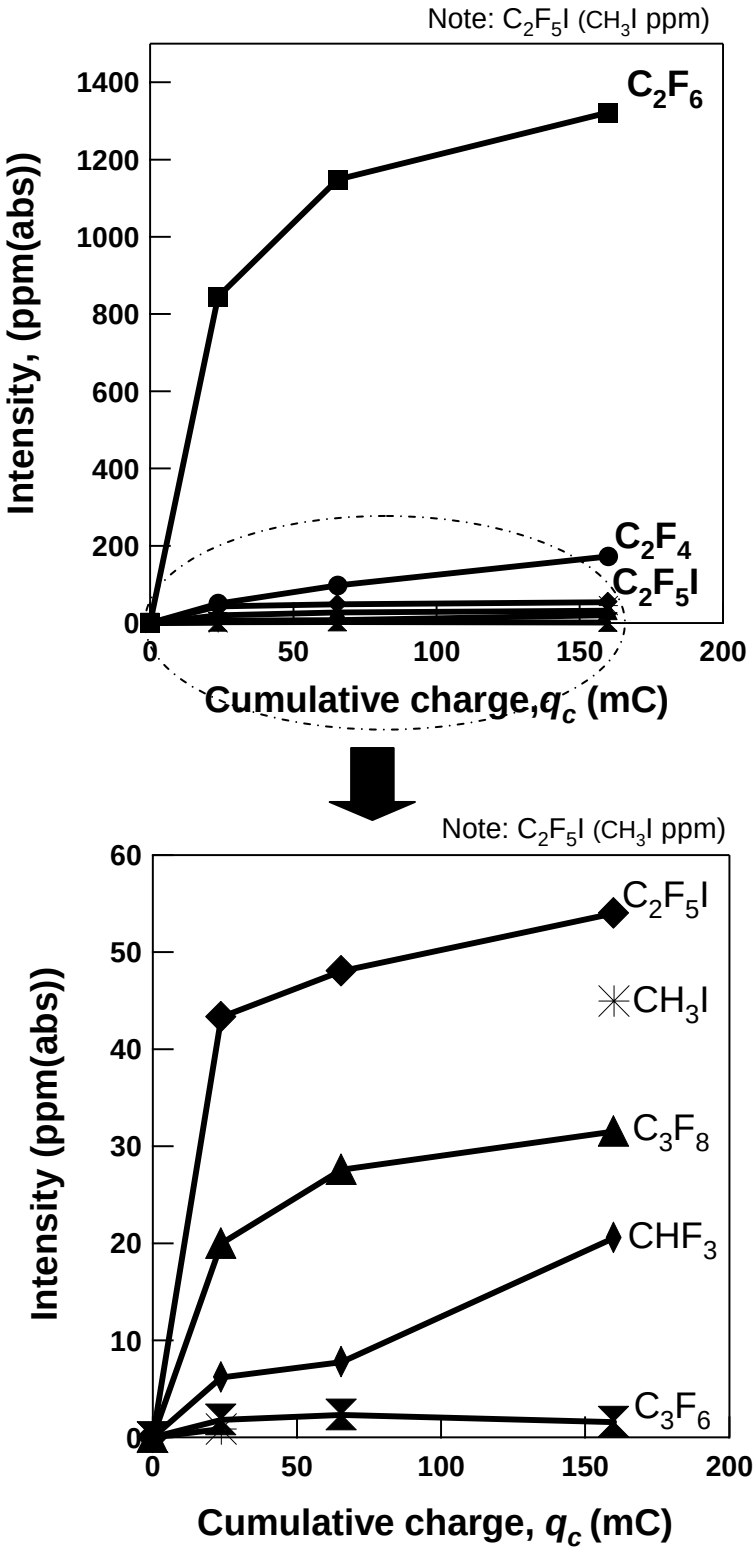

Fig. 5.10 Gaseous by-products as a function of cumulative charge q_c at 18 kVrms (80% of V_s, water content: 250 ~ 400 ppm).

(CF_2), 81 (C_2F_2) and 100 (C_2F_4) were assigned to C_2F_4 as shown in Fig. 5.8. Desorption peak for mass fragments of m/z = 246 (C_2F_5I), 227 (C_2F_4I), 119 (C_2F_5) and 100 (C_2F_4) were assigned to C_2F_5I as shown in Fig. 5.9. The results of mass spectroscopy obtained from the experiment are consistent with that published in National Institute of Standard and Technology (NIST) [8]. Fig. 5.10 depicts the relation between q_c and the dominant gaseous by-products of CF_3I, i.e C_2F_6, C_2F_4 and C_2F_5I with the amount of 1300, 200 and 55(CH_3I) ppm, respectively. The C_2F_5I with the amount of 55(CH_3I) ppm was determined corresponding to the ratio of peak desorption area of C_2F_5I to CH_3I times the peak desorption intensity of CH_3I. The other gaseous by-products such as C_3F_8, CH_3I, CHF_3 and C_3F_6 were detected to be less than 50 ppm. The gaseous by-products seem to abruptly increase with q_c from 0 to 30 mC and gradually increase when q_c exceeded 30mC. Pentafluoro-2-butene (C_4F_8) gas was inherently detected in the virgin gas of CF_3I, thus the larger variance of desorption peak of C_4F_8 after PD test was not detected.

It is generally known that PD gives rise to high-energy electrons, ionic species, ultraviolet light radiation, and local high temperature region. The result shows that C_2F_6 became the dominant gas by-product, suggesting that PD occurrence in CF_3I gas would cause similar reaction as photolysis reaction of CF_3I in direct light exposure as follows [5],

$$2\,CF_3I \xrightarrow{h\nu} 2\,CF_3\bullet \; + \; 2I\bullet \longrightarrow C_2F_6 + I_2 \qquad (5.2)$$

CF_3I gas is chemically and photochemically active due to weak C-I bond compared with that of C-F bond. The bond dissociation enthalpy of C-I is 209 $KJmol^{-1}$ which is lower compared with C-F bond of 552 $KJmol^{-1}$[6]. Thus, it can be said that PDs result in production of C_2F_6 gas and dissociation of I_2. The formation of I_2 is easy due to its lower bonding enthalpy of 148 $\mp$0.2 $KJmol^{-1}$. Although the atomic iodine (I) has desorption peak of *m/z* 127, where *m* is mass and *z* is charge, it was not detected by the GC-MDS analysis. The atomic I was found to be attached on the surface of the plane electrode when it was analyzed with energy dissociation X-ray (EDX) microanalysis. Thus, the reddish brown colour of dry blotch substance on the surface at the centre of the plane electrode shown in Fig. 5.5 was the attachment of the atomic iodine dissociation due to the PD stress.

It also has been suggested that C_2F_6 can be formed from the reaction of trifluoromethyl (CF_3) radicals as written in eq.(5.3)[3],[9],[10]. The CF_3 radicals can be formed from the electron impact excitation (eq.(5.4))[3] or electron impact ionization

(eq.(5.5))[3],[11],[12] as follows

$$^{\bullet}CF_3 + CF_3I \longrightarrow C_2F_6 + {}^{\bullet}I \tag{5.3}$$

$$CF_3I \longrightarrow CF_3I^{*} \longrightarrow {}^{\bullet}CF_3 + I^{\bullet} \tag{5.4}$$

$$CF_3I \longrightarrow CF_3I^{+} + e^{-} \longrightarrow I^{+} + {}^{\bullet}CF_3 + e^{-} \tag{5.5}$$

The CF_3 radicals where desorption peaks for mass fragments of m/z = 69 were identified to exist in the mass spectroscopy of C_2F_6, C_2F_4 and C_2F_5I gas as shown in Fig. 5.7. 5.8 and 5.9, respectively. The existence of the CF_3 radicals well corresponds to the consideration of CF_3 radical formation from electron impact excitation or electron impact ionization as indicated in eq.(5.4) and eq.(5.5), respectively. Thus, it is apparent that the high probability of CF_3 radical reaction yields to the formation of C_2F_6 by-product as written in eq.(5.3).

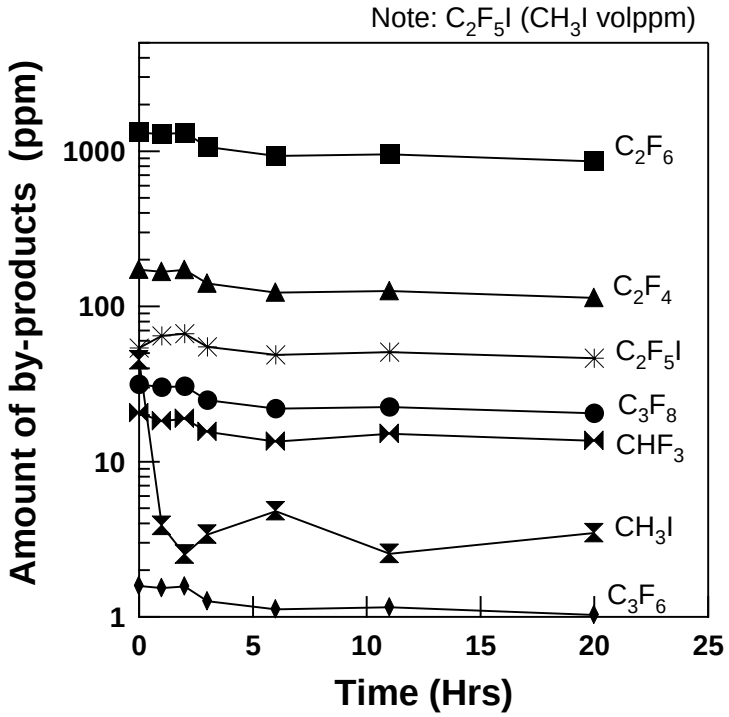

Fig. 5.11 Temporal change of amount of gaseous by-products of CF_3I

In addition, the temporal change of the amount of decomposition products after the PD test has been analyzed. Fig. 5.11 depicts the plot of temporal change of the amount of the gaseous by-products of CF_3I. The results revealed that the amount of the by-products of CF_3I gas suffering PD almost remained for 20 hours after the PD test except CH_3I. There is no significance reformation of CF_3I to the initial state after the PD stress.

5.4 Conclusions

The gas decomposition of CF_3I suffering PD was analyzed. The dominant gaseous by-products were C_2F_6, C_2F_4 and C_2F_5I with the amount of 1300, 200 and 55(CH_3I)ppm for the cumulative charge q_c of 30, 67 and 161 mC, respectively. The other gaseous by-products were C_3F_8, CHF_3, C_3F_6 and CH_3I whose amounts were less than 30 ppm. Moreover, the by-products of CF_3I suffering PD almost remained for 20 hours after the PD test except CH_3I.

References

[1] Tadasu Takuma, Osamu Yamamoto and Shoji Hamada, "Gases as dielectric", Gaseous Dielectrics X, pp.195-204, 2004.

[2] Lutz Niemeyer, "A systematic search for insulation gases and their environmental evaluation", Gaseous Dielectric VIII, pp.459-464, 1998.

[3] Nozomi Nakayama, Elizabeth E. Ferrenz, Denise R.Ostling, Andrea S. Nichols, Janelle F. Faulk and Christopher R. Arumainayagam, "Surface chemistry and radiation chemistry of CF_3I on Mo(110)", Journal of Phys. Chem. B, 108(13), pp.4080-4085, 2004.

[4] M. Kimura, Y. Morokuma and Y. Nakamura, "A measurement of ionization coefficients in pure trifluoro-iodo-methane", Paper of Technical Meetings on Electrical Discharges, IEE Japan, ED-02-98, pp.13-18, 2002 (in Japanese)

[5] S.M Webb, D. Jaksch, R.A. McPheat, E. Drage, E. Vasekova, P. Limao-Vieira, N.J. Mason and K.M. Smith, "High-resolution, temperature dependent, fourier transform infrared spectroscopy of CF_3I", Journal of Quantitative Spectroscopy & Radiative Transfer, 94, pp.425-438, 2005.

[6] Gann R.G., "Photodegradation of CF_3I", Fire Suppression System Performance of Alternative Agents in Aircraft Engine and Dry Bay Laboratory Simulations, Vol. 1, Section 3. NIST SP 890, pp.77-95, 1995.

[7] K. Kiyama, N. Yokoyama, S. Ohtsuka, S. Matsumoto, S. Kaneko, S. Okabe and M. Hikita, "Examination of partial discharge characteristics by discharge light emission in CO_2 and SF_6 gases ", The 12^{th} Asian Conf. on Electrical Discharge, pp.265-268, 2005.

[8] Chemistry webbook, NIST standard reference database, http://webbook.nist.gov

[9] I. McAlpine and H. Sutcliffe, "A comparison of the radiolysis of liquid bromotrifluoromethane with the radiolysis of liquid trifluoroiodomethane", The Journal of Physical Chemistry, Vol. 76, No. 15, pp.2070- 2071, 1972.

[10] Tacheng Hsieh and Robert J. Hanrahan, "Gas phase radiation chemistry of trifluoromethyl iodide", Radiat. Phys. Chem., Vol. 12, pp.153-160, 1978.

[11] I. McAlpine and H. Sutcliffe, "The radiolysis of liquid trifluoroiodomethane", The of Physical Chemistry, Vol. 74, No. 7, pp.1422-1425, 1970.

[12] I. McAlpine and H. Sutcliffe, "The radiolysis of trifluoroiodomethane in the gas phase", The of Physical Chemistry, Vol. 73, No. 10, pp.3215-3218, 1969.

Chapter 6

Summary

6.1 Summary

Sulfur hexafluoride (SF_6) gas is an inorganic compound used as an insulator because it has high dielectric strength, excellent arc extinction properties, harmless and inactive in nature. Moreover with implementation of SF_6 gas in power substation and transmission, the occupied area of power apparatus can be reduced. That is why many utilities have implemented SF_6 gas in power substation or transmission extensively. However according to COP3 the emission of SF_6 gas to the atmosphere due to the leakage of power apparatus would affect the GWP. Due to this reason it became a mandatory requirement to protect environment friendly condition in order to have a healthy life. Many researchers all over the world are trying all their best to search the best solution to minimize or to avoid the greenhouse gas emission and it became an ethically hoped.

Vacuum is one of the promising environmental friendly dielectric media that has an excellent dielectric strength. Vacuum circuit breaker (VCB), for an example, is a device that may be employed to replace the usage of SF_6 gas insulated apparatus in the future. Most of the VCB used in power systems are in medium voltage class and research for the development of higher rated voltage is proceeding now. The successful of high rated voltage development may expand the application of vacuum technology in circuit breaker and switchgear for power substation. In fact, from numerous numbers of reports, the application of VCB to high rated voltage may realize in future. Thus from this point of view it also indicates the diagnostic devices to monitor the performance of VI is highly recommended in future.

At the same time, recently, an extremely low GWP effect gas with relatively low toxicity such as trifluro-iodo-methane (CF_3I) was innovated. CF_3I gas is colorless, nonflammable and has lower environmental impact to the effect of GWP less than 5 and 0.0001 of ozone depleting potential (ODP). CF_3I gas may eventually replace SF_6 gas

because recent studies have demonstrated the limiting electric field $(E/N)_{lim}$ (at α-η=0) under uniform configuration has relatively higher of 440Td compared to that SF_6 gas[10]. However, since it is innovative gas, there are still many uncertain items that should be investigated such as the insulation properties under non-uniform electric field of different electric field utilization factor and water content, partial discharge (PD) properties and by-product analysis of pure CF_3I and CF_3I mixture gas, the influence of gaseous by-products on electrical insulation properties of solid insulating material and the PD mechanism of CF_3I. Solving these issues would lead to contribution of design guideline for utilizing CF_3I gas as insulating medium of environmental friendly gas insulating power apparatus. Eventually it would also propose to the idea of diagnostic technique of the gas insulation performance.

From the statement above it is apparent that the high voltage apparatus development concerning the environmental friendly aspects is greatly important. Since the VI in high voltage application as well as CF_3I gas was among the high potential media on replacement of the usage of SF_6 gas, the research in this thesis dealt with the diagnosis of vacuum performance in VI and decomposition by-products analysis of CF_3I gas.

6.2 Summary of the findings obtained from the investigations

In chapter 2, described mainly were about the experimental construction of the research related to the VI and the CF_3I gas together with measuring systems. For VI, the construction of the measurement circuit was performed to measure PD properties, phase resolve discharge pattern and the optical properties of PD occurrence in VI at various pressures. Meanwhile for CF_3I gas analysis, the construction of the experimental setup was performed to measure all PD charge quantity with cumulative charge and to analyze gaseous by-products of CF_3I suffering PD.

In chapter 3, the properties of discharge and emitted electromagnetic wave spectrum in low vacuum region of VI were discussed. The experiment was conducted in closed and open contact conditions with ceramic type VI. Only two level of pressure was available at 1 (133 Pa) and 5 Torr (665 Pa) of air. A CT and loop antenna were used to measure the discharge current and EMW spectrum emitted by the discharge occurring in VI. PDIV in both pressures was measured and compared to the Paschen's curve of breakdown voltage in air. The results gave good agreement between them and also indicated that the discharge was occurring in VI. The relation between the applied

voltage V_a and discharge current pulse in the closed contact condition showed that the peak of current pulse increased when V_a increased from PDIV to 5 kVrms and then decreased when V_a increased further. The same situation also happened to the spectrum intensity of the EMW. The results of measured spectra revealed that two peaks of spectrum intensity appeared at 6 MHz and 24 MHz. The 6 MHz frequency component was attributed to LC resonance of the external circuit. On the other hand, the 24 MHz frequency component was considered to arise from the nature of discharge itself occurring in VI. The discharge was considered to occur between the electrode and the shield of VI since the reflections appearing in the waveform might be due to large impedance of the stray capacitance C_s, resulting in an impedance mismatching in the external circuit. In the open contact condition, the gap distance dependence of the discharge current in region A ($pd \leq 20$ Torr·mm) was found to obey an exponential growth with the gap length. Therefore the discharges were considered to occur between the fixed and the movable electrode. The current intensity in region B ($20 \leq pd \leq 100$ Torr·mm)decreased abruptly to 30 ~ 50 mA as *pd* increased from 20 to 60 Torr・mm. Based on the measured current waveforms, it can be considered that the discharge occurs between the electrode and the shield, since the current intensity in region B was almost same irrespective of *pd*.

In chapter 4, the PD properties and the determination of gas pressure in VI based on PD was introduced. The PD properties in low vacuum region of practical vacuum interrupter filled with air and SF_6 gas were investigated. In this experiment, the glass vessel of VI was used for a better understanding of optical PD properties in the low vacuum region and to know the location of PD occurrence as the pressure varied at a constant V_a. In order to simulate the possible leakage due to slow leak, the pressures were set at 1 Pa to 1 kPa order. The measurement of PD occurring inside the vacuum interrupter was performed with CT, PMT, ICCD camera and PD measurement device. From the result of the experiment, it is found that the pressure of vacuum interrupter can be distinguished on the basis of the rise time, peak intensity and width of the discharge light pulse. For air, a relatively longer rise time of 2μs with a smaller magnitude (less than 0.5mA) was attributed to a Townsend-like discharge at pressure 260 Pa while a sharper rise time of 10-100ns with a larger magnitude (greater than 1mA) was characterized as a streamer-like discharge above 260 Pa. For the vacuum interrupter filled with SF_6 gas, the discharge pulses at pressures below 50 Pa had the relatively larger rise time of 100ns order, larger pulse width of 2μs order and the intensity of the ratio of 0.1 from that in 50 Pa above. While at pressures above 50 Pa, the rise time had relatively smaller value of 10 ns and pulse width of 0.1μs order. The result shows

significant difference of discharge characteristics compared with that in low vacuum of vacuum interrupter filled with air. Eventually, the estimation of gas pressure in VI based on phase-resolved discharge characteristics utilizing artificial neural network was proposed. The PDs generated at each pressure level in VI was measured with PMT and special designed PD measuring device which represented in ϕ-i-n (ϕ: phase angle of V_a; i: PD light intensity; n: number of PD pulses distributed during 300 cycles of V_a) patterns during 300 cycles of the applied voltage (V_a). Only the ϕ-n patterns were considered to used in determination of gas pressure of VI because i of PD light pulses varies with the distance of PMT from the specimen. The gas pressure inside VI was determined using the data of ϕ-n patterns with the back propagation neural network approach (BP NN). The neural network assistant software was adopted in this analysis. The normalized numbers of pulses of 100 samples were assigned for learning and testing algorithm for different pressure levels. The optimum hidden layer and number of iterations were suggested by considering the minimum recognition error of BP NN. The estimation of gas pressure based on PD phase-angle characteristics using the NN approach gave a recognition success rate from 93 to 98 %. Thus the proposed of neural network algorithm is applicable to the discrimination of gas pressure in VI using ϕ-n patterns.

Chapter 5 discussed about the sparkover voltage properties and gaseous by-products analysis of CF_3I gas under non-uniform electric field configuration. The investigation on quantitative relation between cumulative charge of PD and by-products of CF_3I gas after PD occurrence was conducted. The cumulative charge of PD at 0.1 MPa was obtained using the developed PD measuring system for a given time under the non-uniform electric field configuration. The electrode configuration was the needle-plane electrode where the needle electrode was in hemispherical shape with diameter tip of 1mm and gap of 10mm under the pressure of 0.1MPa. These electrode configurations were found to give an optimum cumulative charge of PD occurrence in CF_3I gas test. The plane electrode had a diameter of 68mm and connected to the ground. After the test, the amount of gaseous by-products of CF_3I gas was measured with a GC/MS detector for a given cumulative charge q_c to discuss the quantitative relation between q_c and the amount of the by-products. It is generally known that PD gives rise to high-energy electrons, ionic species, ultraviolet light radiation, and local high temperature region. The results revealed that the dominant by-products were C_2F_6, C_2F_4, and C_2F_5I with the amount of 1300, 200 and 55 (CH_3I) ppm for the cumulative charge q_c of 30, 67 and 161 mC, respectively. This suggests that PD in CF_3I gas would cause similar reaction as photolysis reaction of CF_3I gas. The other gaseous by-products were

C_3F_8, CHF_3, C_3F_6 and CH_3I whose amounts were less than 30 ppm. After the PD test, reddish brown color of dry blotch obviously been observed on the center of plane electrode and changed to very light reddish brown with bright white color of dry blotch for 20 hours of PD occurrence. Probably iodine may be attached on the surface of the plane electrode.

Moreover, after the PD test, temporal change of the amount of the gaseous by-products was analyzed with GC/MS. The results revealed that except CH_3I the amount of the by-products of CF_3I gas suffering PD almost remained for 20hous after the test. Thus, the result indicates no significance reformation of CF_3I at initial stage as before PD stress. In addition, the AC sparkover voltage V_s, PD inception voltage V_{PDI+} and V_{PDI-} were also obtained at 0.1 MPa to 0.2 MPa. The experimental results revealed that the negative V_{PDI-} of CF_3I gas was almost same as that of SF_6 gas, while V_s of CF_3I was smaller than that of SF_6 gas. The result suggests that CF_3I has different dielectric performance with SF_6 gas under non-uniform electric field of AC applied voltage. The difference of the pressure dependence of V_s in CF_3I gas and SF_6 gas may arise from the difference in corona stabilization effect.

6.3 Practical significance of the result obtained in present work

So far there have been no adequate studies on PD characteristics and optical observation of PD occurrence especially using practical VI. Most of them were utilizing the vacuum chamber in their experiments work. This work is the first one ever proposed utilizing the practical VI with the construction of experimental circuit that simulating the actual situation in cubicle-gas insulated switchgear (C-GIS) in order to investigate the PD properties and to propose the diagnostic technique based on PD by neural network approach. The results revealed from the experiment are very useful and important as a fundamental knowledge to the estimation of VI performance without any detachment at medium voltage (MV) and HV application. The PD properties in low pressure of air and SF_6 gas were well explained and understood by measuring the PD light pulses and observation of PD location. It gives knowledge as a guideline to improve the design of VI especially for the HV development purpose.

For the CF_3I gas, the knowledge corresponding to insulation performance, gaseous by-products and the other aspects related to electrical GIS apparatus is not well defined. Although the research on CF_3I gas was conducted previously, and CF_3I gas is known to undergo rapid photolysis in the presence of sunlight which generates C_2F_6 and reformation of CF_3I. The analysis of decomposition by-products of CF_3I gas under PD stress is very

important to be studied. It is because PD occurring in electrical power apparatus contributes to pre-breakdown phenomena prior to failure when various kinds of defects exist in the apparatus. The results reported in this dissertation is useful to provide a design guideline for realizing CF_3I gas as insulating medium of environmental friendly gas insulation power apparatus. The apparent of the gaseous by-products due to PD stress also would contribute a guideline for the development of diagnostic system on insulation performance of CF_3I based on chemical detection method.

6.4 Future works and developments

6.4.1 Development of diagnostic system for insulation performance of vacuum interrupter

From the knowledge of ϕ-*n* pattern of PD recognition technique with the neural network back propagation approach, the sophisticated diagnostic system for determination of VI performance can be developed. Since the VI is expected to be implemented in high voltage application, the diagnostic system allowing to monitor the pressure level of VI on-line and real time is highly recommended.

6.4.2 PD measurement and by-product analysis of CF_3I

PD measurement and by-products analysis of CF_3I under PD stress at various parameters such as gas pressure, electric field utilization factor (needle electrode tip radius, gap length etc.) and the influence of water content should be further investigated in future to obtain an optimum condition of higher dielectric strength. In addition, it is also essential to perform the PD measurement and investigate the gaseous by-products analysis of CF_3I mixture for the design purpose. The investigation of various parameters would provide an obvious knowledge and advanced guideline for the development of CF_3I gas in electrical power apparatus for replacing the SF_6 gas.

6.4.3 The influence of the gaseous by-products of CF_3I on electrical insulation properties

The influence of gaseous by-products on electrical insulation properties of solid insulating material such as epoxy resin and polymer should be investigated. This hypothesis is greatly important to have a better understanding for the design of solid electrical insulation when CF_3I gas is utilized in electric power apparatus.

6.4.4 Investigation on partial discharge mechanism of CF_3I gas

This dissertation reported the AC V_s and PDIV properties under non-uniform electric field at 0.1 to 0.2 MPa have different dielectric performance with that SF_6 gas. Further investigation on PD mechanism of CF_3I is needed to clarify the reason of different dielectric performance with SF_6 gas.

PD mechanism of CF_3I gas should be clarified by sophisticated observation technique such as ultra-high speed electrical and optical measuring methods.

Appendix A

A.1 Determination of distance between the shield and the grounded metal plate by using Coulomb 3D electric field calculation

The distance D, between the shield and grounded metal plate was calculated automatically by adding the value of stray capacitance at 10pF. Fig. A.1 shows the diagram of the VI using Coulomb 3D electric field software to determine the distance between the shield and the grounded metal plate.

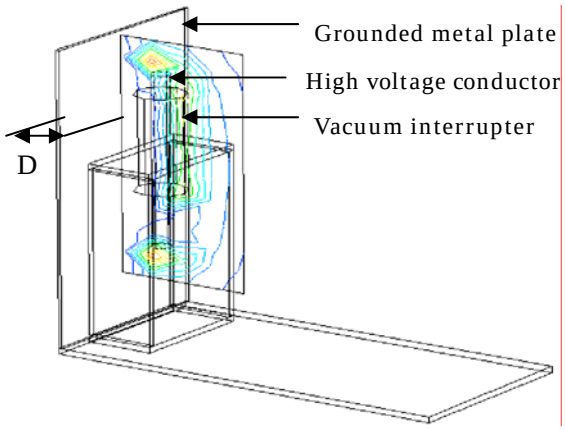

Cs (pF)	D (mm)
8.2	34
8.4	30
11.2	28
10	26.8

Fig. A.1: Diagram VI using Coulomb 3D electric field software to determine gap between the shield and the grounded metal plate giving stray capacitance, *Cs* = 10pF

A.2 Electromagnetic Wave Spectrum of Emitted Discharge in Low Vacuum

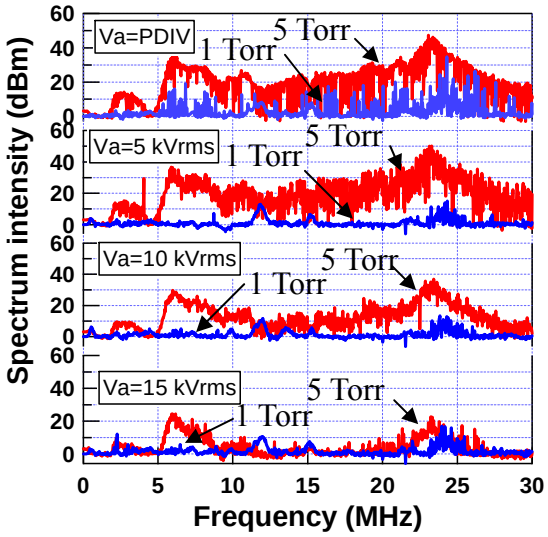

Fig. A.2.1 EMW spectrum measured by loop antenna at closed contact condition of ceramic type VI as applied voltage varies

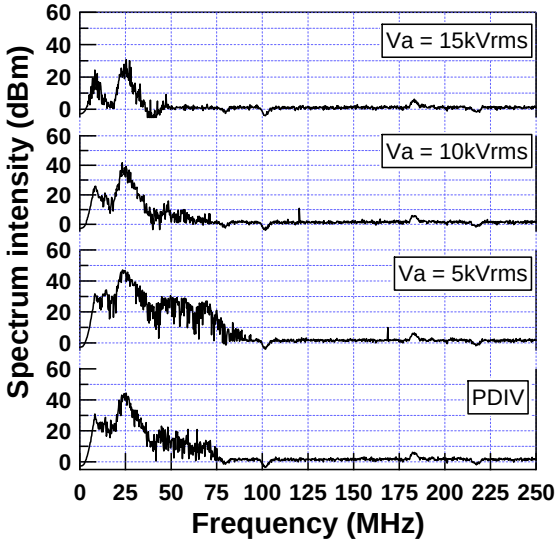

Fig A.2.2 EMW spectrum measured by CT at closed contact condition of ceramic type VI as applied voltage varies for pressure 5 Torr

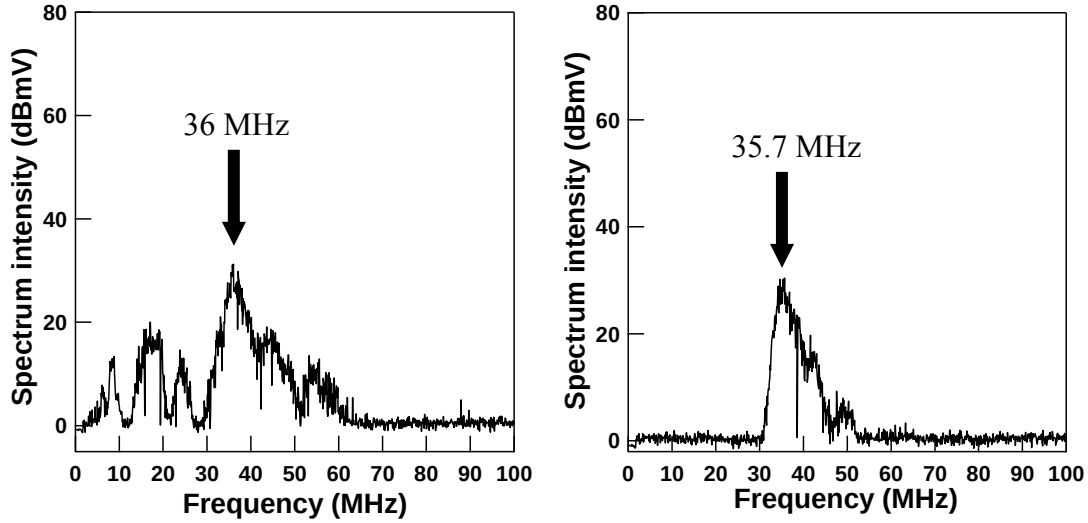

a) l = 1m, h = 0.5m　　b) l = 0.4m, h = 0.2m

Fig. A.2.3 EMW spectrum of discharge measured by bar antenna at closed contact condition of glass type VI with air for different cable length l and height from the ground h. (P = 10 Torr; Va = PDIV (2.8 kVrms))

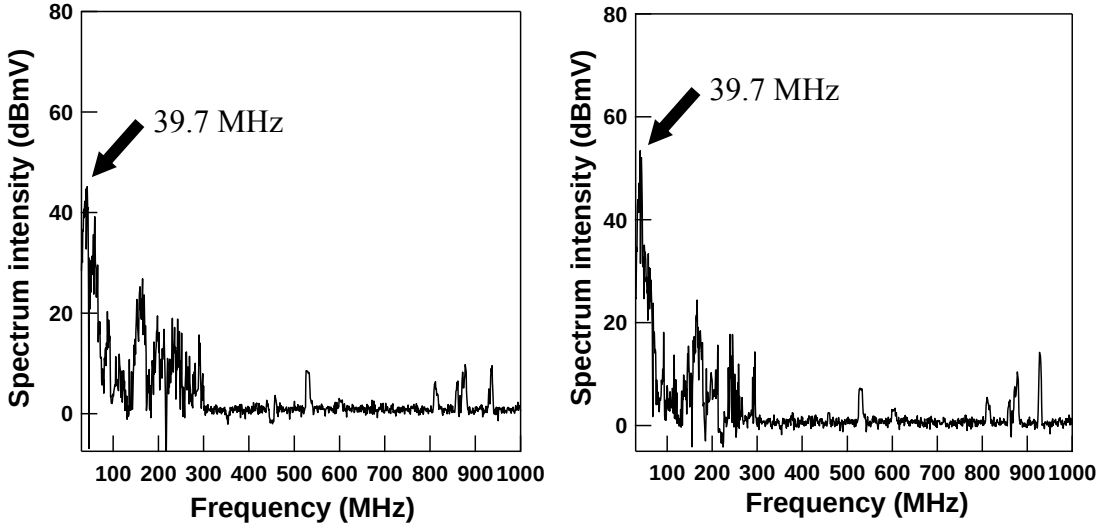

a) l = 1m, h = 0.5m　　b) l = 0.4m, h = 0.2m

Fig. A.2.4 EMW spectrum of discharge measured by log periodic antenna at closed contact condition of glass type VI with air for different cable length l and height from the ground h. (P = 10 Torr; Va = PDIV (2.8 kVrms))

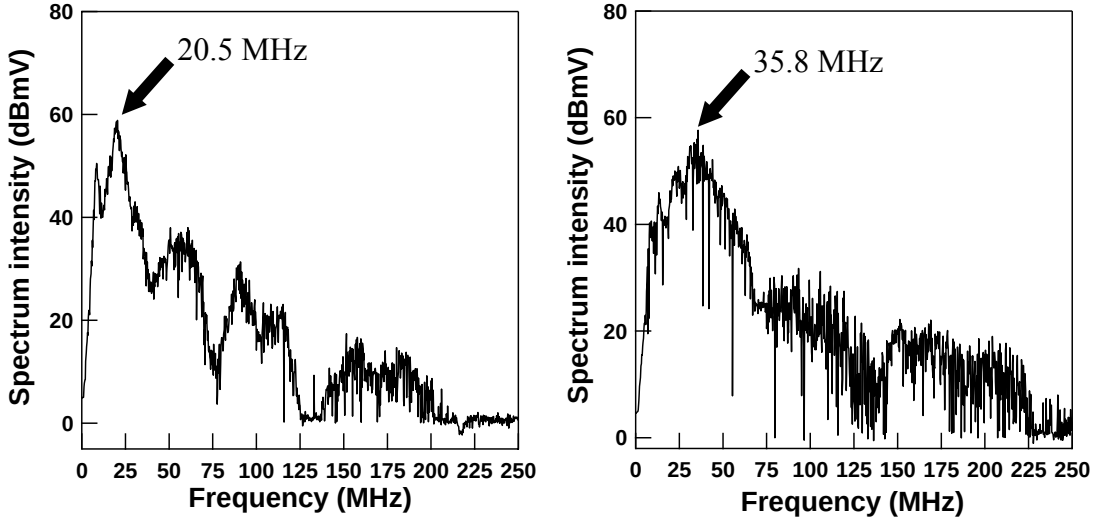

a) l = 1m, h = 0.5m b) l = 0.4m, h = 0.2m

Fig. A.2.5 EMW spectrum of discharge measured by CT at closed contact condition of glass type VI with air for different cable length l and height from the ground h. (P = 10 Torr; Va = PDIV (2.8 kVrms))

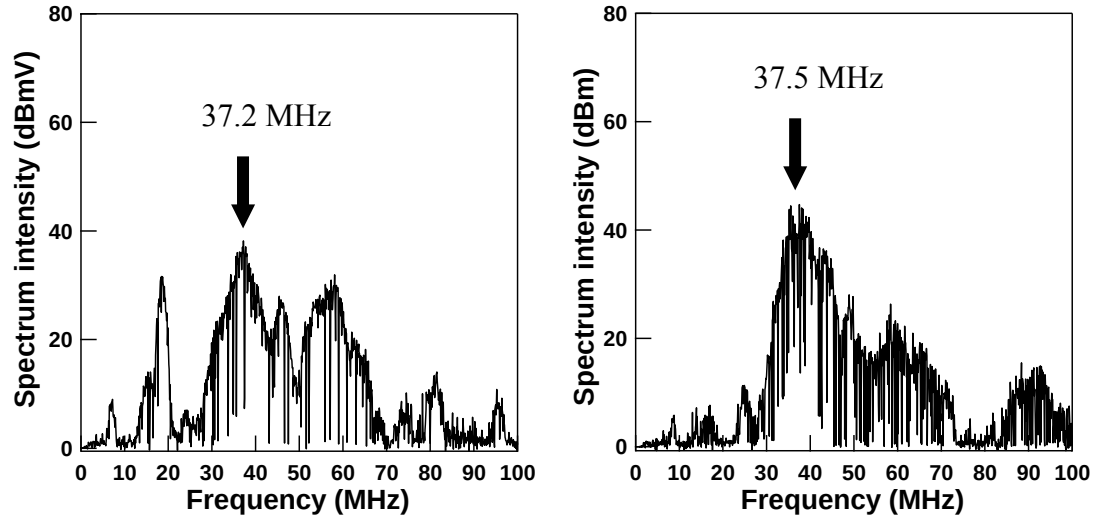

a) l = 1m, h = 0.5m b) l = 0.4m, h = 0.2m

Fig. A.2.6 EMW spectrum of discharge measured by bar antenna at closed contact condition of glass type VI with SF_6 for different cable length l and height from the ground h. (P = 10 Torr; Va = PDIV (4.4 kVrms))

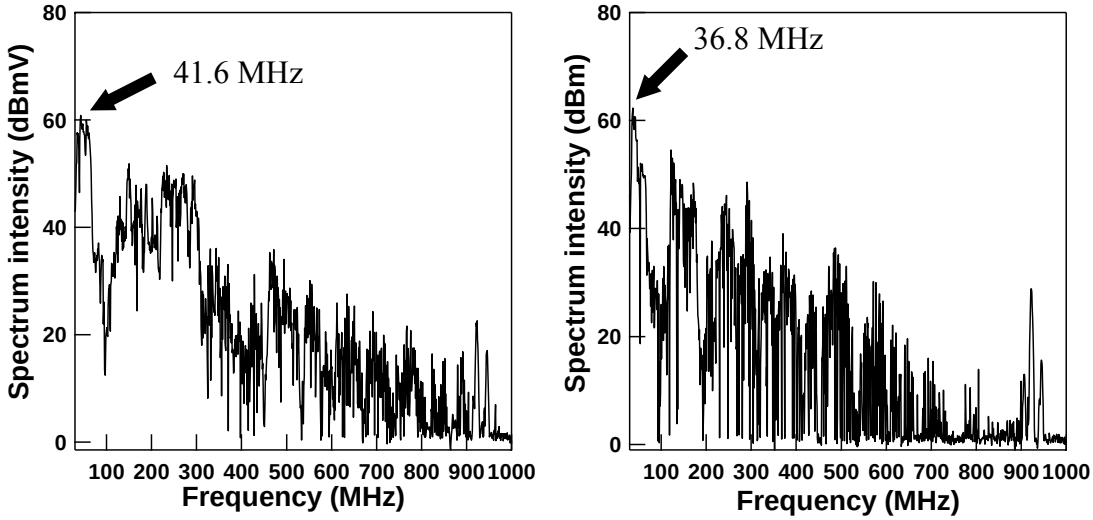

a) l = 1m, h = 0.5m　　b) l = 0.4m, h = 0.2m

Fig. A.2.7 EMW spectrum of discharge measured by log periodic antenna at closed contact condition of glass type VI with SF_6 for different cable length l and height from the ground h. (P = 10 Torr; Va = PDIV (4.4 kVrms))

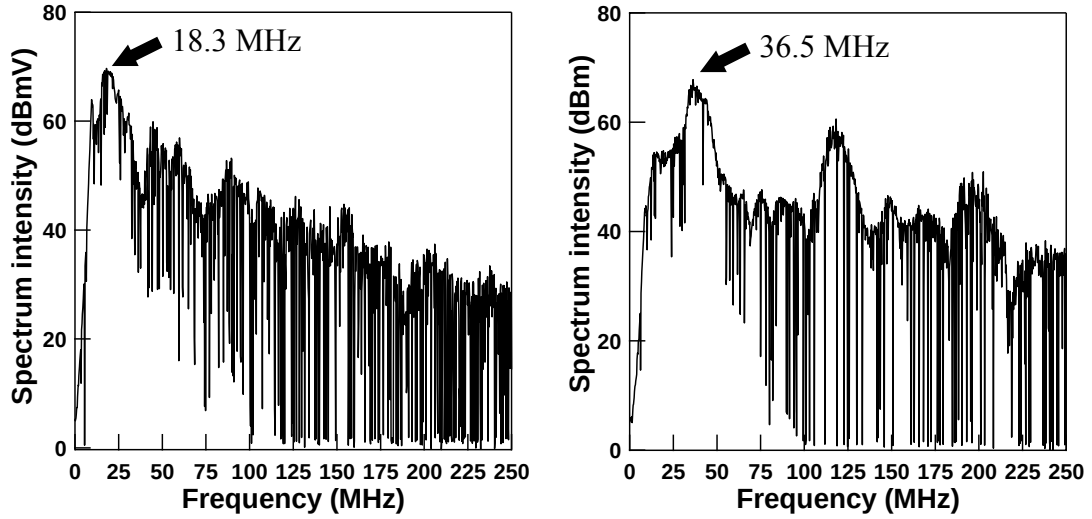

a) l = 1m, h = 0.5m　　b) l = 0.4m, h = 0.2m

Fig. A.2.8 EMW spectrum of discharge measured by CT at closed contact condition of glass type VI with SF_6 for different cable length l and height from the ground h. (P = 10 Torr; Va = PDIV (4.4 kVrms))

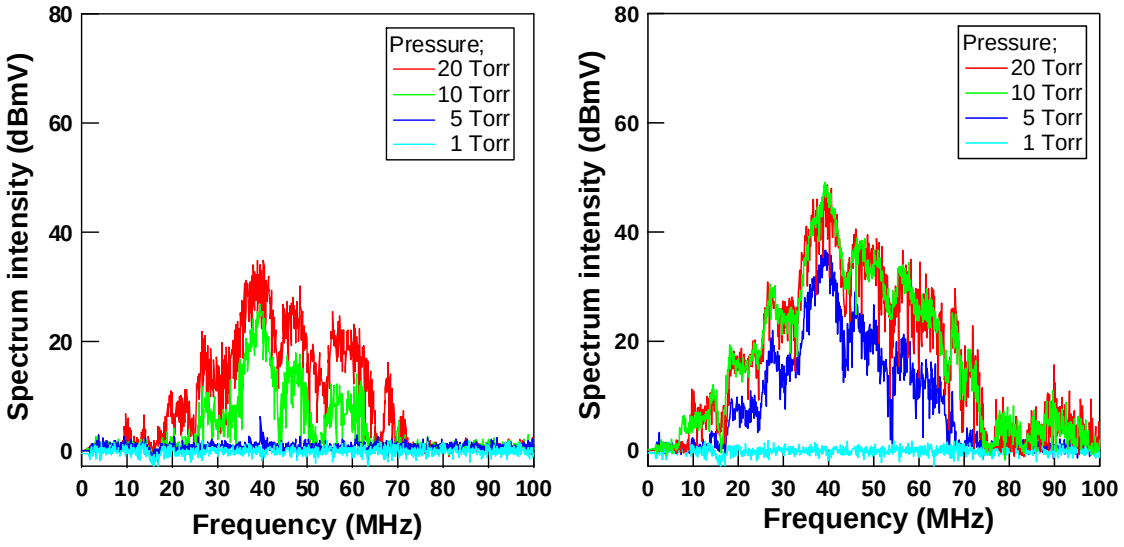

a) Air b) SF_6

Fig. A.2.9 EMW spectrum of discharge measured by bar antenna at applied voltage 12 kVpeak under closed contact condition of glass type VI for different level of pressure**.**

A.3 Discharge Pulses in Low Vacuum of Vacuum Interrupter

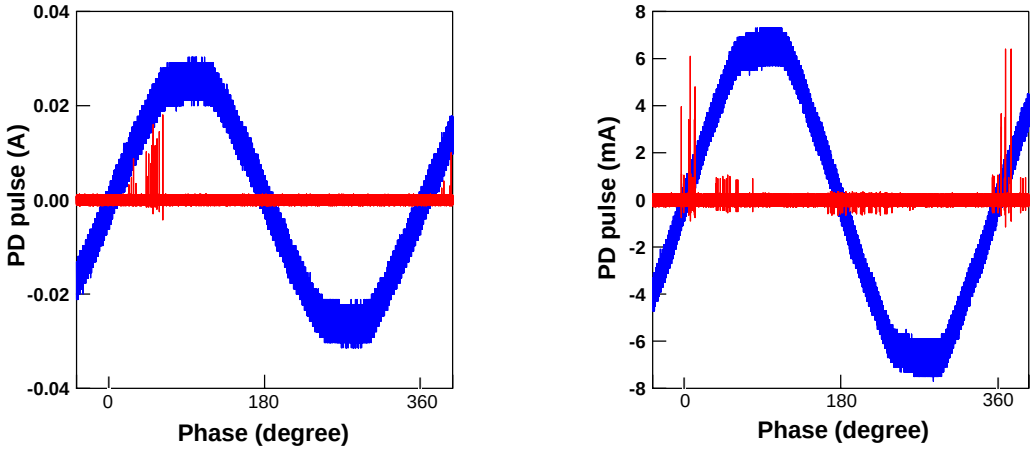

a) *Va* = 1.1 times PDIV (1.9 kVrms) b) *Va* = 1.6 times PDIV (1.9 kVrms)

Fig. A.3.1 Phase angle dependence of discharge pulses accumulated for 15 cycles of different ac applied voltages under closed contact condition of glass type VI with air at pressure 5 Torr.

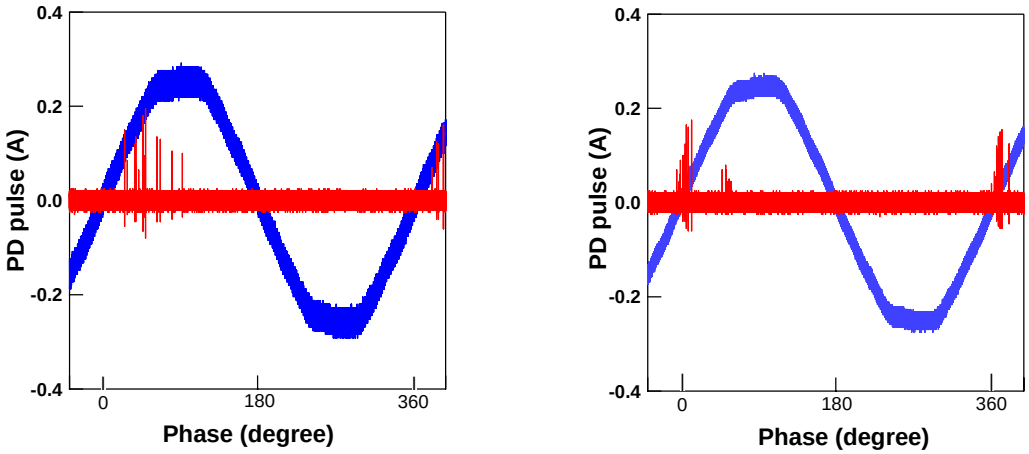

a) *Va* = 1.1 times PDIV (2.8 kVrms) b) *Va* = 1.6 times PDIV (2.8 kVrms)

Fig. A.3.2 Phase angle dependence of discharge pulses accumulated for 15 cycles of different ac applied voltages under closed contact condition of glass type VI with air at pressure 10 Torr.

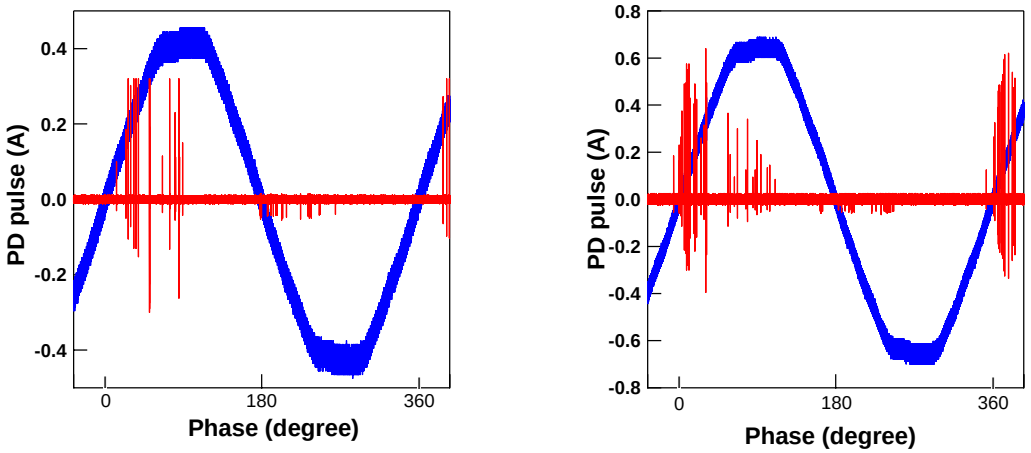

a) *Va* = 1.1 times PDIV (3.9 kVrms)　　b) *Va* = 1.6 times PDIV (3.9 kVrms)

Fig. A.3.3 Phase angle dependence of discharge pulses accumulated for 15 cycles of different ac applied voltages under closed contact condition of glass type VI with air at pressure 20 Torr

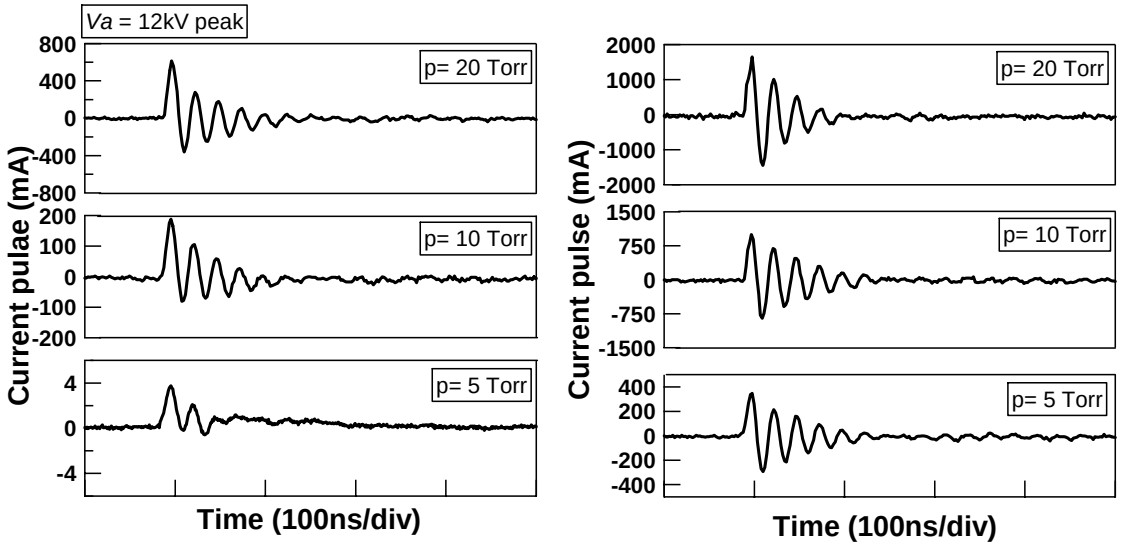

a) air　　b) SF_6

Fig. A.3.4 Typical discharge current pulses at different pressure level under closed contact condition of glass type VI for applied voltage 12 kVpeak

Appendix B

B.1 Phase dependence of discharge light pulses

The discharges having pulse-type discharge. Figs. B.1 (a) and (b) portray the resulting of phase dependence of discharge light pulses accumulated in 15 cycles of various applied voltage against pressures measured with PMT. The results revealed that no pulse less discharges or dc-component discharges appeared at the applied voltage for pressure from 13 Pa to 6.6 kPa.

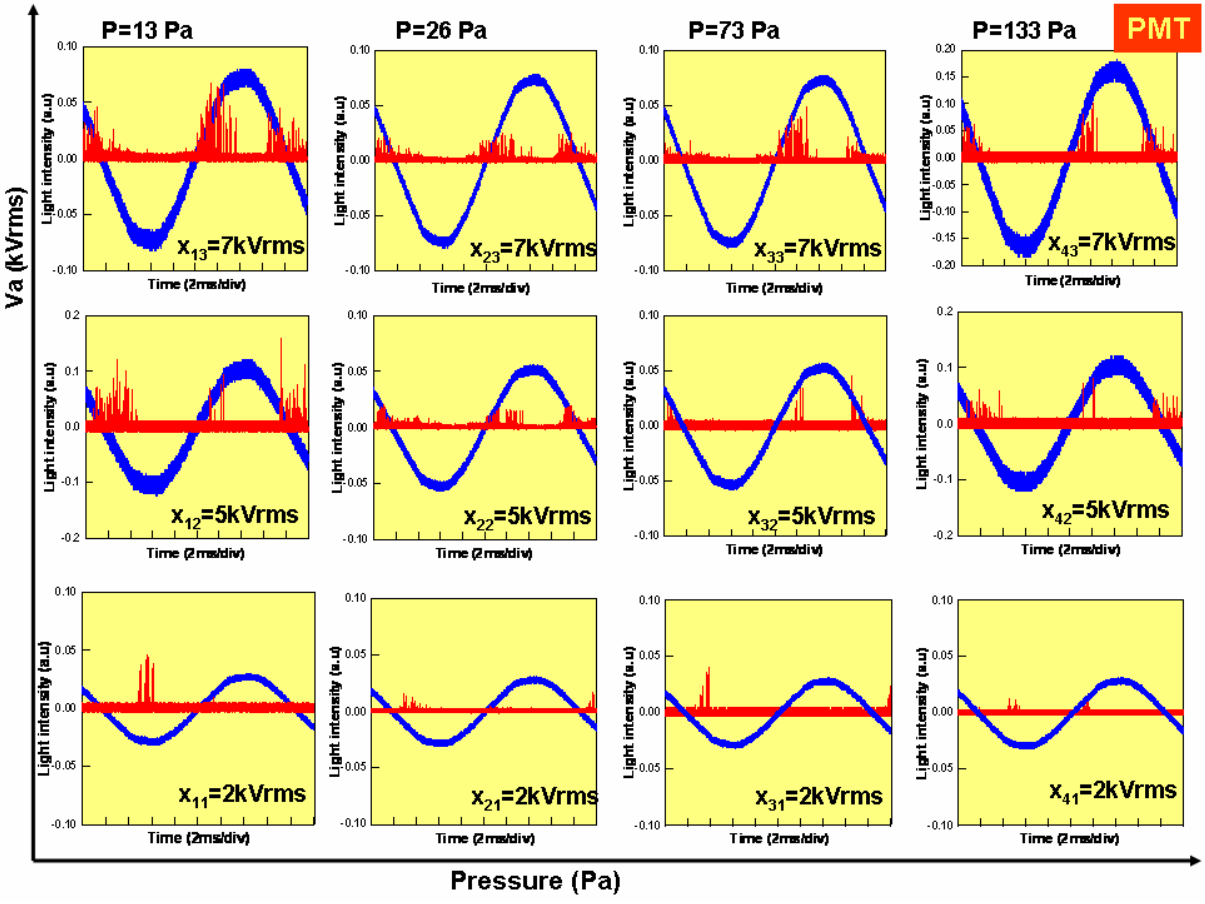

Fig. B.1 (a) Phase dependence of discharge light pulses accumulated in 15 cycles of various applied voltage against pressures measured with PMT

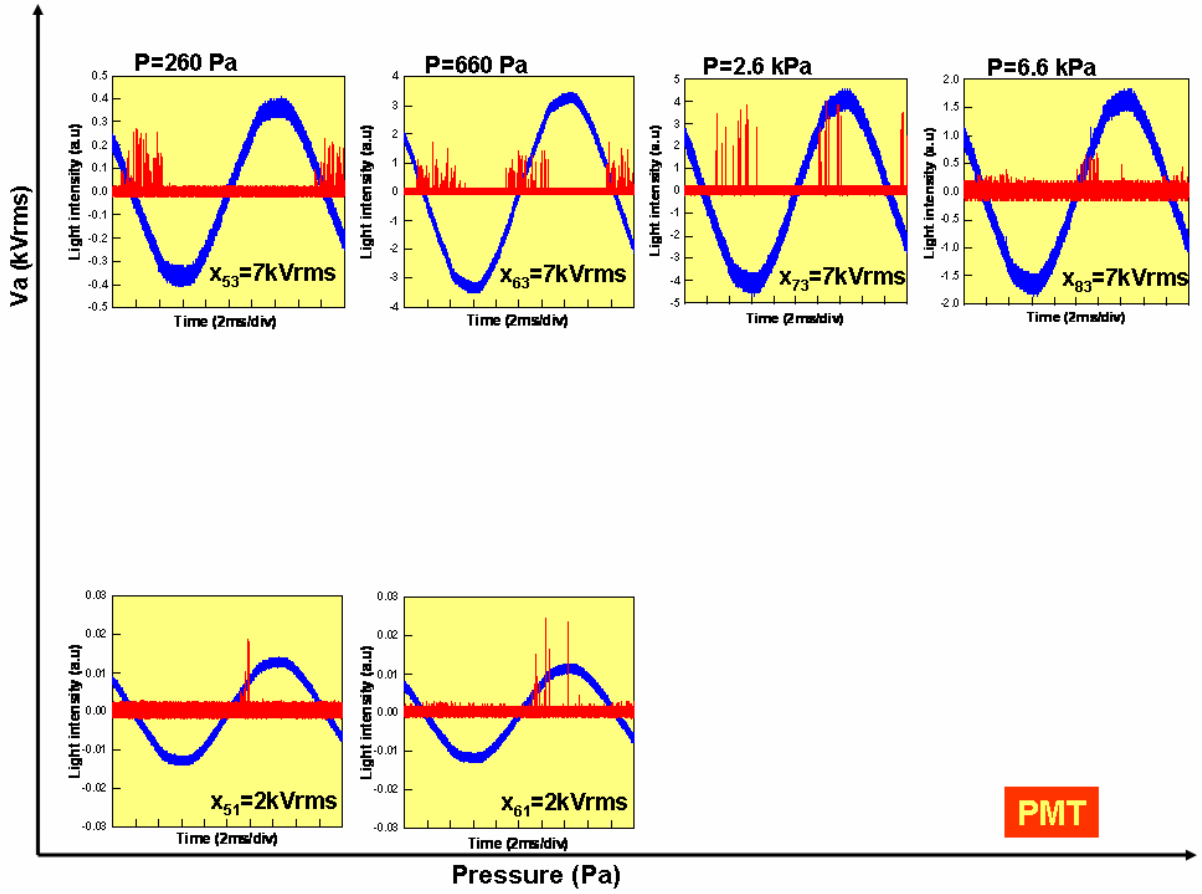

Fig. B.1 (b) Phase dependence of discharge light pulses accumulated in 15 cycles of various applied voltage against pressures measured with PMT

B.2 PD light pulses

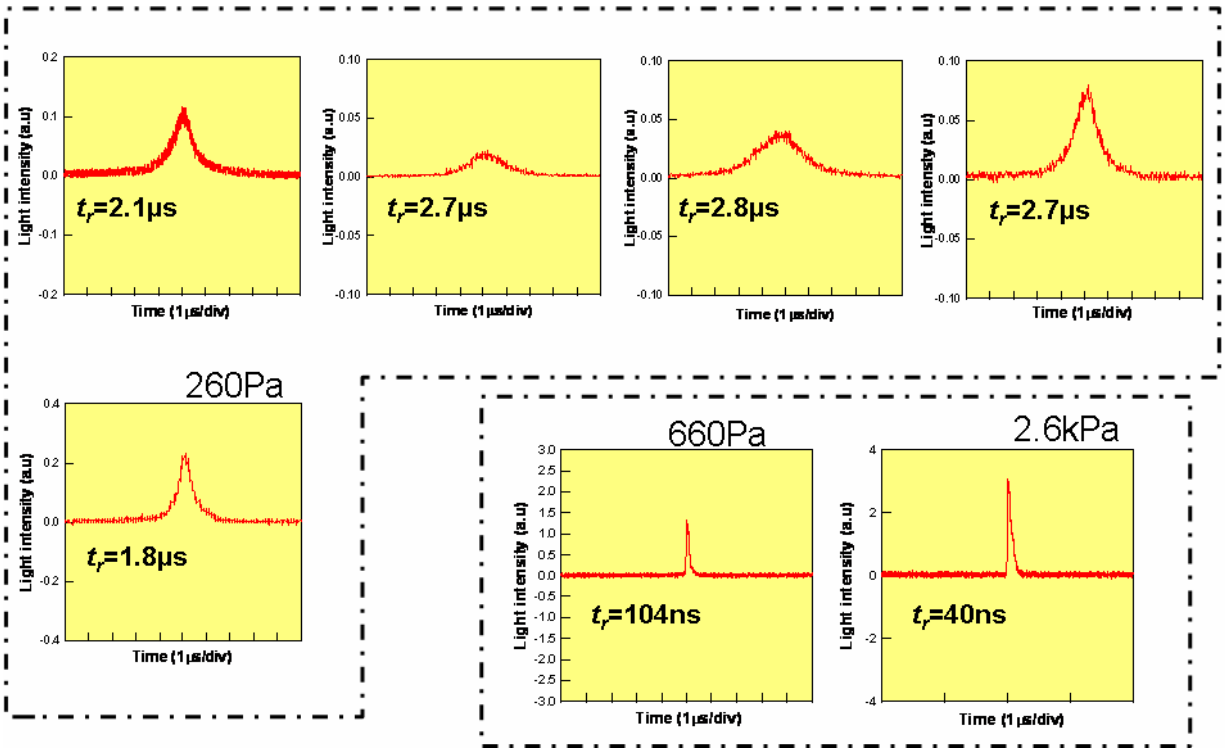

Fig. B.2.1 Typical discharge light pulses for various pressures of air measured with PMT at 7 kVrms applied voltage

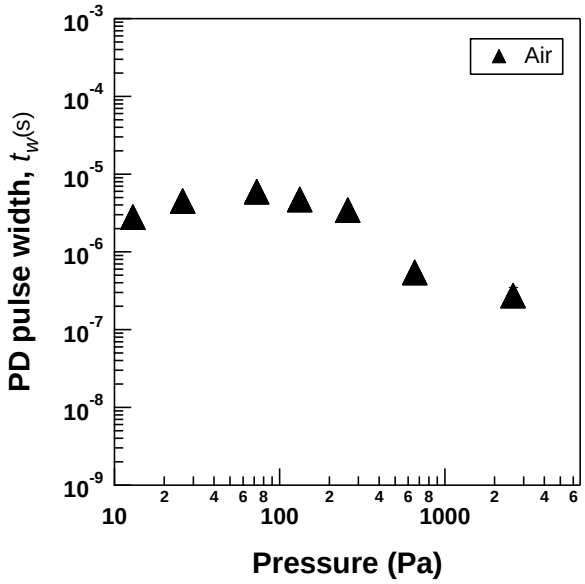

Fig. B.2.2 PD light pulses width as a function of various pressures of air at 7 kVrms applied voltage.

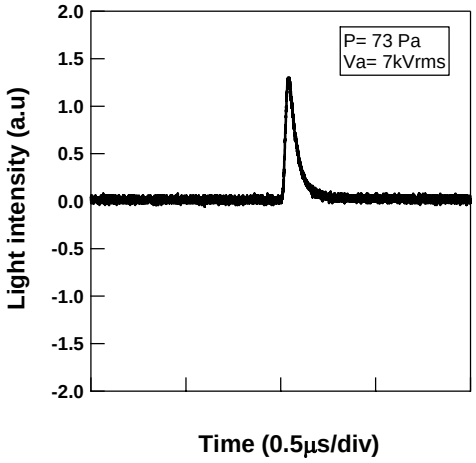

a) p = 73 Pa

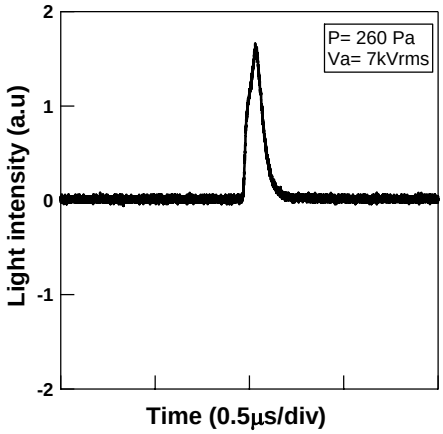

b) p = 260 Pa

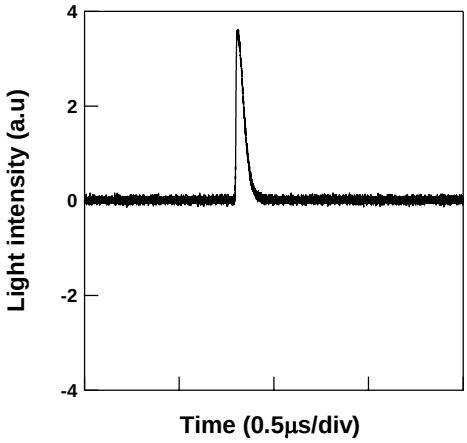

c) p = 1300 Pa

Fig. B.2.3 Typical discharge light pulses for various pressures of SF_6 measured with PMT at 7 kVrms of applied voltage

B. 3 Phase-resolved discharges

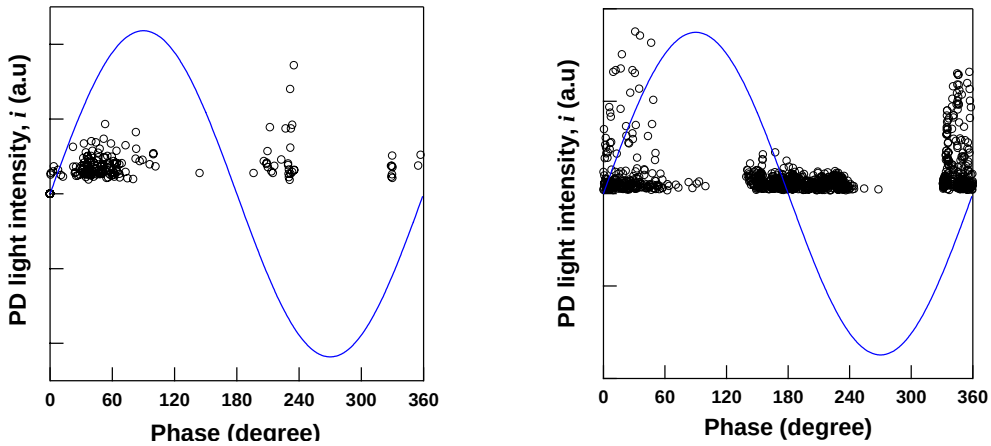

a) p = 66 Pa

b) p = 130 Pa

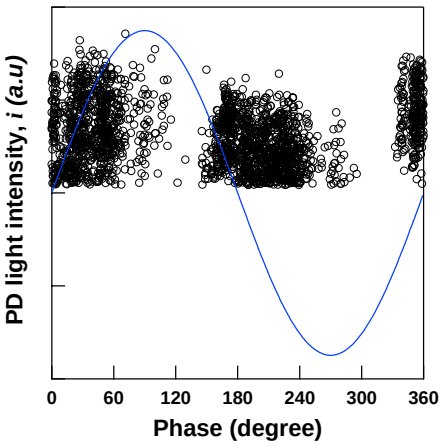

c) p = 660 Pa

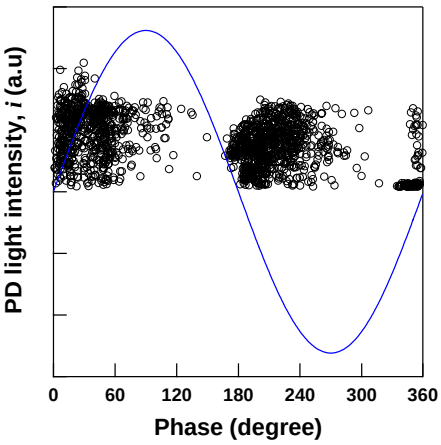

d) p = 1300 Pa

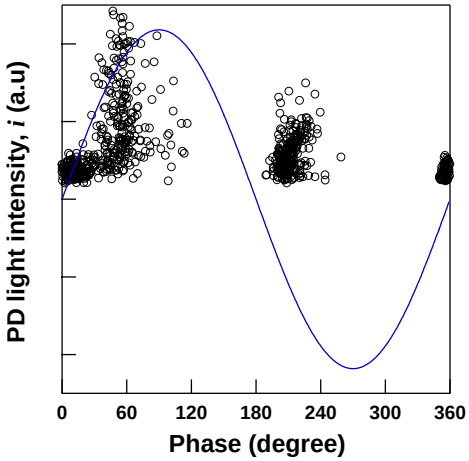

e) p = 2600 Pa

Fig. B.3.1 Typical phase resolved discharge for various pressures of air measured with PMT and PARADISE at 7 kVrms of applied voltage.

B.3 Drawing of glass vessel Vacuum Interrupter

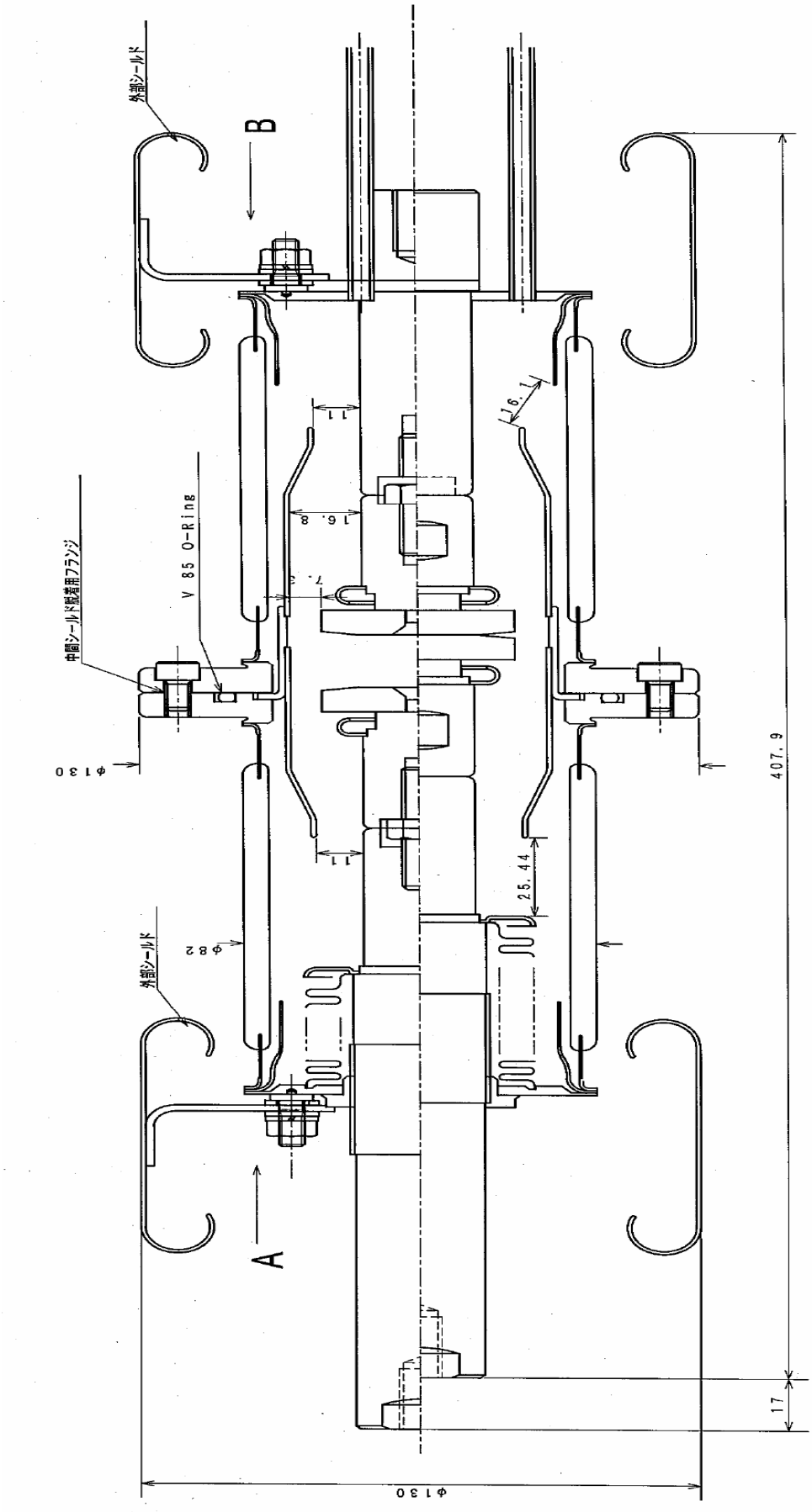

Appendix C

C.1 Optimum condition for obtain a maximum cumulative charge

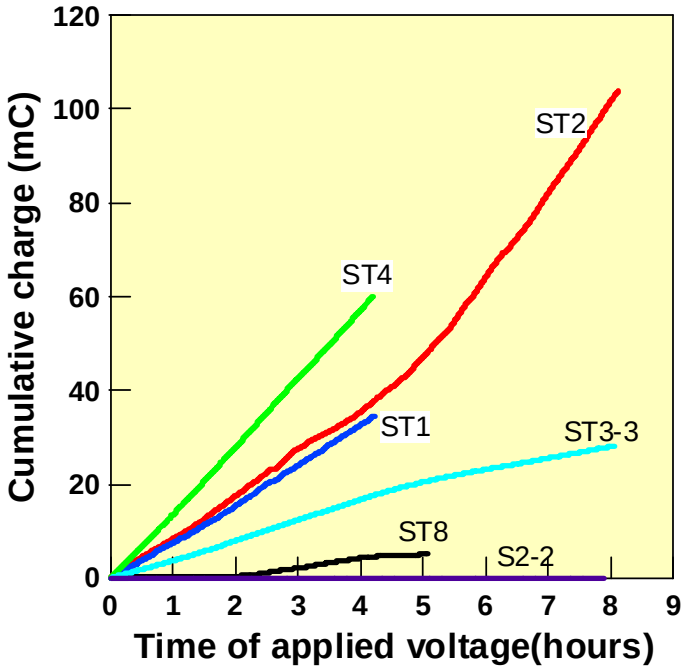

ST1, ST2 & ST4 :
Ø = 1mm, g= 10mm
p= 0.1 MPa
Va = 18 kVrms (80% Vs)

ST3-3 :
Ø = 0.5mm, g= 10mm
p= 0.1 MPa
Va= 20 kVrms (80% Vs)

ST8 :
Ø = 1mm, g= 10mm
p= 0.2 MPa
Va= 17 kVrms (80% Vs)

S2-2 :
Ø = 1mm, g= 10mm
p= 0.2 MPa
Va= 19 kVrms

Fig. C.1.1 Cumulative charge as a function of time of applied voltage for various conditions

C.2 Photograph of typical features after breakdown and partial discharge occurrence.

ST2 (BD & PD)

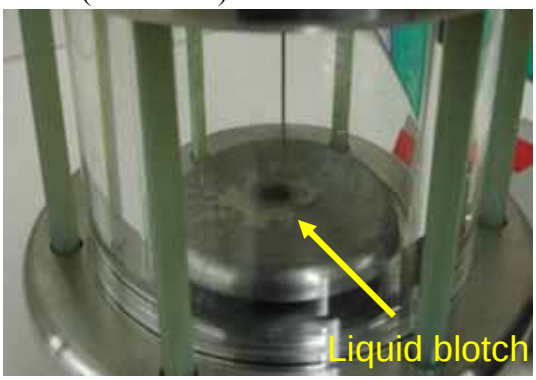

P= 0.1MPa
BD ≈ 23 kVrms (2 ~ 3 times)
PD at Va= 18 kVrms (8 hours)
ϕ= 1 mm, g= 10 mm

Water Vapor: 1050 (vol ppm)

ST4 (PD only)

P= 0.1MPa
PD at Va= 18 kVrms (4 hours)
ϕ= 1 mm, g= 10mm

Water Vapor: 135 (vol ppm)

Liquid blotch:
water vapor content > 1000 (vol ppm)

⇔

***Humidity**
***Temperature**
***charge, q**

Fig. C.2.1 Photograph of blotch substance after PD and breakdown test

ST2-Just after BD & PD)

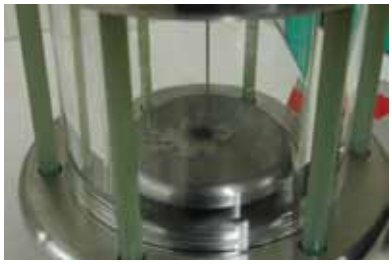

Yellow color was not observed on the surface of acrylic

ST6- Just after BD & PD

Light yellow color appear on the surface of acrylic

ST8- Just after BD & PD

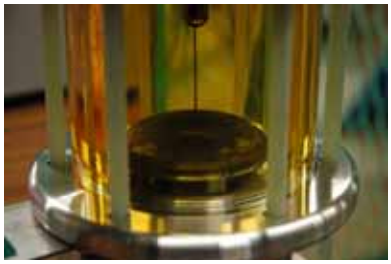

Bright yellow color appear on the surface of acrylic

0.1 MPa → **0.15 MPa** → **0.2 MPa**

Fig. C.2.2 Photograph of transformation to yellow color as pressure increases

Sample: ST8

P= 0.2 MPa

PD at Va = 17 kVrms (4 hours)

ϕ= 1 mm, g= 10mm

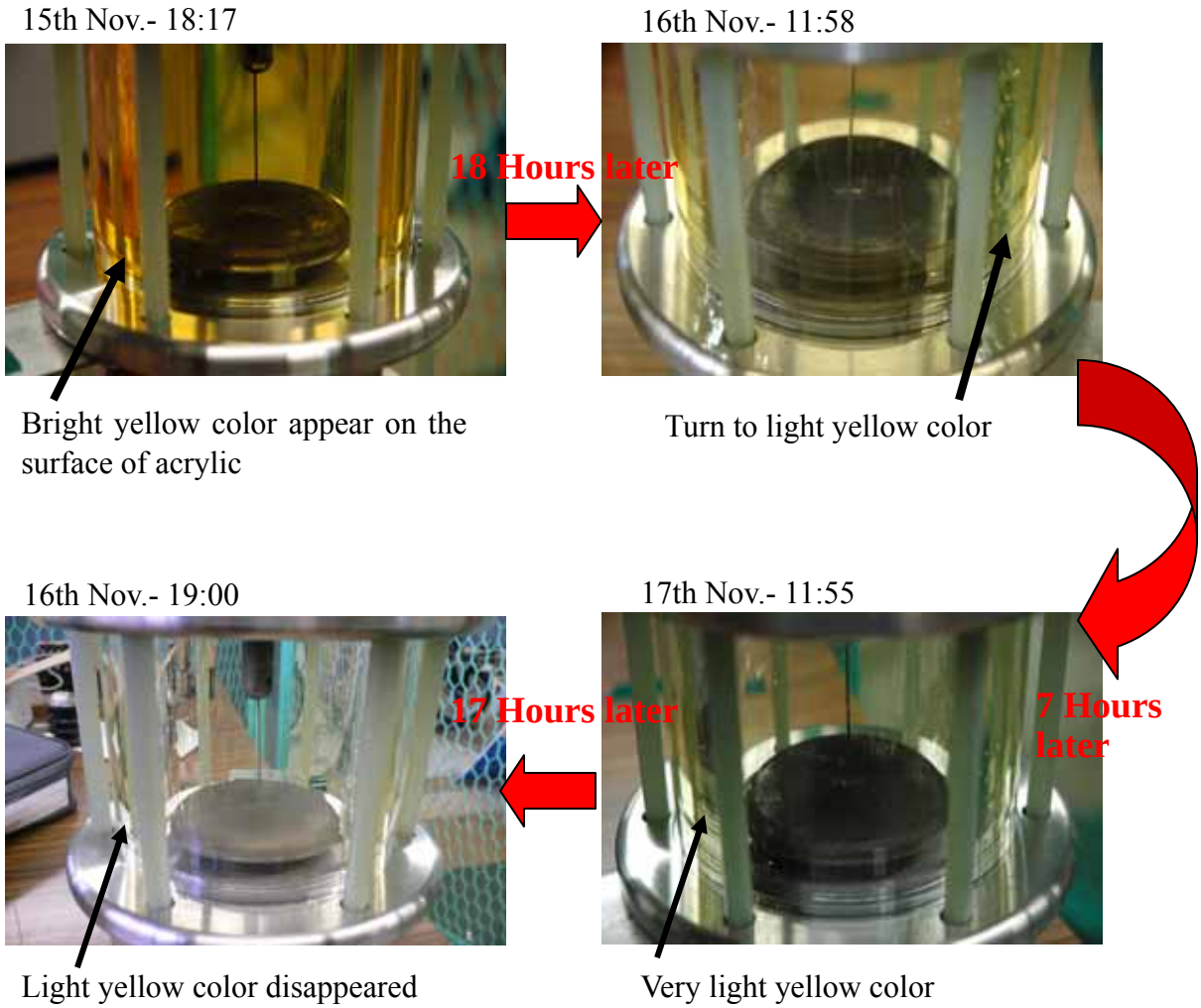

Fig. C.2.3 Photograph for observation of temporal disappeared of yellow color

SM-1 & SM-2
P= 0.1 MPa
PD at Va = 18 kVrms (80% V_s)
ϕ= 1 mm, g= 10mm

SM-1

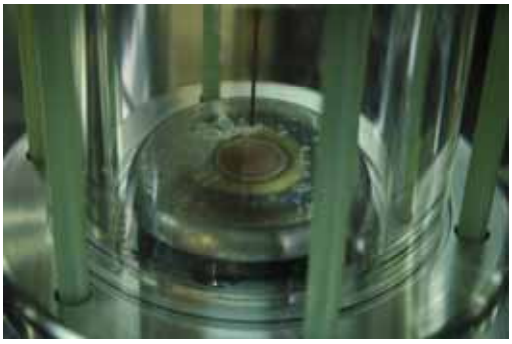

Time of PD occurrence: 8 hours
Cumulative charge: 30 mC

SM-2

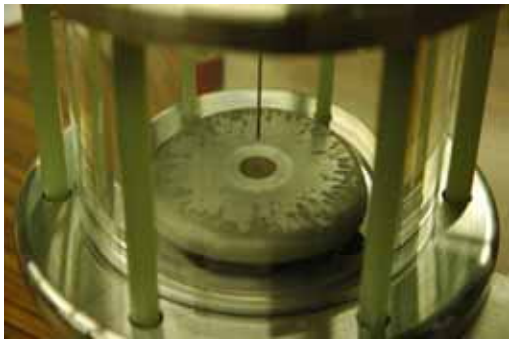

Time of PD occurrence: 12 hours
Cumulative charge: 67 mC

Fig. C.2.4 Photograph of blotch substance of SM-1 and SM-2

C.3 Quantitative value determination for C_2F_5I

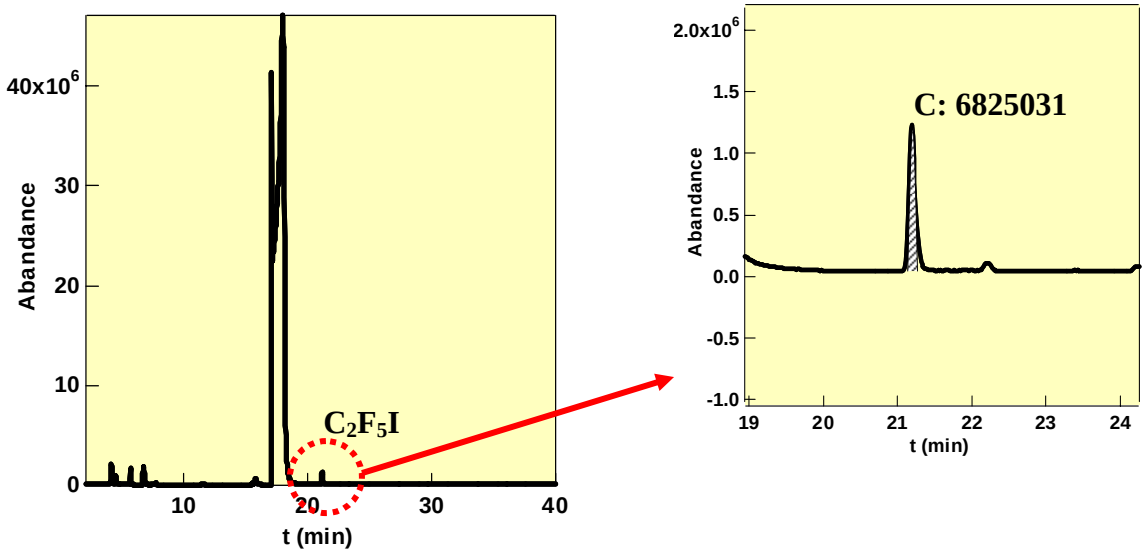

STD gas
CH_3I : B=130 ppm ,
A =18472783

Quantitative value = $\frac{\mathbf{C \times B}}{\mathbf{A}}$

= 48.03 (Volppm, CH_3I correspond value)

C.4 Energy dissociation X-ray microanalysis (EDX)

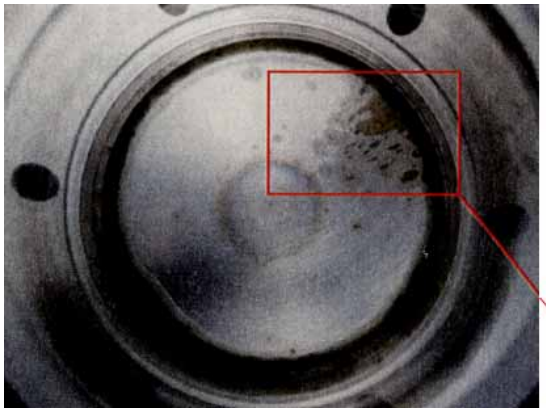

EDX analysis result of the blotch sticking on the plane electrode surface

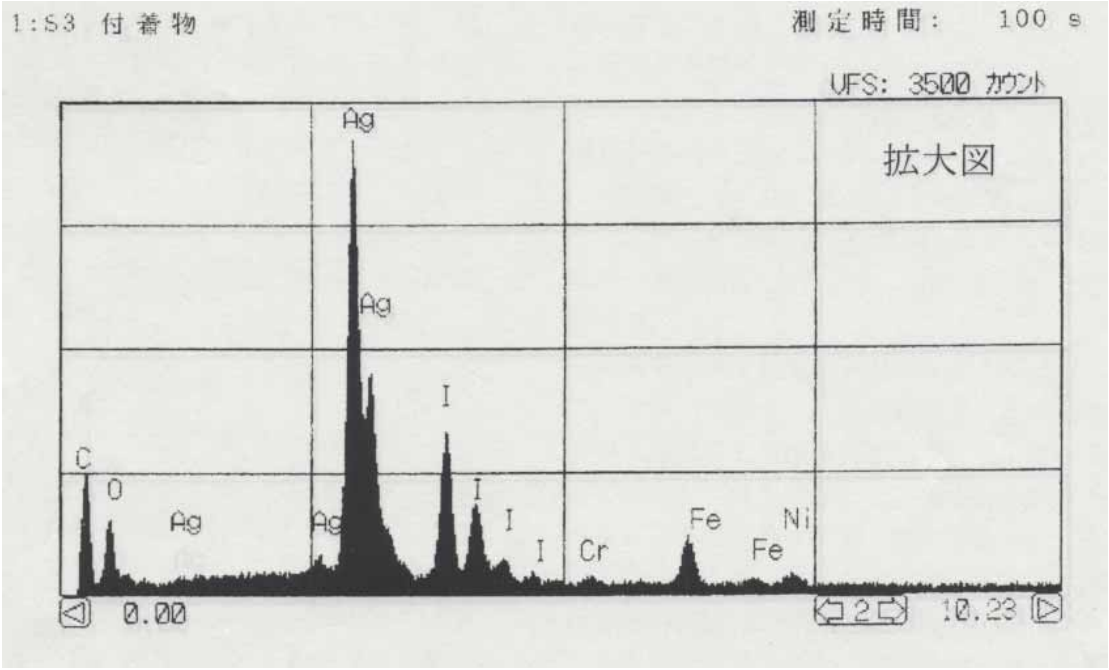

C.5 Drawing of CF_3I container

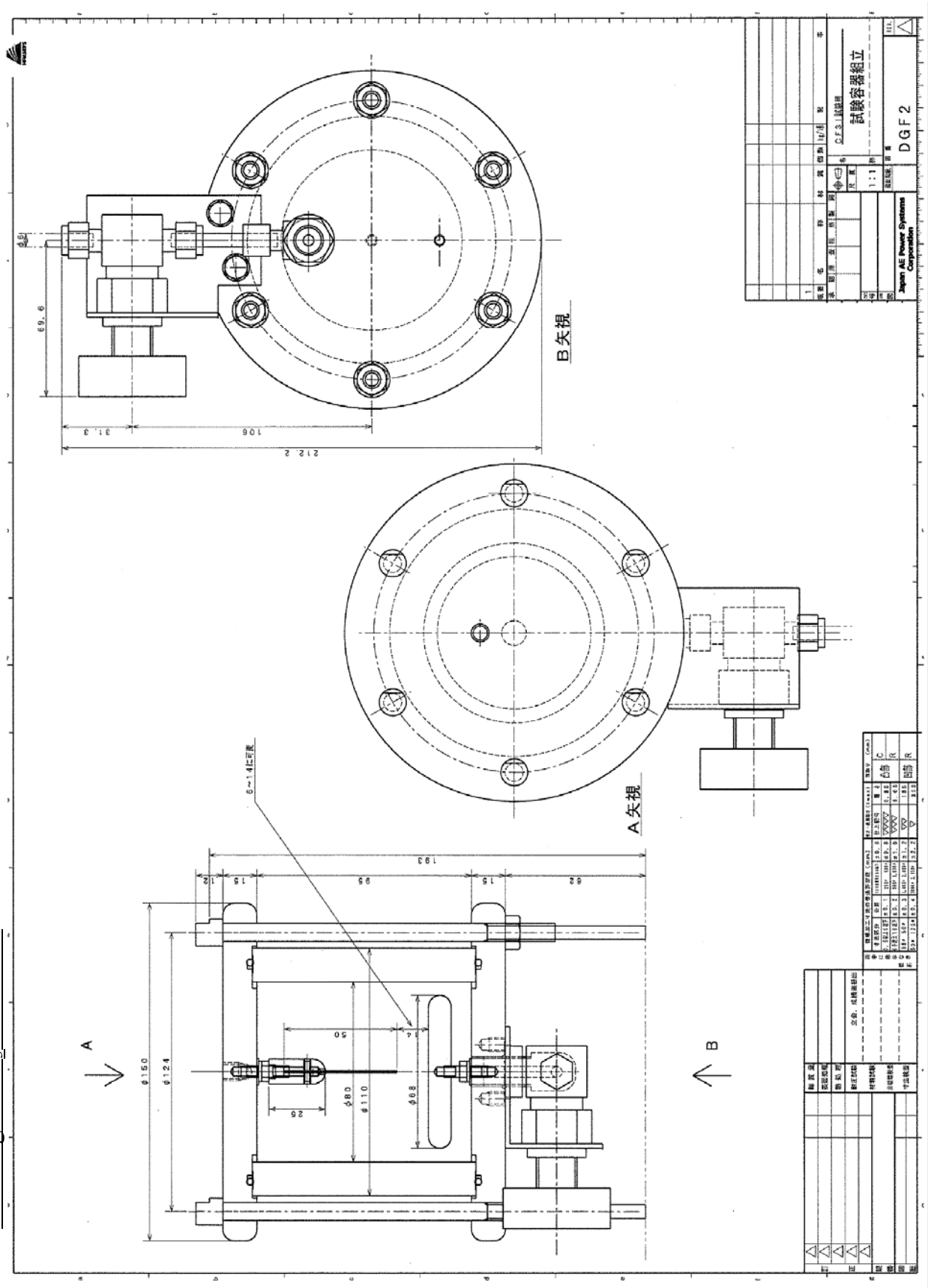

C.6 Impedance matching circuit

Impedance matching circuit (IMC) with 50 ohm of input and output impedance is a self developed PD measurement device. The IMC enable to measure PD current signal which has frequency range up to 400 MHz. The equivalent circuit of IMC is shown in Fig. C.6.1. The IMC consists of chip-type impedance, capacitance, inductance, amplifier and arrestor. The chip-type impedance was connected in π shape, work as attenuator to attenuate in case of high PD current pulse flow, so that the measurement device such as oscilloscope can be protect. The impedance of 50 ohm was well matching to measuring cables and devices. Arrestor and operational amplifier (MAV-3) with a wide-band frequency range were placed in IMC in order to have an extra protection from the surge pulses generated at breakdown. The power source of the IMC is DC 12V. The frequency response characteristic of the IMC device is shown in Fig. C.6.2. The frequency response of IMC was measured with network analyzer (Anritsu).

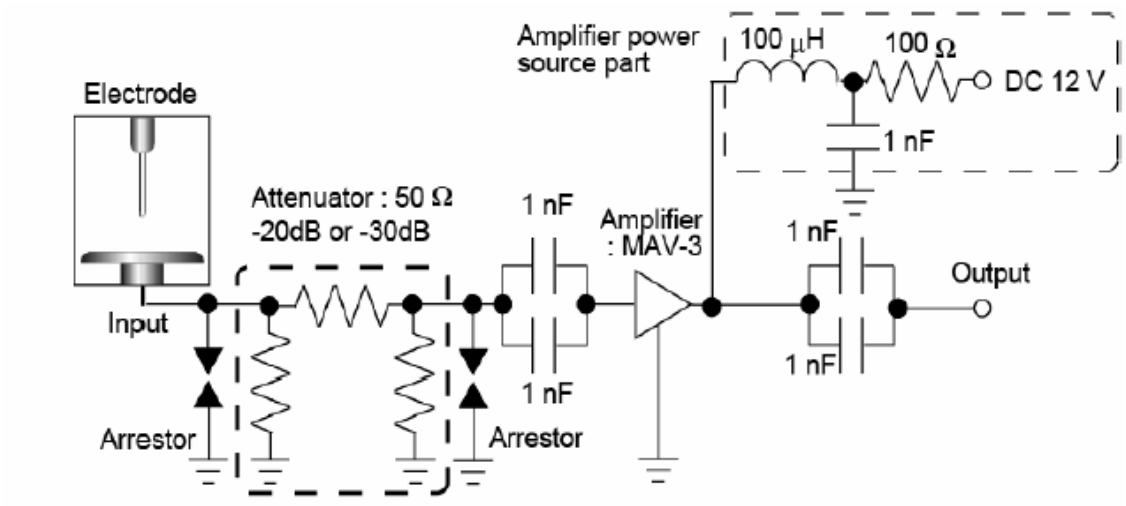

Fig. C.6.1 Equivalent circuit of impedance matching circuit (IMC)

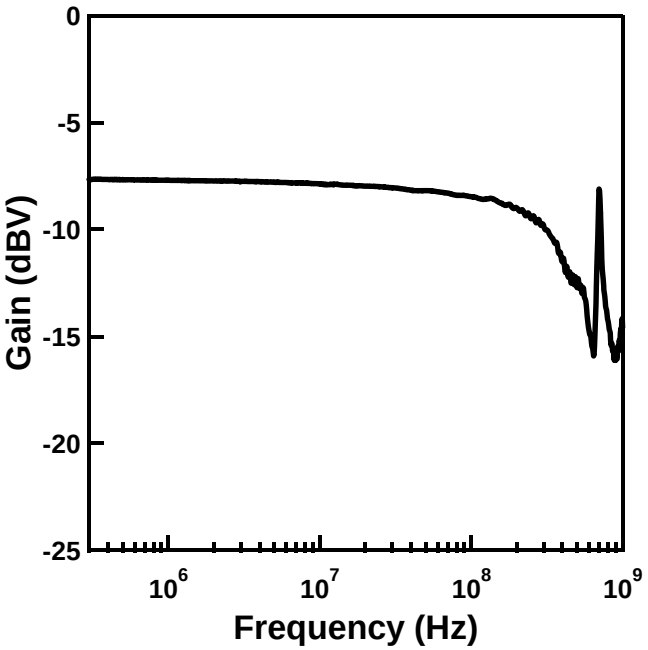

Fig. C.6.2 Frequency response of IMC

Acknowledgment

In the name of Allah, Most Gracious, Most Merciful

The author is deeply indebted to his research advisor, Professor Dr. Masayuki Hikita, Department of Electrical Engineering, Kyushu Institute of Technology, for all his insightful guidance, valuable discussion and great encouragement to this research work. Working with him has been the most valuable experience of the author's life.

The author would like to express his great appreciation to Associate Professor Dr. Shinya Ohtsuka, Department of Electrical Engineering, Kyushu Institute of Technology, for all his kindness advice and helpful comments through this research work.

The author would like to express his appreciation to Professor Dr. Ken Kimura and Professor Dr. Satoshi Matsumoto for his intelligent advice and comments through this research work.

The author would like also to express his great pleasure and special thanks to Japan AE Power Systems Corporation for contributing a collaboration research with Kyushu Institute of Technology by providing materials and financial support. The author would like to give his great appreciation to Dr. Hitoshi Saitoh, Dr. Masayuki Sakaki and Dr. Masanori Tsukushi, the person in charge of Japan AE Power Systems Corporation, for all their valuable discussion and helpful comment to succeed this research. The research cannot be carried out without strong support from them.

The author would also like to thank to University Science Malaysia and Ministry of High Education, the Government of Malaysia whose give an opportunity and financial support to the author to pursue his study in master and doctoral degree course in Kyushu Institute of Technology.

The author would like to thanks to all the members of Professor Hikita's Laboratory, who have offered generous support and gave full cooperation to this research work.

Finally, the author would like to express his sincere thank to his wife, Hazizon binti Hamid and his children, Noraina Syafiqah, Mohamad Farid and Amira Raheema for their patients and giving him the great encouragement and inseparable support to proceed this work successfully.

Tobata, February 2008

Mohamad Kamarol bin Mohd Jamil

List of Publications

Journals

1. Discharge Properties and Emitted Electromagnetic Wave Spectrum in Low Vacuum Region of Vacuum Interrupter

   IEEJ Transactions on Power and Energy, Vol. 125, No.8, pp.797-802, Aug. 2005.

   Authors: *Mohamad Kamarol*, Shinya Ohtsuka, Hitoshi Saitou, Masayuki Sakaki and Masayuki Hikita

2. Determination of Gas Pressure in Vacuum Interrupter Based on Partial Discharge

   IEEE Transactions on Dielectric and Electrical Insulation, Vol. 14, No. 3, pp.593-599, June 2007.

   Authors: *Mohamad Kamarol*, Shinya Ohtsuka, Hitoshi Saitou, Masayuki Sakaki and Masayuki Hikita

3. Discharge properties in Low Vacuum Region of Vacuum Interrupter Filled with SF_6 Gas

   IEEJ Transactions on the Fundamentals and Materials, Vol. 127, No.11, pp.709-713, Nov. 2007.

   Authors: *Mohamad Kamarol*, Shinya Ohtsuka, Hitoshi Saitou, Masayuki Sakaki and Masayuki Hikita

Proceedings

1. Discharge Properties and Emitted Electromagnetic Wave Spectrum in Low Vacuum Region of Vacuum Interrupter

   Proceeding of International Workshop on High Voltage Engineering (IWHV), Vol. 1, pp.117-122, Oct. 2004.

   Authors: *Mohamad Kamarol*, Shinya Ohtsuka, Hitoshi Saitou, Masayuki Sakaki and Masayuki Hikita

2. Discharge Phenomena in Low Vacuum Region of Glass Tube Vacuum Interrupter under AC Applied Voltage

   Proceeding of International Symposium on Electrical Insulating Materials (ISEIM), Vol.1, pp. 36-39, Jun. 2005.

   Authors: *Mohamad Kamarol*, Shinya Ohtsuka, Hitoshi Saitou, Masayuki Sakaki and Masayuki Hikita

3. Investigation of Discharge Characteristic for Diagnosis of Degree of Vacuum in Glass Type Vacuum Interrupter

   Proceeding of the 14^{th} International Symposium on High Voltage Engineering (ISH), pp.171, Beijing, Aug. 2005.

   Authors: *Mohamad Kamarol*, Shinya Ohtsuka, Hitoshi Saitou, Masayuki Sakaki and Masayuki Hikita

4. Diagnosis of Vacuum Degree in Vacuum Interrupter Based on Partial Discharge

   Proceeding of $XXII_{nd}$ International Symposium on Discharges and Electrical Insulation in Vacuum (ISDEIV), Vol.1, pp.165-168, Matsue, Sept. 2006.

   Authors: *Mohamad Kamarol*, Shinya Ohtsuka, Hitoshi Saitou, Masayuki Sakaki and Masayuki Hikita

5. Discharge properties in Low Vacuum Region of Vacuum Interrupter Filled with SF_6 Gas

   Proceeding of 13^{th} Asian Conference on Electrical Discharge (ACED), P-1-20, Hokkaido, Oct. 2006.

   Authors: *Mohamad Kamarol*, Shinya Ohtsuka, Hitoshi Saitou, Masayuki Sakaki and Masayuki Hikita

6. Gas decomposition analysis of CF_3I under AC partial discharge of non-uniform electric field configuration

   Proceeding of Japan-Korea Joint Symposium on Electrical Discharge and High Voltage Engineering, pp.161-164, Tokyo, Nov. 2007.

   Authors: *Mohamad Kamarol*, Yuta Nakayama, Tomoki Hara, Shinya Ohtsuka and Masayuki Hikita

7. Diagnostic technique of insulation performance in vacuum interrupter based on partial discharge

   Proceeding of International Symposium on EcoTopia Science, ISBN: 978-4-903263-01-4, pp.475-481, Nagoya, Nov. 2007.

   Authors: *Mohamad Kamarol*, Shinya Ohtsuka, Hitoshi Saitou, Masayuki Sakaki and Masayuki Hikita

8. Investigation of Discharge Properties in Low Vacuum Region by Optical Observation for Glass Type Vacuum under Closed Contact Condition.

   Proceeding of National Convention of IEEJ, Vol. 6, pp. 424-425, Mar. 2005.

   Authors: *Mohamad Kamarol*, Shinya Ohtsuka, Hitoshi Saitou, Masayuki Sakaki and Masayuki Hikita

9. Discharge Properties in Low Vacuum Region of Vacuum Interrupter at Open Contact Condition

   Proceeding of Joint Conference of Electrical and Electronics Engineers in Kyushu, pp.95, 2004

   Authors: *Mohamad Kamarol*, Shinya Ohtsuka, Hitoshi Saitou, Masayuki Sakaki and Masayuki Hikita

10. Partial Discharge Properties in Low Vacuum Region of Vacuum Interrupter

    Proceeding of National Convention of IEEJ, Vol. 6, pp. 347, 2004

    Authors: *Mohamad Kamarol*, Shinya Ohtsuka, Mengu Cho, Hitoshi Saitou, Masayuki Sakaki and Masayuki Hikita

11. Optical Properties of Discharge in Vacuum Interrupter Filled with Air at Low Vacuum Region

    Proceeding of Institute of Engineers on Electrical Discharge in Japan (IEEDJ) Annual Meeting, A-1-3, 2005

    Authors: *Mohamad Kamarol*, Shinya Ohtsuka, Hitoshi Saitou, Masayuki Sakaki and Masayuki Hikita

12. AC Sparkover Voltage and PD Inception Voltage Properties in CF_3I gas under non-uniform electric field configuration

    Proceeding of Annual Meeting Record IEE Japan, Vol.6, pp.441, March 2007

    Authors: *Mohamad Kamarol*, Yuta Nakayama, Shinya Ohtsuka, Hitoshi Saitou, Masayuki Sakaki and Masayuki Hikita

13. Construction of time and space-resolved spectroscopy system of PD phenomena and its application to observation of PDs in SF_6 gas

    Proceeding of Annual Meeting Record IEE Japan, Vol.1, pp.38, March 2007. (in Japanese)

    Authors: Shinya Ohtsuka, Yuta Nakayama, S Nawata, *Mohamad Kamarol* and Masayuki Hikita

14. Application of time spectroscopic system to investigate of PD phenomena in SF_6 gas

    Proceeding of Annual Meeting Record IEE Japan, Vol.1, pp.39, March 2007. (in Japanese)

    Authors: Yuta Nakayama, *Mohamad Kamarol*, S Nawata, Masayuki Hikita and Shinya Ohtsuka

Award

1. Chatterton Young Investigator Award from ISDEIV 2006

   Proceeding of $XXII_{nd}$ International Symposium on Discharges and Electrical Insulation in Vacuum (ISDEIV), Vol.1, pp.165-168, Matsue, Sept. 2006.